

**SYNTHESIS AND STRUCTURAL CHARACTERIZATION OF
CHIRAL SCHIFF BASE METAL COMPLEXES AND THEIR
CATALYTIC ACTIVITY**

**A THESIS
SUBMITTED FOR THE DEGREE OF
DOCTOR OF PHILOSOPHY**

**BY
MADDELA PRABHAKAR**



**SCHOOL OF CHEMISTRY
UNIVERSITY OF HYDERABAD
HYDERABAD 500 046
INDIA**

SEPTEMBER 2006



School of Chemistry
University of Hyderabad
Hyderabad-500046, India

STATEMENT

I hereby declare that the matter embodied in the thesis entitled **“Synthesis and Structural Characterization of Chiral Schiff Base Metal Complexes and Their Catalytic Activity”** is the result of investigations carried out by me in the School of Chemistry, University of Hyderabad, Hyderabad, India, under the supervision of **Prof. P. S. Zacharias** and **Dr. Samar K. Das**. In keeping with the general practice of reporting scientific observations, due acknowledgements have been made wherever the work described is based on the findings of other investigators. Any omission, which might have occurred by oversight or error is regretted.

Maddela Prabhakar



**School of Chemistry
University of Hyderabad
Hyderabad-500046, India**

CERTIFICATE

Certified that the work contained in the thesis entitled **“Synthesis and Structural Characterization of Chiral Schiff Base Metal Complexes and Their Catalytic Activity”** has been carried out by Mr. Maddela Prabhakar under our supervision and the same has not been submitted elsewhere for a Ph. D. degree.

**Hyderabad
September 2006**

**Prof. P. S. Zacharias
(Supervisor)**

**Dean
School of Chemistry**

**Dr. Samar K. Das
(Co-supervisor)**

Dedicated to my parents
Kamamma, Ramulu
and
Sons of the Soil

ACKNOWLEDGEMENTS

I express my sincere gratitude to my research supervisors **Prof. P. S. Zacharias** and **Dr. Samar K. Das** for their invaluable guidance, inspiration and constant encouragement through out the course of this research work.

I am extremely thankful to Dean, School of Chemistry, former Deans and faculty members of the School of Chemistry for their kind help and encouragements at various stages of my research work.

I am highly grateful to Prof. M. Periasamy and Prof. D. Basavaiah for their helps and suggestions and permit me HPLC analysis in favour of catalytic studies with the help of their students during my research career.

I am thankful to financial assistance from DST and UGC/UPE, Govt. of India is gratefully acknowledged. The infrastructure support from UGC (UPE Program) and DST (National Single Crystal X-ray diffractometer facility) is also acknowledged.

I thank my seniors and labmates Prof. A. Ramachandraiah, Dr. Mohan Rao, Dr. N. Arulsamy, Dr. Ch. Ramakrishna Rao, Dr. Ameerunisha Begum, Dr. H. Aneetha, Dr. K. Srinivas Rao, Dr. Sunil Kumar, Dr. N. Mangayarkarasi, Dr. Tin Htwe, Dr. Vamsee Krishna, Dr. Pradeep for creating cheerful work atmosphere. I thank Dr. T. Jana and his group Arun, Arindam and Murali for creating a pleasant working atmosphere.

All the non-teaching staff of the School of Chemistry, CIL and Spinco-Biotech people has been extremely helpful, I thank them all. Especially I thank Raghavaiah, Asia Perwez, Suresh, Satyanarayana, Bhasker Rao, Prasad and Rangaiah for their helps throughout my research work. I thank Prashanth, Shaik Anwar, Chandra Shaker and Abhik Mukhopadhyay and all University of Hyderabad friends for their helps in various occasions.

I thank all my teachers who taught me at various levels of my academic career. Prof. T. P. Radhakrishnan and Prof. S. Pal are specially acknowledged. I would like to thank Polam Venkat Reddy.

I thank my friends of M.Sc., B.Sc., Intermediate, School and memorable childhood friends Dasari Sailu and Padmaiah. A special thank to Shaker and Ravi.

I am extremely grateful to my relatives and their families for their affection and encouragement in various occasions. They are always there for me whenever I am in need.

My stay in my Uncle's house is made pleasant by my Mama (B. Jeevaratnam), Aunty, Moses, Rani and Rupa. I heart fully acknowledge each and every one of them. They are always there for me whenever I am in need.

My entire life and academic career is only blessings of my God and Parents; without them I would not have reached this stage. The credit of all my achievements goes to them. Secondly, the credit of all my achievements goes to my Brothers, Sister, Brother-in-law, Sisters-in-law, Niece and Nephews; because of their affection and support. I heart fully acknowledge each and every one. They are always there for me whenever I am in need.

My acknowledgements would not be complete without mentioning the unique support of my wife in favour of my research work. I am grateful to my precious wife Grace Prabhakar for her marvelous grace, patience and constant encouragement. Finally, I thank to my beloved son (John Romel) and daughter (Crystal Percy).

Maddela Prabhakar

CONTENTS

STATEMENT	i
CERTIFICATE	ii
ACKNOWLEDGEMENTS	iii
<i>Chapter 1: Introduction</i>	1
<i>Chapter 2: Synthesis of some chiral Schiff base metal complexes and their catalytic epoxidation reactions using un-functionalized olefins</i>	27
2.1. Abstract	27
2.2. Introduction	28
2.3. Experimental	28
2.4. Results and discussion	36
2.5. Catalysis	54
2.6. Conclusion	61
2.7. References	62
<i>Chapter 3: Chiral Schiff base metal complexes derived from 4-methyl 2,6-di[(S)-(+)-1-phenylethyliminomethyl]phenol and relevant catalysis</i>	65
3.1. Abstract	65
3.2. Introduction	66
3.3. Experimental	67
3.4. Results and discussion	73
3.5. Catalysis	88
3.6. Conclusion	94
3.7. References	94

Chapter 4: Synthesis of some optically active binuclear metal complexes and their catalytic activities towards organic oxidation 97

4.1. Abstract	97
4.2. Introduction	98
4.3. Experimental	99
4.4. Results and discussion	104
4.5. Catalysis	113
4.6. Conclusion	118
4.7. References	118

Chapter 5: Synthesis and structural characterization of some chiral acyclic and macro cyclic binuclear metal complexes and epoxidation reactions 121

5.1. Abstract	121
5.2. Introduction	122
5.3. Experimental	123
5.4. Results and discussion	129
5.5. Catalysis	140
5.6. Conclusion	146
5.7. References	146
LIST OF PUBLICATIONS	149

Chapter 1

Introduction

1.1. Abstract

In this chapter, the importance of chiral Schiff base metal complexes and their catalytic activities has been briefly discussed. The aim of the present investigation, in the background of known chemistry of chiral Schiff base metal complexes and their catalytic activities has been stated.

1.2. Introduction

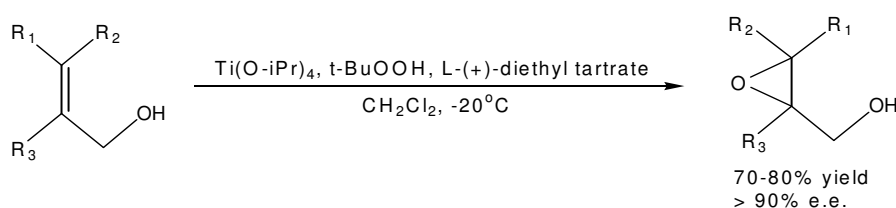
Discovery of new asymmetric catalysts involve interdisciplinary research that combines organic, inorganic, organometallic and biomimetic chemistry. To make efficient new chiral ligands, a number of strategies including combinatorial design of structurally innovative ligand framework are adopted. Consideration of steric, electronic and conformational properties is necessary to prepare effective ligands. The design of new metal catalysts bearing optically active ligands plays an important role in the development of asymmetric organic synthesis. Most asymmetric catalysts consist of metal complexes with chiral ligands. Several synthetic routes are available for the preparation of such ligands.

Successful examples of catalytic reactions include asymmetric epoxidation of allylic alcohols by titanium(IV) alkoxide in the presence of optically active tartrate,¹ *cis*-dihydroxylation of un-functionalized alkenes by OsO₄-chiral alkaloid system² and more recently the asymmetric epoxidation of un-functionalized alkenes catalysed by chiral manganese(III) Schiff base complexes.³ Among the various chiral compounds employed in asymmetric metal catalysis, those containing C₂ symmetric binaphthyl groups have been widely studied.⁴ The design of catalysts that ensures high enantioselectivity in the epoxidation of non-functionalized alkenes constitutes one of the most significant importance in the asymmetric synthesis.

1.3. Oxidation catalysts

1.3.1. Titanium-catalyst

Dialkyl tartrates have been successfully employed as chiral ligands in the titanium-based enantioselective epoxidation of allylic alcohols and the most efficient procedures involve *t*-butyl hydroperoxide (*t*-BuOOH) as the oxidant.⁵ The hydroxyl moiety of the substrate has an activating and stereo-directing role by binding the metal centre thereby providing high enantioselectivities in the epoxidation reaction. The catalyst is *in situ* prepared from titanium-*iso*-propoxide and the enantiomerically pure diethyl tartrate. Using 5-20 mol% of the titanium-*iso*-propoxide, high enantioselectivities (>90%) and yields (>80%) were obtained for a range of substituted allylic alcohols (Scheme 1.1).⁶



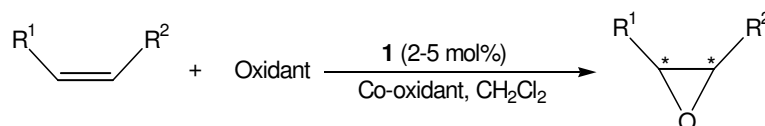
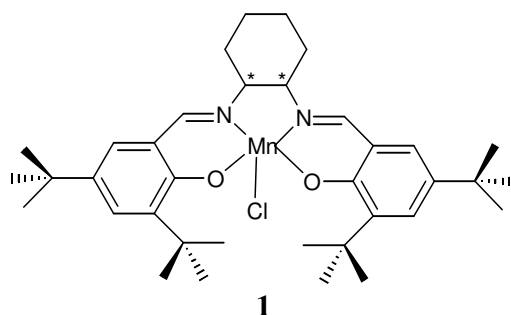
Scheme 1.1. Sharpless asymmetric epoxidation of allylic alcohols.

1.3.2. Manganese complexes

Kochi *et al.* reported that cationic manganese(III) complexes of the salen ligand [*N,N'*-ethylene bis(salicydeneaminato)] are effective catalysts for the epoxidation of various olefins with iodosylbenzene as the terminal oxidant. The presence of electron-withdrawing groups, such as 5,5'-dichloro or dinitro substituents enhances the catalytic activity of the (salen)Mn(III) catalyst in measure with the electron-deficient character of the cationic complex as evaluated by standard reduction potential E° . Various types of olefins, including substituted styrenes, stilbenes, cyclic and acyclic alkenes are epoxidized in 50–75% yields within 15 minutes at ambient temperatures in acetonitrile.⁷ The development of catalysts that mediate enantioselective group transfer to un-functionalized olefins is an important goal in organic chemistry.⁸ Catalytic systems that are effective for directed

epoxidation⁹ and hydrogenation¹⁰ have been discovered, but the substrates must bear specific functional groups to achieve the pre-coordination required for high enantioselectivity. Enantio-selective epoxidation of simple olefins constitutes a challenging and important synthetic problem and chiral-salen based complexes have recently emerged as promising catalysts for these reactions.¹¹

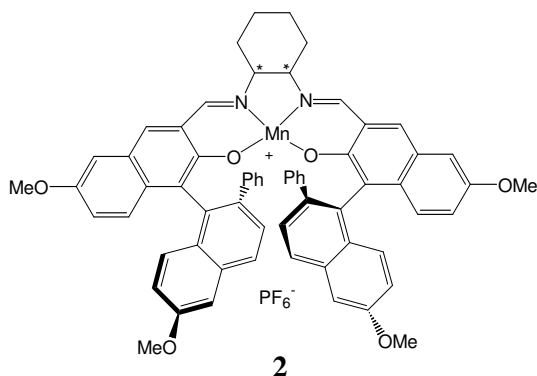
Jacobsen *et al.* designed the chiral Mn(III)-Schiff base complex (**1**) which is currently the most efficient catalyst for the enantioselective epoxidation of unfunctionalized olefins.¹² Enantioselective epoxidation of simple olefins using Jacobsen's catalyst gives yields up to 97% with an asymmetric induction as 98% enantiomeric excess depending on the substrate in an organic solvent such as dichloromethane. The source of oxygen used can be either an aqueous oxidant such as sodium hypochlorate or an organic peracid, for example *m*-chloroperbenzoic acid. In both the cases, the presence of an additive has a significant effect on the catalysis rate, yield and enantioselectivity of the epoxidation (Scheme 1.2).



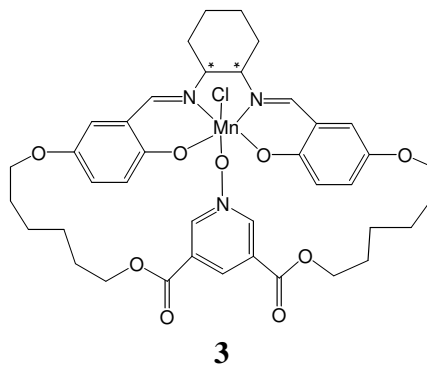
Scheme 1.2. Catalytic asymmetric epoxidation reaction of simple olefins.

Katsuki and his colleagues developed¹³ a new set of manganese complexes. The important thing in the ligand design was the introduction of two extra stereogenic groups in the place of the tertiary alkyl groups at the C-3 and C-3' positions of the aryl

groups. Using these interesting complexes (**2**) Katsuki studied the enantioselective epoxidation of un-functionalized olefins but observed lower asymmetric induction than Jacobsen. This group also first showed¹⁴ that a donor ligand such as N-methylmorpholine N-oxide improves the enantioselectivity of the system.

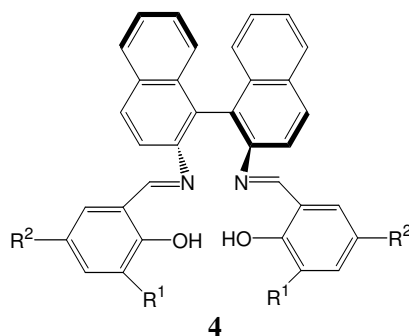


Jacobsen examined the importance of these 'additives' with the Mn(salen) complex (**3**) in which the additive is present as part of the ligand structure.¹⁵ The enantioselective epoxidation of olefins catalyzed by salen-Mn(III) complexes can be effected under anhydrous conditions with a variety of primary oxidant systems. The combination of m-chloroperbenzoic acid (m-CPBA) and N-methylmorpholine N-oxide (NMO) is particularly effective, allowing for epoxidation reactions to be carried out at -78°C . Under these low temperature conditions, a variety of un-functionalized olefins undergo epoxidation with a significant increase in enantioselectivity relative to reaction using aqueous bleach.¹⁶



New class of tetradentate chiral picolinamide-salicylidene ligands and their corresponding manganese complexes as catalysts for epoxidation of olefins have been synthesized. The manganese complexes catalyzed asymmetric epoxidation of olefins by sodium hypochlorite with up to 74% enantiomeric excess for *trans*- β -methyl styrene.¹⁷ Chiral pentadentate dihydrosalen ligand, carrying an imidazole group as the fifth donor, was synthesized in enantiomerically enriched form. The corresponding manganese(III) complex catalyzed the epoxidation of olefins with dilute hydrogen peroxide. With 1,2-dihydronaphthalene as substrate and 10% of catalyst, enantiomeric excess up to 64% was achieved.¹⁸

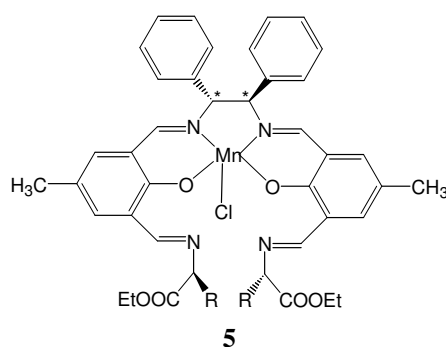
The binaphthyl Schiff bases (**4**) are capable of activating Cu(II) and Mn(III) towards catalytic oxygen-atom transfer to alkenes. Enantioselective formation of organic epoxides from the PhIO oxidation of alkenes catalyzed by the Mn(III)+**4** system has been demonstrated. The chiral inducing ability of the dinitro-substituted auxiliary ligands could be enhanced by attaching small alkyl groups at the C-3 and C-3' positions. Addition of donor ligands such as substituted imidazole or pyridine N-oxide did not result in enantiomeric excess (ee) enhancement.¹⁹



The manganese(III) derivatives mediate the catalytic asymmetric epoxidation of alkenes by iodosylbenzene (PhIO) and the highest enantiomeric excess in this system so far has been achieved at -20 °C in low-polarity toluene²⁰ in contrast to the planar structures observed for Jacobsen-type catalysts.²¹

Natural L-amino acids would be ideal chiral sources, as they are inexpensive and readily available. The asymmetric epoxidation catalyzed by chiral salen-Mn

complexes is one of the most intensively studied with the results showing that the size and configuration of the C-3 and C-3' groups on the salen structure play very important roles on directivity or chiral induction.²² Therefore this is a suitable system for evaluating amino acid Schiff-base groups, which are incorporated at the C-3 and C-3' positions of the Katsuki salen-Mn catalysts.²³ The mononuclear new chiral Mn(III)-Schiff base complexes with L-amino acid ethyl esters were found to be highly effective catalysts (**5**) for the enantioselective epoxidation of conjugated olefins while the corresponding binuclear Mn(III) complexes showed lower enantioselectivity.²⁴



The development of direct and selective epoxidation of olefins catalyzed by transition metal complexes with molecular oxygen and a suitable reductant that can accept one oxygen atom from molecular oxygen to perform the reaction is of current interest.²⁵ Mukaiyama and coworkers reported manganese(III) complexes of optically active N,N'-ethylene bis(α -alkoxycarbonyl- β -ketoimine) as a catalyst for the asymmetric aerobic epoxidation of simple olefins, such as 1,2-dihydronaphthalene derivatives, to afford the corresponding optically active epoxides with good to high enantioselectivities.²⁶

Kureshy *et al.* reported²⁷ on enantioselective epoxidation of non-functionalized olefins by chiral Ru(II), Ru(III), Co(II), Ni(II) and Mn(III) Schiff base complexes and in pursuit of better selectivity through electronic tuning in the catalysts of dissymmetric Mn(III) chiral Schiff base complexes derived from 1*R*,2*R*(-)-1,2-diaminocyclohexane with 3-acetyl 4-hydroxy 6-methyl 2-pyrone, 2-hydroxy

benzaldehyde and substituted (5-chloro-, 5-methoxy-, 5-nitro, 3-tertiary butyl- and 3,5-ditertiary butyl) 2-hydroxy benzaldehydes. These complexes were used for aerobic enantioselective epoxidation of 1-hexene, 1-octene and 1,2-dihydronaphthalene using molecular oxygen in presence of 2-methylpropanal as sacrificial reductant. Good to excellent conversions and epoxide selectivity for all the substrates were obtained with all the catalysts while enantiomeric excess was relatively better in the case of 1,2-dihydronaphthalene.²⁸

1.3.3. DNA binding/cleaving of [salen-Mn(III)]⁺

The salen-Mn(III) mediates the cleavage of right-handed double-helical DNA in the presence of terminal oxidant.²⁹ Combination of salen-Mn(III) and oxidant produces single-strand cleavage as well as double-strand cleavage which derives from independent, proximal nicks on opposite DNA strands. Cleavage is effected selectively from the DNA minor groove in segments rich in A:T base pairs and is consistent with a mechanism involving deoxyribose C–H activation by an oxidatively activated intermediate such as [salen-Mn(V)O]⁺.³⁰

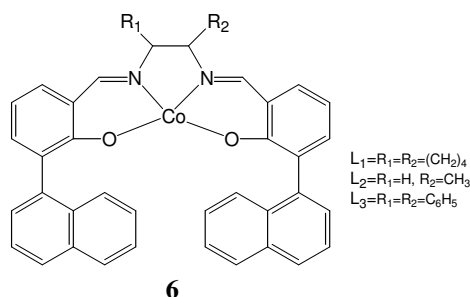
Recently J. H. Griffin *et al.* reported twenty-six derivatives of [salen Mn(III)]⁺ bearing halogen, nitro, amino, ether and alkyl or aryl substituents on the aromatic ring and/or at the imine positions or containing 1,3-propane-, 1,2-phenylene- and 1,2-cyclohexane- or 1,2-diphenylethylenediamine in place of ethylenediamine as the bridging moiety. The DNA binding/cleaving properties of these complexes in presence of terminal oxidants have been examined using DNA affinity cleaving techniques. Active derivatives produced DNA cleavage from the minor groove at sites containing multiple contiguous A:T base pairs. For aryl-substituted derivatives, DNA cleavage efficiency was found to vary with both the identity and position of attachment of substituents.

The precise patterns of cleavage at A:T target sites varied with the position of attachment of substituents, but not with the identity of the substituents. These results suggest that substituents alter specificity through both steric and electronic effects. DNA cleavage efficiency for the complex derived from (*R,R*)-cyclohexyldiamine was

5 times greater than that of the (*S,S*)-enantiomer. Cleavage patterns produced by the enantiomeric complexes at A:T rich target sites were different, demonstrating enantiospecific recognition and cleavage of right-handed double helical DNA.³¹

1.3.4. Cobalt complexes

A class of chiral salen-Co(II) complexes derived from α -naphthyl salicylaldehyde with 1*S*,2*S*(+)-diaminocyclohexane, 1*R*,2*R*(-)-diaminodiphenylethane and *S*(+)-1,2-diaminopropane have been reported. Epoxidation reactions of unfunctionalized prochiral olefins viz. styrene, *trans*-3-octene and *trans*-4-nonene was achieved by the combined use of an atmospheric pressure of molecular oxygen and sacrificial reductant *iso*-butaraldehyde catalyzed by these chiral Co(II) complexes (**6**) with and without pyridine N-oxide as co-oxidant.³²



1.3.6. Nickel complexes

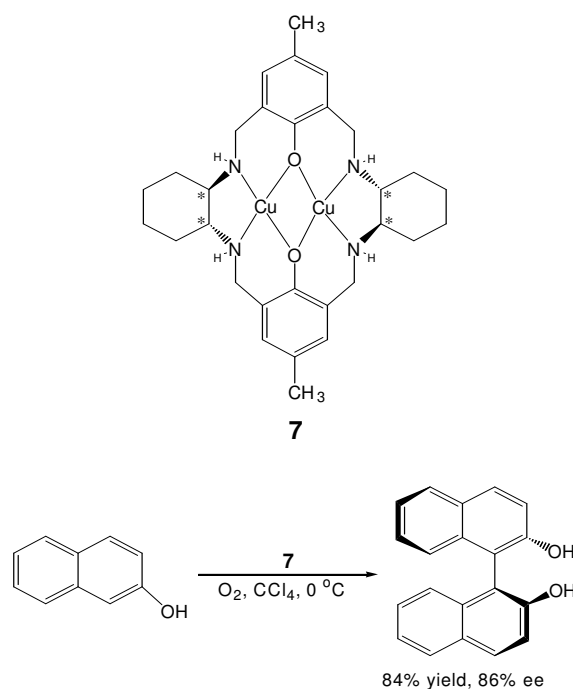
Only a few investigations have focused on nickel catalysis for alkene epoxidation. Soluble nickel(II) salts are unlike their iron(II), manganese(II), cobalt(II) and copper(II) counterparts; completely ineffective in the catalytic epoxidation of alkenes with iodosylbenzene (PhIO) as terminal oxidant.³⁵ However, complexation of nickel(II) to tetraaza macrocycles as well as to other ligands affords systems that can act as catalysts for alkene epoxidation.³⁶ The nickel(II) system was found to be a better catalyst than the nickel(III) system. The nickel(II) complexes can achieve catalytic epoxidation of a variety of alkenes with iodosylbenzene as terminal oxidant, but the reaction is non-stereospecific as epoxidation of *cis*- β -methylstyrene afforded a 2:1 mixture of the *cis*- and *trans*-epoxides.³⁶ Iodosylbenzene and nickel(II) complex probably form an oxonickel(IV) intermediate that transfers oxygen to alkene in a similar way as the other oxo-transition metal complex systems.

Transition metal-catalyzed transfer of oxygen atoms to organic substrates is of interest in the study of bioinorganic mechanisms and the development of efficient catalysts for laboratory and industrial organic synthesis.³⁷ Certain nickel(II) catalysts have recently joined the group of metallo-porphyrin complexes capable of facilitating this reaction using OCI^- and PhIO or KHSO_5 as terminal oxidant.³⁸ The high-valent nickel-oxo species may be responsible for substrate oxidation.³⁹ Burrows and his coworkers have reported⁴⁰ an unusual pH dependence of the OCI^- based reactions with dramatic rate acceleration in olefin epoxidation at reduced pH.

1.3.7. Oxidative coupling catalysts

Binaphthol enantiomers and their derivatives are important chiral ligands for a wide range of asymmetric synthesis.⁴¹ The facile conversion of binaphthol to 2,2'-(diphenylphosphanyl)-1,1'-binaphthyl (BINAP) is particularly noteworthy because BINAP greatly expanded the synthetic utilities of binaphthol in asymmetric catalysis.⁴² Existing catalysts for the asymmetric preparation of chiral binaphthols include copper complexes of chiral amines or their derivatives⁴³ and V(IV)=O complexes with either one or two stereogenic metal centers.⁴⁴ In the above reports, the

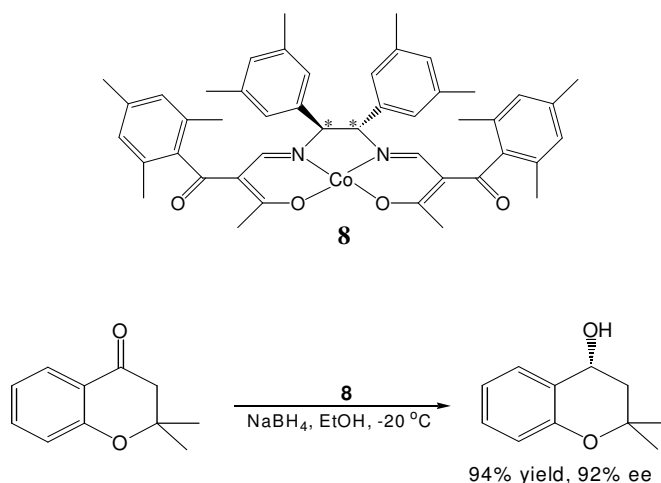
catalytic metal complexes were prepared *in situ* by reacting a chiral ligand with a desired metal ion (Cu(I), Cu(II) or V(IV)=O). Recently Jian Gao *et al.* reported⁴⁵ the synthesis and crystal structures of a family of dicopper catalysts (**7**) for the asymmetric oxidative coupling of 2-naphthol (Scheme 1.3).



Scheme 1.3. Catalytic asymmetric oxidative coupling of β -naphthol.

1.4. Reduction catalysts

The first example of enantioselective hydrogenation was reported in 1939 using PtO₂ and cinchonine as a chiral modifier.⁴⁶ 8% enantiomeric excess was measured for the reduction of β -methylcinnamic acid. With a silk fibroin support, up to 66% enantiomeric excess was reached.⁴⁷ In the late 1960s, Knowles⁴⁸ and Kagan⁴⁹ independently developed Rh(I) complexes of chiral chelating phosphines leading to 90% enantiomeric excess. With Noyori's BINAP ligand, almost 100% enantiomeric excess was achieved.⁵⁰ Mukaiyama *et al.* reported⁵¹ reduction of ketones with NaBH₄ and catalytic amount of optically active cobalt(II) complexes (**8**) having β -oxoaldimine ligands (Scheme 1.4).

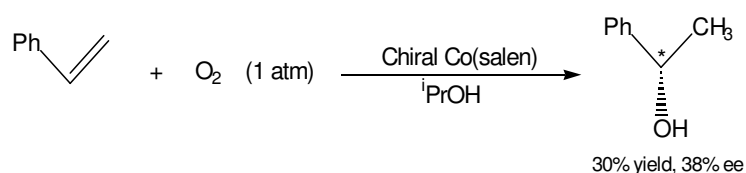


Scheme 1.4. Catalytic enantioselective hydrogenation reaction.

1.5. Hydroxylation catalysts

1.5.1. Iron complexes

Variety of iron porphyrin complexes are capable of catalyzing oxidation reactions employing H_2O_2 as oxidant.⁵² Que *et al.* studied extensively the non-hemo iron epoxidation catalyst based on the tripodal tetradentate ligand tris(2-pyridylmethyl)amine (tpa).⁵³ This study was extended by replacing the tripodal tetradentate ligand with a tetradentate N,N'-bis(2-pyridylmethyl)-N,N'-dimethyl-1,2-ethylenediamine (bpmen) ligand containing an ethylenediamine backbone. Subsequently ethylene backbone was replaced by a chiral *trans*-1,2-diaminocyclohexane. The use of the corresponding chiral iron complex as catalyst provided 2,3-octane-diol in 38% yield and 82% enantiomeric excess starting from *trans*-octene.



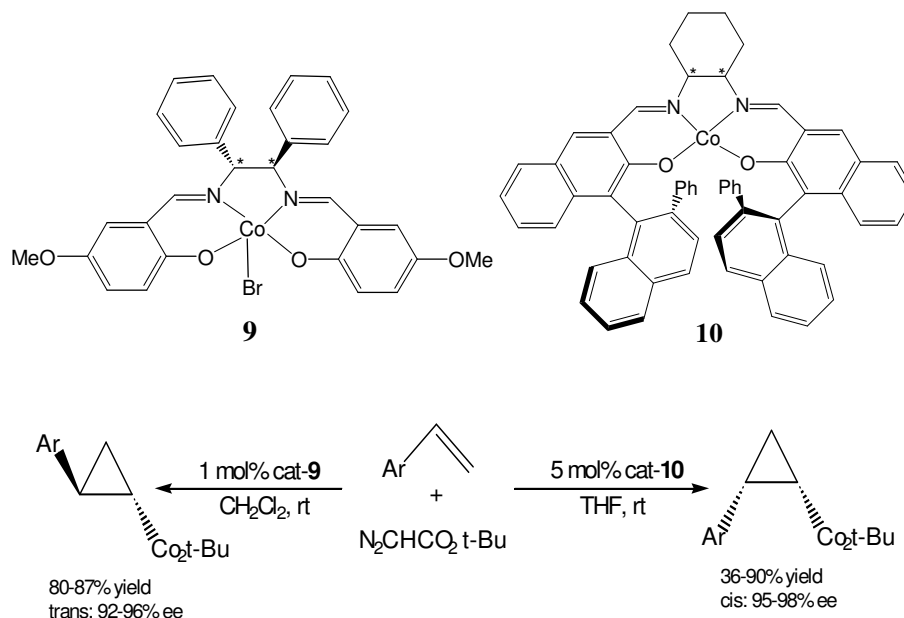
Scheme 1.5. Catalytic asymmetric hydroxylation reaction of styrene.

Nishinaga *et al.* described⁵⁴ the hydroxylation of styrene using the optically active Co(salen) complex to produce 1-phenylethanol in modest yield with 38% enantiomeric excess as shown in Scheme 1.5. Katsuki showed⁵⁵ that the chiral substituents at the C-3 and C-3' positions of the aryl groups of the Mn(salen) complex such as **2** enabled asymmetric benzylic hydroxylation (64% ee) carried out using iodosylbenzene as oxidant in solvents of high polarity (e.g. chlorobenzene).

1.6. Corbylation catalysts

1.6.1. Cobalt complexes

The cyclopropanation of olefins with diazoesters involving carbene transfer from metal to olefins is similar to the epoxidation reactions. Katsuki demonstrated high yields and *trans*-enantioselectivity with cobalt complexes (**9**) that have no substituents at the C-3 and C-3' positions of the salen ligand.⁵⁶ Katsuki has also developed high *cis*-enantioselectivity with Co(II)-salen complex (**10**)⁵⁷ as shown in Scheme 1.6. The product yields are higher and catalyst shows exceptional enantioselectivity (>90% ee). The process to *trans*-cyclopropane products seems especially practical due to accessibility of the salen ligand.



Scheme 1.6. Katsuki enantio-selective cyclopropanation reactions.

1.6.2. Nickel complexes

Nickel Schiff bases play an important role as polymerization catalysts and are able to stabilize a reactive cationic nickel complex. In order to stabilize cationic intermediate nickel complexes, the Schiff bases are prepared using hindered aromatic amines (eg. 2,6-diisopropylaniline) with diketones. Although Ni(salen) complexes have not found many applications in catalysis, their planar coordination geometry constitutes an interesting platform to coordinate other metals. The Schiff bases are able to act as a metallo-crown and interesting structures containing different metals can result. Ni(salen) bearing another metal can behave as a bifunctional catalyst.⁵⁸

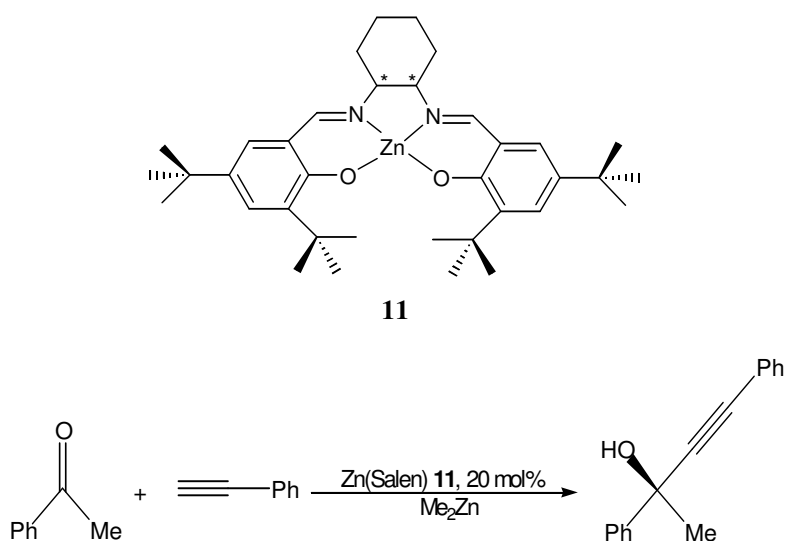
1.6.3. Copper complexes

Copper Schiff bases have found more extensive use, since copper(I) can be stabilized by Schiff bases and are used in nitrene transfer. Schiff bases derived from two types of diamine have also been described.⁵⁹ The preparation of the complexes generally uses copper(I), but copper(II) sources have also been considered. Similar results obtained in nitrene transfer are probably due to the fact that a reduction of copper(II) to copper(I) takes place, determined by the nitrene source. Due to the particular geometry and properties of the Schiff base, Cu(salen) is able to coordinate ions, *via* the interaction with the oxygen of the Schiff base.⁶⁰ The complexes are prepared by the reaction of salen with copper acetate in ethanol. The Cu(salen) is stable when exposed to air and moisture and it is possible to perform enantioselective alkylation in phase transfer conditions.

1.6.4. Zinc complexes

There are many reports on the synthesis of Zinc(II)-salen complexes from either Zn(OAc)₂ or ZnCl₂/Et₂N. However, these routes create some difficulties in isolating pure metalated product. In some cases a mixture of the complex and the free salen is isolated. A more direct route is the treatment of Schiff bases with the reactive alkyl derivatives ZnMe₂ or ZnEt₂. This strategy has an advantage compared to the use of Zn salts, since both alkyls are commercially available in toluene solution or hexane solution. Isolation of Zn(salen) and its characterization by X-ray analysis, are

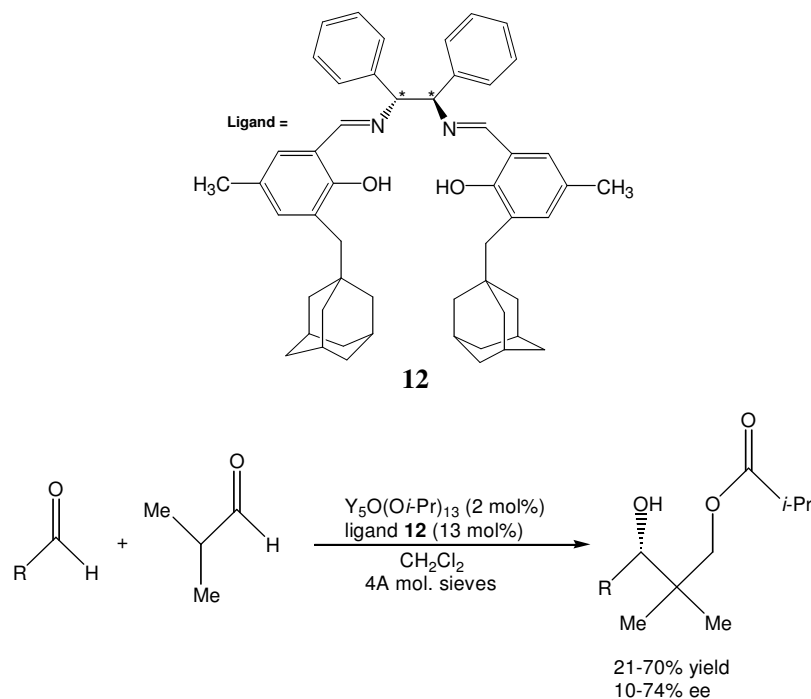
facilitated by the use of pyridine. On the other hand, without pyridine the complex can be isolated in polymeric form, where the oxygen of the Schiff base coordinates the zinc of another molecule of salen. Another possible zinc derivative for the synthesis of Zn Schiff bases is $\text{Zn}[\text{N}(\text{SiMe}_3)_2]_2$. Use of this reagent is particularly suited for bidentate Schiff bases because it is possible to avoid the formation of fully coordinated Zn-Schiff base complexes.



Scheme 1.7. Catalytic alkynyl addition reaction of ketone.

The intermediate $\text{Zn}(\text{Schiff base})$ -hexamethylsilamide can be used as a starting material for the preparation of three mixed coordinated unsaturated (salicylaldiminato)- $\text{Zn}(\text{OR})$ complexes (where $\text{R}=\text{Me}$, Ph or COMe) which are useful for catalytic applications. As in the case of $\text{Al}(\text{salen})$, chiral $\text{Zn}(\text{salen})$ shows interesting photophysical properties and the luminescence of the complex is well recognized during its preparation.⁶¹ Due to their stability in aqueous systems Schiff bases can be suitable for carrying active metals and investigating photophysical properties in biological systems. One of the reasons why it is difficult to crystallize anhydrous $\text{Zn}(\text{II})$ salen complexes can be ascribed to the ability of salen oxygen to coordinate metal and salts, even after chelation. This property can be used advantageously to develop new catalytic reactions. $\text{Zn}(\text{salen})$ (**11**) can catalyze the

addition of ZnEt_2 to aldehydes. Cozzi *et al.* reported⁶² the use of salen in this reaction and Kozlowski has modified the structure of salen, using the same concepts and enhancing the reactivity of the system.⁶³



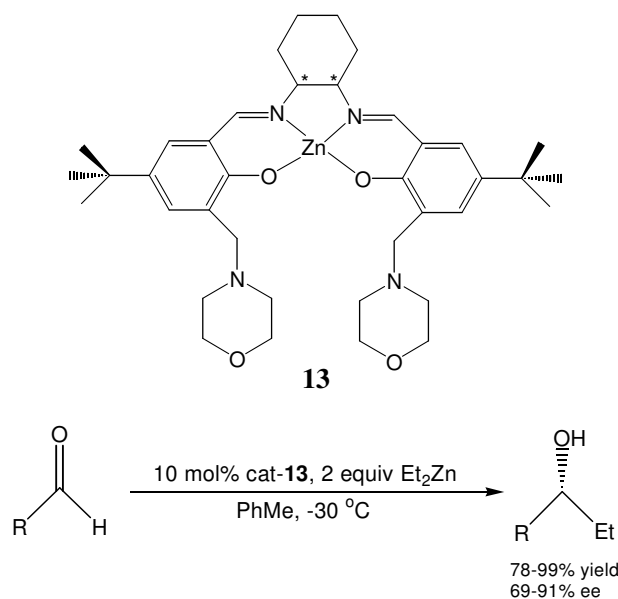
Scheme 1.8. Y(III)-catalysed aldol-Tischenko reaction.

Salen can act as a bifunctional catalyst mimicking the common aminoalcohols widely used in Zn-mediated additions of Et_2Zn to aldehydes. $\text{Zn}(\text{salen})$ has the ability to promote the addition of other organometallic reagents as well. Alkynylation has attracted considerable interest in recent years as propargylic alcohols are valuable synthetic precursors. The undeveloped addition of alkynyl zinc reagents to ketones can be realized using $\text{Zn}(\text{salen})$ as a catalyst leading to new perspectives in the formation of quaternary stereocenters (Scheme 1.7).⁶⁴

1.6.5. Carbonyl addition reactions

Recently several other salen-catalyzed asymmetric transformations involving C–C bond formation have been studied. Chiral Y(III) complex (**12**) was used to catalyze the first enantioselective catalytic aldol-Tischenko reaction (Scheme 1.8).⁶⁵

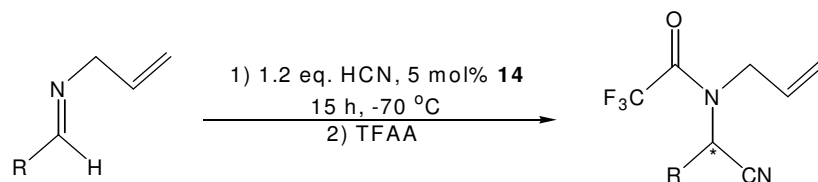
In this case the ligand structure was systematically varied to optimize for enantioselectivity. Chiral Zn(salen) was also found to catalyze asymmetric addition of diethyl zinc to aldehydes shown in Scheme 1.9.⁶⁶ This catalyst (**13**) provides for electrophile activation by the metal centre and nucleophile activation by the secondary basic groups.



Scheme 1.9. Asymmetric addition of Et_2Zn to aldehydes by chiral zinc catalyst.

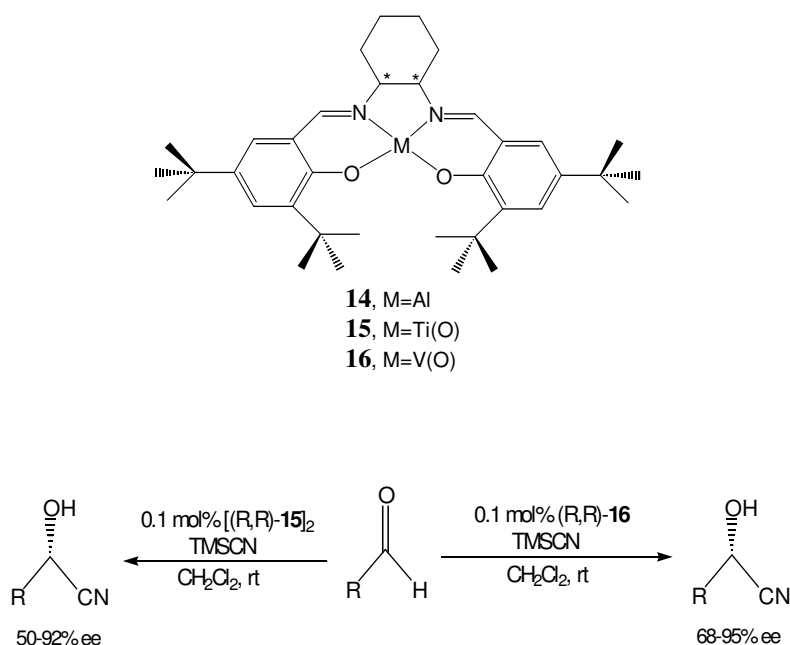
1.6.6. Hydrocyanation reactions

Jacobsen recently described the first example of a metal-catalyzed enantioselective Strecker reaction which occurred using a chiral Al(III) complex (**14**) (Scheme 1.10).⁶⁷ The addition of HCN to *N*-allylbenzalimine afforded the expected product in 91% yield and 95% enantiomeric excess.



Scheme 1.10. Chiral(salen)Al-catalyzed Strecker reaction of an imine.

Various *N*-allyl imines were evaluated in this reaction to give the corresponding products in good yields and moderate to excellent enantioselectivities. They simultaneously used and described parallel approaches for the discovery and optimization of ligands in terms of chiral Schiff base catalysts useful for the asymmetric Strecker reactions.⁶⁸ Salen metal complexes are found to be active for the addition of cyanide to the carbonyl compounds. The Ti(IV)oxo-dimer (**15**) and the V(IV)oxo (**16**) complexes were found to be good catalysts for the hydrocyanation reactions (Scheme 1.11) in terms of reactivity or selectivity for all the substrates investigated.⁶⁹

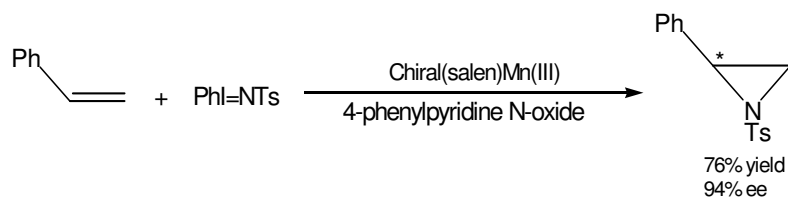


Scheme 1.11. Asymmetric hydrocyanation of carbonyls.

1.7. Aziridine synthesis

Aziridines are useful building blocks in the organic synthesis and their chiral derivatives have served as ligands in asymmetric catalysis.⁷⁰ Aziridines can be obtained in chiral form by starting from the chiral pool (by cyclization of amino acids, for example⁷¹) or by asymmetric metal catalysis. There are two main catalytic ways to synthesize such compounds, the asymmetric metal-catalyzed nitrene transfer to olefins or the transfer of carbenes to imines. Copper-chiral bis(oxazoline) systems

allowed both reactions but with low yields and enantiomeric excess (<12%).⁷² Dissymmetric chiral diamine ligands having a 1,1'-binaphthyl or 1,1'-biphenyl moiety have been determined with copper for the aziridination of styrene derivatives. But enantiomeric excess values do not surpass 22%.⁷³



Scheme 1.12. Catalytic asymmetric aziridination of styrene.

Katsuki *et al.* discovered with chiral (salen) manganese(III) complexes results are up to 94% enantiomeric excess and yield reached to 74% for the aziridination of styrene derivatives (Scheme 1.12).⁷⁴ Additives play an important role in the reaction for activation of the catalyst (for example, trifluoroacetic anhydride and toluenesulfonic anhydride). Most of the time, the use of pyridine *N*-oxide is crucial to reach high enantioselectivity.⁷⁵

1.8. Aim of the present investigation

In the previous sections we have discussed the different types of chiral Schiff base metal complexes and their catalytic activity. The design and synthesis of new metal catalysts bearing optically active auxiliary ligands is important in the development of asymmetric organic synthesis. Most asymmetric catalysts consist of metal complexes with chiral ligands.

Kochi *et al.* reported that the cationic manganese(III) complexes of the salen ligand [*N,N'*-ethylene bis(salicydeneaminato)] are effective catalysts for the epoxidation of various olefins with iodosylbenzene as the terminal oxidant.

Jacobsen *et al.* designed the chiral Mn(III)-Schiff base complex which is currently the most efficient catalyst for the enantio-selective epoxidation of unfunctionalized olefins.¹²

Katsuki and his colleagues developed¹³ set of manganese complexes. The important thing in the ligand design was the introduction of two extra stereogenic axes in place of the tertiary alkyl groups at the C-3 and C-3' positions of the aryl groups. Using these complexes such as **2**, Katsuki studied the enantioselective epoxidation of un-functionalized olefins. This group also first showed¹⁴ that a donor ligand such as N-methylmorpholine N-oxide improves the enantioselectivity of the system.

Discovery of new asymmetric catalysts involve interdisciplinary research that combines organic, inorganic, organometallic and biomimetic chemistry. To make efficient new chiral ligands, a number of strategies including combinatorial design of structurally innovative ligand framework are adopted. Consideration of steric, electronic and conformational properties is necessary to prepare effective ligands.

The aim of present work is synthesis and structural characterization of new chiral Schiff base ligands, their metal complexes and investigation of their catalytic activity.

1.9. References

1. (a) T. Katsuki and K. B. Sharpless, *J. Am. Chem. Soc.*, **1980**, 102, 5974; (b) M. G. Finn and K. B. Sharpless, *Asymmetric Synthesis*, J. D. Morrison, Ed., Academic Press, New York, **1985**, vol. 5, p. 247.
2. H. C. Kolb, M. S. Van Nieuwenhze and K. B. Sharpless, *Chem. Rev.*, **1995**, 94, 2483.
3. (a) E. N. Jacobsen, *Catalytic Asymmetric Synthesis*, I. Ojima, Ed., VCH, New York, **1993**, p. 159; (b) J. F. Larrow and E. N. Jacobsen, *Organomet. Chem.*, **2004**, 6, 123; (c) T. Katsuki, *Coord. Chem. Rev.*, **1995**, 140, 189.
4. C. Rosini, L. Franzini, A. Raffaelli and P. Salvadori, *Synthesis*, **1992**, 502.
5. T. Katsuki and K. B. Sharpless, *J. Am. Chem. Soc.*, **1980**, 102, 5974.
6. (a) K. B. Sharpless and T. R. Verhoeven, *Aldrichimica Acta.*, **1979**, 12, 63; (b) A. Phenninger, *Synthesis*, **1986**, 89; (c) R. M. Hanson and K. B. Sharpless,

- J. Org. Chem.*, **1986**, 51, 1922; (d) S. S. Wood, M. G. Finn and K. B. Sharpless, *J. Am. Chem. Soc.*, **1991**, 113, 106; (e) M. G. Finn and K. B. Sharpless, *J. Am. Chem. Soc.*, **1991**, 113, 113; (f) R. A. Johnson and K. B. Sharpless, In *Catalytic Asymmetric Epoxidation of Unfunctionalized Olefins in Catalytic Asymmetric Synthesis*, I. Ojima, Ed., VCH, New York, **1993**, 103.
7. K. Srinivasan, P. Michaud and J. K. Kochi, *J. Am. Chem. Soc.*, **1986**, 108, 2309.
8. (a) J. T. Groves and R. S. Myers, *J. Am. Chem. Soc.*, **1990**, 112, 2801; (b) K. Tani, M. Hanafusa and S. Otsuka, *Tetrahedron Lett.*, **1979**, 3017; (c) R. Curci, M. Fiorentino and M. Serio, *J. Chem. Soc. Chem. Commun.*, **1984**, 155; (d) R. Sinigalia, R. A. Michelin, F. Pinna and G. Strukul, *Organometallics*, **1987**, 6, 728; (e) Y. Naruta, F. Tani and K. Maruyama, *Chem. Lett.*, **1989**, 1269; (f) S. O' Malley and T. Kodadek, *J. Am. Chem. Soc.*, **1989**, 111, 9116; (g) T. Hayashi, Y. Matsumoto and Y. Ito, *J. Am. Chem. Soc.*, **1989**, 111, 3426; (h) E. N. Jacobsen, I. E. Marko, W. S. Mungall, G.W. Schroder and K. B. Sharpless, *J. Am. Chem. Soc.*, **1988**, 110, 1968; (i) J. S. M. Wai, I.E. Marko, J. S. Svendsen, M. G. Finn, E. N. Jacobsen and K. B. Sharpless, *J. Am. Chem. Soc.*, **1989**, 111, 1123; (j) R. L. Halterman, K. P. C. Vollhardt, M. E. Welker, D. Blaser and R. Boese, *J. Am. Chem. Soc.*, **1987**, 109, 8105.
9. (a) T. Katsuki and K. B. Sharpless, *J. Am. Chem. Soc.*, **1980**, 102, 5974; (b) Y. Gao, R. M. Hanson, J. M. Klunder, S. Y. Ko, H. Masamune and K. B. Sharpless, *J. Am. Chem. Soc.*, **1987**, 109, 5765.
10. (a) H. Takaya, T. Ohta, N. Sayo, H. Kumobayashi, S. Akutagawa, S. Inoue, I. Kasahara and R. J. Noyori, *J. Am. Chem. Soc.*, **1987**, 109, 1596; (b) T. Hayashi, N. Kawamura and Y. Ito, *J. Am. Chem. Soc.*, **1987**, 109, 7876; (c) K. E. Koenig, In *Asymmetric Synthesis*, J. D. Morrison, Ed., Academic, New York, **1985**, vol. 5, p. 71.
11. (a) W. Zhang, J. L. Loebach, S. R. Wilson and E. N. Jacobsen, *J. Am. Chem. Soc.*, **1990**, 112, 2801; (b) W. Zhang and E. N. Jacobsen, *J. Org. Chem.*, **1991**,

- 56, 2296; (c) R. Irie, K. Noda, Y. Ito and T. Katsuki, *Tetrahedron Lett.*, **1991**, 32, 1055.
12. (a) E. N. Jacobsen, In *Comprehensive Organometallic Chemistry II*, Eds. E. W. Abel, F. G. A. Stone and E. Pergamon, New York, **1995**, vol. 12, p. 1097.
13. (a) T. Katsuki, *J. Mol. Catal. A: Chemical*, **1996**, 113, 87; (b) T. Katsuki, *Chem. Soc. Rev.*, **2004**, 33, 437; (c) L. Canali and D. C. Sherrington, *Chem. Soc. Rev.*, **1999**, 28, 85.
14. R. Irie, K. Noda, Y. Ito, N. Matsumoto and T. Katsuki, *Tetrahedron Asymm.*, **1991**, 2, 481.
15. N. S. Finney, P. J. Pospisil, S. Chang, M. Palucki, R. G. Konsler, K. B. Hansen and E. N. Jacobsen, *Angew. Chem. Int. Ed.*, **1997**, 36, 1720.
16. M. Palucki, G. J. Mc Cormick and E. N. Jacobsen, *Tetrahedron Lett.*, **1995**, 36, 5457.
17. S.-H. Zhao, P. R. Ortiz, B. A. Keys and K. G. Davenport, *Tetrahedron Lett.*, **1996**, 37, 2725.
18. S.-H. Zhao, P. R. Ortiz, B. A. Keys and K. G. Davenport, *Tetrahedron Lett.*, **1993**, 34, 4785.
19. C.-W. Ho, W.-C. Cheng, M.-C. Cheng, S.-M. Peng, K.-F. Cheng and C.-M. Che, *Dalton trans*, **1996**, 405.
20. M.-C. Cheng, M. C.-W. Chan, S.-M. Peng, K.-K. Cheung and C.-M. Che, *Dalton trans*, **1997**, 3479.
21. (a) W. Zhang, J. L. Loebach, S. R. Wilson and E. N. Jacobsen, *J. Am. Chem. Soc.*, **1990**, 112, 2801; (b) P. J. Pospisil, D. H. Carsten and E. N. Jacobsen, *Chem. Eur. J.*, **1996**, 2, 974.
22. (a) W. Zhang and E. N. Jacobsen, *J. Org. Chem.*, **1991**, 56, 2296; (b) W. Zhang, J. L. Loebach and E. N. Jacobsen, *J. Am. Chem. Soc.*, **1990**, 112, 2801; (c) A. Hatayama, N. Hosoya, R. Irie, Y. Ito and T. Katsuki, *Synlett.*, **1992**, 407; (d) H. Sasaki, R. Irie and T. Katsuki, *Synlett.*, **1993**, 300; (e) H. Sasaki, R.

- Irie and T. Katsuki, *Synlett.*, **1994**, 356; (f) N. Hosoya, A. Hatayama, R. Irie, H. Sasaki and T. Katsuki, *Tetrahedron*, **1994**, 50, 4311.
23. (a) Y. N. Ito and T. Katsuki, *Bull. Chem. Soc. Jpn.* **1999**, 72, 603; (b) B. S. Lane, M. Vogt, V. J. DeRose and K. Burgess, *Synlett.*, **1994**, 255; (c) P. Pietikainen, *Tetrahedron Lett.*, **1994**, 35, 941.
24. X.-W. Liu, N. Tang, Y.-H. Chang and M.-Y. Tan, *Tetrahedron Asymm.*, **2004**, 15, 1269.
25. (a) K. Imigawa, T. Nagata, T. Yamada and T. Mukaiyama, *Chem. Lett.*, **1994**, 527; (b) T. Mukaiyama, T. Takai, T. Yamada and O. Rhode, *Chem. Lett.*, **1990**, 1661; (c) T. Yamada, T. Takai, O. Rhode and T. Mukaiyama, *Bull. Chem. Soc. Jpn.* **1991**, 64, 2109.
26. T. Mukaiyama, T. Yamada, T. Nagata and K. Imagawa, *Chem. Lett.*, **1993**, 327.
27. (a) R. I. Kureshy, N. H. Khan, S. H. R. Abdi and K. N. Bhatt, *Tetrahedron Asymm.*, **1993**, 4, 1693; (b) R. I. Kureshy, N. H. Khan and S. H. R. Abdi, *J. Mol. Catal.*, **1995**, 96, 117; (c) R. I. Kureshy, N. H. Khan, S. H. R. Abdi and A. K. Bhatt, *J. Mol. Catal.*, **1996**, 110, 33; (d) R. I. Kureshy, N. H. Khan, S. H. R. Abdi, P. Iyer and A. K. Bhatt, *J. Mol. Catal.*, **1997**, 120, 101; (e) R. I. Kureshy, N. H. Khan, S. H. R. Abdi, P. Iyer and A. K. Bhatt, *J. Mol. Catal.*, **1998**, 130, 41.
28. R. I. Kureshy, N. H. Khan, S. H. R. Abdi, P. Iyer and S. T. Patel, *Polyhedron*, **1999**, 18, 1773.
29. D. J. Gravert and J. H. Griffin, *J. Org. Chem.*, **1993**, 58, 820.
30. K. Srinivasan, P. Michaud and J. K. Kochi, *J. Am. Chem. Soc.*, **1986**, 108, 2309.
31. D. J. Gravert and J. H. Griffin, *Inorg. Chem.*, **1996**, 35, 4837.
32. R. I. Kureshy, N. H. Khan, S. H. R. Abdi, A. K. Bhatt and P. Iyer, *J. Mol. Catal.*, **1997**, 121, 25.

33. (a) B. Meunier, *Bull. Soc. Chim. Fr.* **1986**, 578; (b) B. Meunier, *Bull. Soc. Chim. Fr.* **1983**, 345.
34. T. Yamamoto and M. Kimura, *J. Chem. Soc. Chem. Commun.*, **1977**, 948.
35. R. B. VanAtta, C. C. Franklin and J. S. Valentine, *Inorg. Chem.*, **1984**, 23, 4121.
36. (a) A. Fusi, R. Ugo and G. M. Zanderighi, *J. Catal.*, **1974**, 34, 175; (b) J. D. Koola and J. K. Kochi, *Inorg. Chem.*, **1987**, 27, 908.
37. (a) R. A. Sheldon and J. K. Kochi, *Metal-Catalyzed Oxidations of Organic Compounds*; Academic: New York, **1981**; (b) K. A. Jorgensen, *Chem. Rev.*, **1989**, 89, 431.
38. (a) J. F. Kinneary, T. R. Wagler and C. J. Burrows, *Tetrahedron Lett.*, **1988**, 29, 877; (b) J. F. Kinneary, J. S. Albert and C. J. Burrows, *J. Am. Chem. Soc.*, **1988**, 110, 6124; (c) H. Yoon and C. J. Burrows, *J. Am. Chem. Soc.*, **1988**, 110, 4087; (d) T. R. Wagler and C. J. Burrows, *Tetrahedron*, **1988**, 29, 5091; (e) T. R. Wagler, Y. Fang and C. J. Burrows, *J. Org. Chem.*, **1989**, 54, 1584; (f) J. D. Koola and J. K. Kochi, *Inorg. Chem.*, **1987**, 27, 908.
39. (a) C. J. Burrows, In *Inclusion Phenomena and Molecular Recognition*; J. L. Atwood, Ed. Plenum: New York, **1989**; (b) M. V. George and K. S. Balachandran, *Chem. Rev.*, **1975**, 75, 491; (c) L. M. Moroney, R. S. C. Smart and M. W. Roberts, *J. Chem. Soc., Faraday Trans I*, **1983**, 1769.
40. H. Yoon, T. R. Wagler, K. J. O'Connor and C. J. Burrows, *J. Am. Chem. Soc.*, **1990**, 112, 4568.
41. (a) M. Shibasaki and N. Yoshikawa, *Chem. Rev.*, **2002**, 102, 2187; (b) M. Shibasaki, H. Sasai and T. Arai, *Angew. Chem. Int. Ed.*, **1997**, 36, 1236; (c) R. Noyori, *Asymmetric Catalysis in Organic Synthesis*, Wiley, New York, **1994**; (d) K. Ishihara, H. Nakamura and H. Yamamoto, *J. Am. Chem. Soc.*, **1999**, 121, 7720; (e) *Comprehensive Asymmetric Catalysis* (Eds.: E. N. Jacobsen, A. Pfaltz and H. Yamamoto), Springer, Berlin, **1999**.

42. (a) A. Miyashita, H. Yasuda, H. Takaya, K. Toriumi, T. Ito, T. Souchi and R. Noyori, *J. Am. Chem. Soc.*, **1980**, 102, 7932; (b) R. Noyori, *Chem. Rev.*, **1989**, 89, 187; (c) R. Noyori and H. Takaya, *Acc. Chem. Res.*, **1990**, 23, 345; (d) R. Noyori, *Angew. Chem. Int. Ed.*, **2002**, 41, 2008.
43. (a) J. Brusse and A. C. A. Jansen, *Tetrahedron Lett.*, **1983**, 24, 3261; (b) M. Hovorka and J. Zavada, *Tetrahedron*, **1992**, 48, 9517; (c) M. Smrcina, M. Lorenc, V. Hanus, P. Sedmera and P. Kocovsky, *J. Org. Chem.*, **1992**, 57, 1993; (d) M. Smrcina, J. Polakowa, S. Vyskocil and P. Kocovsky, *J. Org. Chem.*, **1993**, 58, 4534; (e) M. Smrcina, S. Vyskocil, B. Maca, M. Polasek, T. A. Claxton, A. P. Abbott and P. Kocovsky, *J. Org. Chem.*, **1994**, 59, 2156; (f) M. Nakajima, L. Miyoshi, K. Kanayanma, S. L. Hashimoto, M. Noji and K. Koga, *J. Org. Chem.*, **1999**, 64, 2264; (g) X. Li, J. Yand and M. C. Kozlowski, *Org. Lett.*, **2001**, 3, 1137.
44. (a) C.-T. Chen, S.-W. Hon and S.-S. Weng, *Synlett.*, **1999**, 816; (b) S.-W. Hon, C.-H. Li, J.-H. Kuo, N. B. Barhate, Y.-H. Liu, Y. Wang and C.-T. Chang, *Org. Lett.*, **2001**, 3, 869; (c) N. B. Barhate and C.-T. Chang, *Org. Lett.*, **2002**, 4, 2529; (d) Z. Luo, Q. Liu, L. Gong, X. Cui, A. Mi and M. Jiang, *Chem. Commun.*, **2002**, 914; (e) Z. Luo, Q. Liu, L. Gong, X. Cui, A. Mi and M. Jiang, *Angew. Chem. Int. Ed.*, **2002**, 41, 4532.
45. (a) Jian Gao, J. H. Reibenspies and A. E. Martell, *Angew. Chem. Int. Ed.*, **2003**, 42, 6008.
46. (a) D. Lipkin and T. D. Stewart, *J. Am. Chem. Soc.*, **1939**, 61, 3295; (b) H. U. Blaser and M. Muller, *Heterogeneous Catalysis and Fine Chemicals II*; Elsevier: Amsterdam, **1991**.
47. S. Akabori, S. Sakurai, Y. Izumi and Y. Fujii, *Nature*, **1956**, 323.
48. B. D. Vineyard, W. S. Knowles, M. J. Sabacky, G. L. Bachman and D. J. Weinkauff, *J. Am. Chem. Soc.*, **1977**, 99, 5946.
49. H. B. Kagan, N. Langloirs and T.-P. Dag, *J. Organomet. Chem.*, **1975**, 96, 353.

50. A. Miyashita, A. Yasuda, H. Takaya, K. Totiumi, T. Ito, T. Souchi and R. Noyori, *J. Am. Chem. Soc.*, **1980**, 102, 7932.
51. (a) T. Nagata, K. Yoroze, T. Yamada and T. Mukaiyama, *Angew. Chem. Int. Ed.*, **1995**, 34, 2145; (b) T. Nagata, K. Sugi, T. Yamada and T. Mukaiyama, *Synlett.*, **1996**, 1076; (c) F. Fache, E. Schulz, M. L. Tommasino and M. Lemaire, *Chem. Rev.*, **2000**, 100, 2159.
52. (a) D. Mansuy and P. Battioni, In *Bioinorganic Catalysis*, J. Reedijk, E. Bouwman, Eds; Marcel Dekker, Inc: New York, USA., **1999**; pp 323; (b) K. K. Andeson, W. A. Froland, S. -K. Lee and J. D. Lipscomb, *New. J. Chem.*, **1991**, 15, 411; (c) B. Meunier, *Chem. Rev.*, **1992**, 92, 1411; (d) T. G. Traylor, S. Tsuchiya, Y. -S. Byun and C. Kim, *J. Am. Chem. Soc.*, **1993**, 115, 2775.
53. C. Kim, K. Chen, J. Kim and Jr. L. Que, *J. Am. Chem. Soc.*, **1997**, 119, 5964.
54. A. Nishinaga, H. Yamato, T. Abe, K. Maruyama and T. Matsuura, *Tetrahedron Lett.*, **1988**, 29, 6309.
55. K. Hamachi, R. Irie and T. Katsuki, *Tetrahedron Lett.*, **1996**, 37, 4979.
56. (a) T. Fukuda and T. Katsuki, *Synlett.*, **1995**, 3, 825; (b) T. Fukuda and T. Katsuki, *Tetrahedron*, **1997**, 53, 7201.
57. (a). T. Niimi, T. Uchida, R. Irie and T. Katsuki, *Tetrahedron Lett.*, **2000**, 41, 3647; (b) T. Niimi, T. Uchida, R. Irie and T. Katsuki, *Adv Synth Catal*, **2001**, 343, 79; (c) T. Uchida, B. Saha and T. Katsuki, *Tetrahedron Lett.*, **2001**, 42, 2521.
58. E. F. DiMauro and M. C. Kozlowski, *Organometallics*, **2002**, 21, 1454.
59. P. Muller and C. Fruit, *Chem. Rev.*, **2003**, 103, 2905.
60. Y. N. Belokon, M. North, T. D. Churkina, N. S. Ikonnikov and V. I. Maleev, *Tetrahedron*, **2001**, 57, 2491.
61. P. G. Cozzi, L. S. Dolci, A. Garelli, M. Montalti, L. Prodi and N. Zaccheroni, *New. J. Chem.*, **2003**, 692.
62. P. G. Cozzi, A. Papa and A. Umani-Ronchi, *Tetrahedron Lett.*, **1996**, 37, 4613.

63. E. F. DiMauro and M. C. Kozlowski, *Org. Lett.*, **2001**, 3, 3053.
64. (a) P. G. Cozzi, *Angew. Chem. Int. Ed.*, **2003**, 42, 2895; (b) P. G. Cozzi, *Chem. Soc. Rev.*, **2004**, 33, 410 and refs. therein.
65. (a) C. M. Mascarenhas S. P. Miller, P. S. White and J. P. Morken, *Angew. Chem. Int. Ed.*, **2001**, 40, 601; (b) M. –H. Lin and T. V. Rajanbabu, *Org. Lett.*, **2002**, 4, 1607.
66. (a) E. F. DiMauro and M. C. Kozlowski, *Org. Lett.*, **2001**, 3, 3053; (b) P. G. Cozzi, A. Papa and A. Umani-Ronchi, *Tetrahedron Lett.*, **1996**, 37, 4613.
67. M. S. Sigman and E. N. Jacobsen, *J. Am. Chem. Soc.*, **1998**, 120, 5315.
68. M. S. Sigman and E. N. Jacobsen, *J. Am. Chem. Soc.*, **1998**, 120, 4901.
69. Y. N. Belokon, M. North and T. Parsons, *Org. Lett.*, **2000**, 2, 1617.
70. D. Tanner, *Angew. Chem. Int. Ed.*, **1994**, 33, 599.
71. J. W. Kelly, N. L. Eskew and Jr. S. A. Evans, *J. Org. Chem.*, **1986**, 51, 95.
72. (a) K. B. Hansen, N. S. Finney and E. N. Jacobsen, *Angew. Chem. Int. Ed.*, **1995**, 34, 676; (b) A. M. Harm, J. G. Knight and G. Stemp, *Tetrahedron Lett.*, **1996**, 37, 6189.
73. M. Shi, N. Itoh and Y. Masaki, *J. Chem. Research (S)*, **1996**, 37, 9245.
74. H. Nishikori and T. Katsuki, *Tetrahedron Lett.*, **1996**, 37, 352.
75. S. Manikata, T. Ando, M. Nishimura, I. Kyu and M. Komatsu, *Angew. Chem. Int. Ed.*, **1998**, 37, 3392.
-

Chapter 2

Synthesis of some chiral Schiff base metal complexes and their catalytic epoxidation reactions using un-functionalized olefins

2.1. Abstract

A new class of chiral Schiff base metal complexes, **1–7** derived from 4-bromo-2-formyl-6-(4-methylpiperazin-1-ylmethyl)phenol and (R,R)-*trans*-1,2-diaminocyclohexane has been synthesized. Characterization of the ligand **L**¹ and its metal complexes **1–7** (M = Ni⁺², **1**; Mn⁺³, **2**; Cu⁺², **3**; Co⁺², **4**; Fe⁺², **5**; Zn⁺², **6**; Ni⁺², **7**) were carried out by microanalysis, ¹H-NMR, IR, UV/Vis, CD spectral studies. Structures of the nickel complexes **1** and **7** were determined by single crystal X-ray crystallographic methods. Crystal data for nickel complex **1**: Monoclinic space group *P*2₁, *a* = 21.8997(10) Å, *b* = 8.8129(4) Å, *c* = 22.7230(10) Å, *V* = 4195.0(3) Å³, *Z* = 4. Crystal data for nickel complex **7**: Monoclinic space group *P*2₁/*c*, *a* = 9.0262(6) Å, *b* = 13.2339(8) Å, *c* = 38.974(3) Å, *V* = 4638.2(5) Å³, *Z* = 4. Ligand **L**¹ and its metal complexes **1–7** exhibit circular dichroism signals at room temperature.

To examine the nature of the chiral complexes in the catalytic process, the catalytic activities of the chiral Schiff base complexes towards the epoxidation reactions of the styrene, *cis*-stilbene and *trans*-stilbene were investigated. The epoxidation products were confirmed by ¹H-NMR and quantification of the styrene products were carried out by gas chromatography (GC). The quantification of the *cis*-stilbene and *trans*-stilbene epoxide products was determined by HPLC analysis. Manganese catalyst **2** gives up to 97% yield at room temperature on styrene epoxidation. Epoxidation of *cis*-stilbene catalyzed by **2**, yields up to 40% at room temperature with 74% of enantiomeric excess.

2.2. Introduction

Oxidation of olefins to optically pure epoxides, catalyzed by chiral transition-metal complexes, is one of the important challenges in modern synthetic chemistry.¹ Optically pure epoxides find wide range of applications in pharmaceuticals, agrochemicals, flavors and fragrances.² There is growing awareness about the utility of the desired epoxide and the necessity of disposal of unwanted one, whose negative side effects can far outweigh the beneficial value of the right enantiomer. Catalytic methods represent an efficient route for the synthesis of chiral products using a chiral catalyst.³ Sharpless epoxidation of allylic alcohols was the first example in this field⁴ and this method led to the preparation of a variety of different allylic epoxides of which many have been used for the synthesis of valuable target molecules⁵ with high selectivity. Amongst various catalysts developed so far for enantioselective epoxidation, chiral metalloporphyrins,⁶⁻⁸ hemoenzymes such as cytochrome-c peroxidase,^{6,9} and macrocyclic ligands are of special interest.¹⁰

Recently, Jacobsen and Katsuki have reported an efficient catalytic system¹¹ for several kinds of olefins with moderate to high enantioselectivity depending on the substitution degree of double bond using iodosylbenzene, NaOCl, and H₂O₂ as terminal oxidants. Several other types of metal catalysts for the asymmetric epoxidation of olefins have also been reported. These include: nickel complexes bearing cyclic or acyclic tetraaza multidantate ligands.¹²

The aim of present work is to synthesize new chiral Schiff base ligand **L**¹ and its metal complexes **1–7** analogous to salen-complexes and to examine the catalytic efficiency of the chiral Schiff base metal complexes. Accordingly we have synthesized chiral Schiff base metal complexes **1–7** and made efforts to use them in catalytic epoxidation reactions of styrene, *cis*-stilbene and *trans*-stilbene.

2.3. Experimental

2.3.1. Chemicals and reagents

All chemicals and the solvents used in this work were of analytical grade and were used as obtained. The chemicals and the sources are as follows: 5-

bromosalicylaldehyde and N-methylpiperazine were purchased from Lancaster (England). The 4-bromo-2-formyl-6-(4-methylpiperazin-1-ylmethyl) phenol was prepared according to the literature procedure.¹³ Paraformaldehyde and CDCl₃ were obtained from Acros (India). (R,R)-*trans*-1,2-diaminocyclohexane was separated from the mixture of *cis*- and *trans*-1,2-cyclohexanediamine, according to the literature procedure.¹⁴ All metal salts were purchased commercially and used as received. Iodobenzenediacetate, styrene, *cis*-stilbene and *trans*-stilbene were purchased from Aldrich chemicals. Iodosylbenzene was prepared according to literature procedure.²³ HPLC grade solvents were used for catalysis and spectral analysis.

2.3.2. Physical measurements

¹H-NMR spectra in CDCl₃ solution were recorded on a Bruker DRX-400 spectrometer using Si(CH₃)₄ as an internal standard. Elemental analyses were carried out on a Perkin-Elmer Model 240C CHN analyzer. Infrared spectra were collected by using KBr pellets on a Jasco-5300 FT-IR spectrophotometer. The UV-visible spectra were recorded with a Shimadzu model UV-3101PC spectrophotometer. The CD spectra were measured with a JASCO J-810 spectropolarimeter. Optical rotation was measured with an AUTOPOL-IV automatic polarimeter (readability ±0.01°).

Gas chromatographic analyses were carried out on a Shimadzu GC 14B instrument equipped with a stainless steel packed column (5 m, 5 % SE 30) and a chiral capillary column (Supelco α -DEX 325, 30m length, 0.25mm id, 0.25 μ m film thickness) and a flame ionization detector (FID). HPLC analyses of *cis*-stilbene epoxide and *trans*-stilbene epoxide products were carried out on a Shimadzu SCL-10A instrument equipped with CHIRALCEL OD-H using Class-VP program.

X-ray crystallography

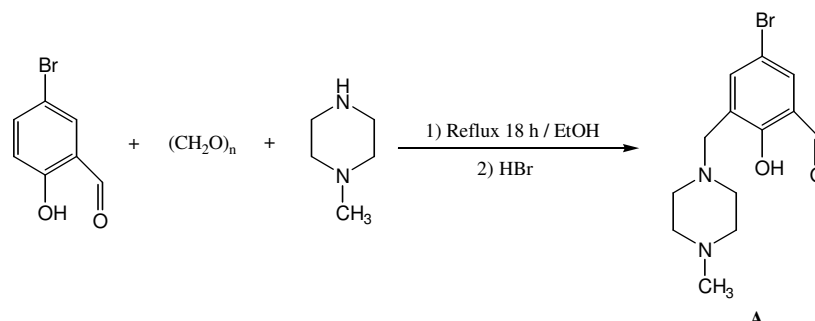
X- ray data were collected for orange red crystals of **1** and **7** on a Bruker-Nonius SMART APEX CCD single crystal diffractometer using graphite monochromated Mo-K α radiation (0.71073Å). The SMART software was used for intensity data acquisition and the SAINT-Plus software¹⁵ was used for data extraction.

In each case, absorption correction was performed with help of SADABS program.¹⁶ The SHELXTL package¹⁷ was used for structure solution and least-squares refinement on F^2 . All the non-hydrogen atoms were refined anisotropically. The ORTEP3¹⁸ and the PLATON¹⁹ softwares were used for molecular graphics.

2.3.3. Synthesis

2.3.3.1. 4-bromo-2-formyl-6-(4-methylpiperazin-1-ylmethyl)phenol, A

(a) The hydrobromide salt: N-methylpiperazine (4.5 g, 45 mmol), paraformaldehyde (2.2 g, 73 mmol) and 5-bromosalicylaldehyde (11.0 g, 55 mmol), were refluxed in ethanol (150 mL) for 18 hours. The initial deep orange solution slowly became paler over this period. The yellow solution was cooled to room temperature and aqueous hydrobromic acid (48%, 15 mL) was added with stirring. The hydrobromide salt precipitated as a pale yellow powder. Recrystallisation from ethanol gave yellow needles of **A**·2HBr (Yield: 13.3 g, 62%). IR Spectra $\nu(\text{C}=\text{O})$ 1650 cm^{-1} .



Scheme 2.1. Schematic representation of the Mannich reaction.

(b) The neutral species (**A**): The salt of **A**·2HBr (8.0 g, 16.4 mmol) was taken in water (200 mL) and neutralized with excess of potassium carbonate (5.0 g, 36 mmol). The intense yellow, cloudy solution was extracted with CH_2Cl_2 ($4 \times 50\text{ mL}$). The extracts were combined and the solvent was removed under reduced pressure with out drying. The resulting sticky yellow oil was taken up in diethyl ether (200 mL), dried over MgSO_4 and filtered. The solvent was removed to give a pale yellow solid.

Recrystallisation from diethyl ether gave yellow crystals of 4-bromo-2-formyl-6-(4-methylpiperazin-1-ylmethyl)phenol **A** (Yield: 4.26 g, 80%). The reaction sequence is shown in Scheme 2.1.

M. W.: 312 g mol⁻¹; M. P: 83-84 °C; IR Spectra: $\nu(\text{C=O})$ 1680 cm⁻¹; ¹H NMR (CDCl₃, δ , ppm): 10.27(s, 1H, H-C=O), 7.77 (d, 1H, Ar-H), 7.39 (d, 1H, Ar-H), 3.73 (s, 2H, CH₂), 2.65 (br s, 4H, CH₂), 2.53 (br s, 4H, CH₂), 2.31 (s, 3H, CH₃).

2.3.3.2. Resolution of cis/trans-1, 2-diaminocyclohexane

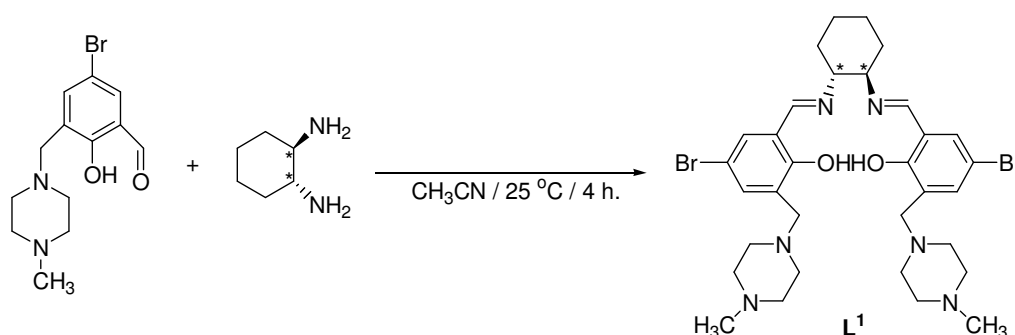
To a 500 mL beaker with a magnetic stirrer was added L-(+)-tartaric acid (75 g, 0.50 mol) and distilled water (200 mL). The mixture was stirred at room temperature until complete dissolution occurred, at which point a mixture of cis- and trans-1,2-diaminocyclohexane (120 mL, 97 mol) was added at a rate such that the reaction temperature just reached 70 °C. To the resulting solution was added glacial acetic acid (50 mL, 0.88 mol) at a rate such that the reaction temperature just reached 90 °C. A white precipitate was formed immediately upon addition of the acid. The slurry was vigorously stirred as it was cooled to room temperature over 2 h.

The mixture was then cooled to ≤ 5 °C in an ice bath for 2 h and the precipitate was collected by vacuum filtration. The wet cake was washed with 5 °C water (50 mL) and then rinsed with methanol (5 x 50 mL). The solid was dried by drawing air through the cake for 1 h. The product was then dried at 40 °C under reduced pressure to yield (R,R)-1,2-diaminocyclohexane mono-(+)-tartarate salt as a white solid (Yield: 80 g, 99%). To the dry compound in a separating funnel, saturated KOH (73 mL) solution was added. The upper layer was separated. The compound was distilled under vacuum at 165–170 °C. The enantiomeric excess of (R,R)-*trans*-1,2-diaminocyclohexane is ≥ 99 %.

2.3.3.3. Synthesis of new chiral Schiff base ligand, L¹

To a solution of 4-bromo-2-formyl-6-(4-methylpiperazin-1-ylmethyl)phenol (0.312 g, 1 mmol), in acetonitrile (25 mL) was added (R,R)-*trans*-1,2-diaminocyclohexane (0.057 g, 0.5 mmol). The reaction mixture was stirred for 4

hours at room temperature. The resulting yellow solution was filtered and the solvent was removed by rotary evaporator. The residue was precipitated by diethyl ether and the precipitate was washed with hexane. Recrystallization from dichloromethane-hexane yielded the desired chiral ligand **L**¹ as a yellow crystalline solid (Yield: 73%). The reaction sequence is shown in Scheme 2.2.



Scheme 2.2. Schematic representation of the chiral Schiff base ligand **L**¹.

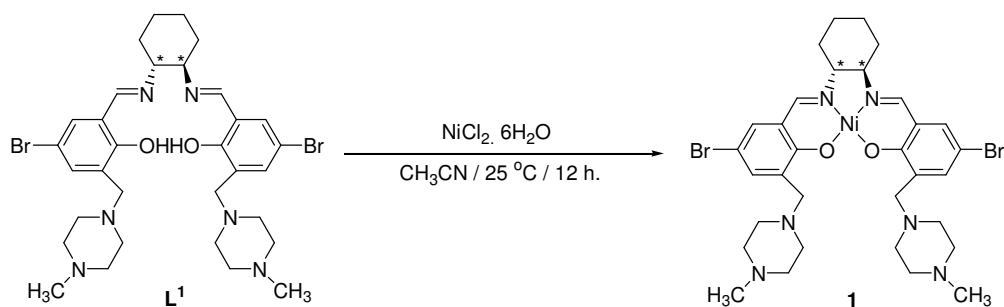
Characterization data for chiral ligand, **L**¹

Optical rotation $[\alpha]_D^{25}$: -225.6 (c 1, ethanol); M. F.: $C_{32}H_{44}N_6O_2Br_2$; M. W.: 704.54 g mol⁻¹; IR (ν cm⁻¹, KBr pellet): 3323, 1633, 1581; ¹H NMR ($CDCl_3$, δ , ppm): 13.5 (br, 2H, C-OH), 8.20 (s, 2H, HC=N), 3.74 (s, 4H, CH₂), 7.26 (d, 4H, Ar-H), 3.56 (q, 2H, CH), 2.54 (br, 8H, CH₂), 2.33 (s, 16H, CH₂), 1.91 (t, 6H, CH₃); CD λ_{max} (mdeg) (CH₃OH): 339 (-4.38), 266 (-6.58), 236 (11.63), 219 (-3.29); UV-Vis (CH₃OH) [λ_{max}/nm (ϵ/dm^3 mol⁻¹ cm⁻¹): 408 (1474), 333 (8880), 253 (20578), 222 (55150); CHN Analysis: Calcd: C, 54.55; H, 6.29; N, 11.93%; Found: C, 53.96; H, 6.04; N, 11.69%.

2.3.3.4. Synthesis of nickel complex, **1**

To a solution of ligand **L**¹ (0.352 g, 0.5 mmol), in acetonitrile (25 mL) was added $NiCl_2 \cdot 6H_2O$ (0.119 g, 0.5 mmol) and stirred for 12 hours at room temperature. The resulting reaction mixture was then filtered and the filtrate was kept at room temperature to allow the solvent evaporate slowly. Orange red crystals suitable for X-

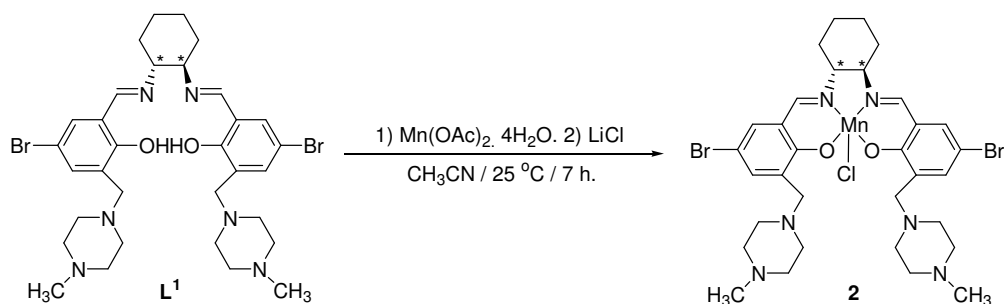
ray single crystal analysis were obtained after ten days (Yield: 67%). The reaction sequence is shown in Scheme 2.3.



Scheme 2.3. Schematic representation of the chiral nickel complex **1**.

2.3.3.5. Synthesis of manganese complex, **2**

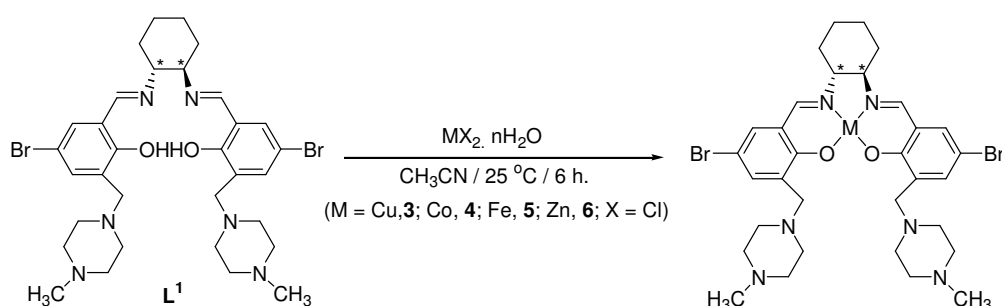
To a solution of ligand **L**¹ (0.704 g, 1 mmol), in acetonitrile (25 mL) was added $\text{Mn}(\text{OAc})_2 \cdot 4\text{H}_2\text{O}$ (0.245 g, 1 mmol). The reaction mixture was stirred for 4 hours at room temperature. To the complex in solution, LiCl (0.086 g, 2 mmol) was added and stirred for another 3 hours at the same temperature. The solvent was removed by rotary evaporator and the residue was washed with hexane and recrystallised from dichloromethane-hexane solutions to obtain a pure sample of chiral manganese complex, **2** as brown solid (Yield: 85%). The reaction sequence is shown in Scheme 2.4.



Scheme 2.4. Schematic representation of the chiral manganese complex **2**.

2.3.3.6. General synthetic procedure for complexes, 3–6

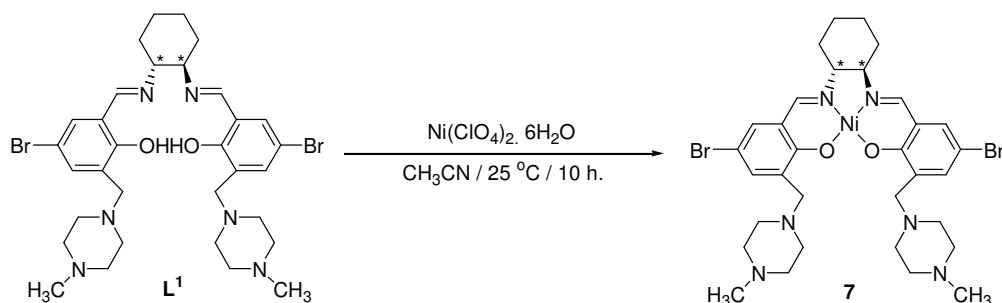
To a solution of ligand **L**¹ (0.704 g, 1 mmol), in acetonitrile (25 mL) was added $\text{MX}_2 \cdot n\text{H}_2\text{O}$ ($\text{M} = \text{Cu}$, **3**; Co , **4**; Fe , **5**; Zn , **6**; $\text{X} = \text{Cl}$; $n = 0-6$) (1 mmol). The reaction mixture was stirred for 6 hours at room temperature and the solvent removed by rotary evaporator. The resulting chiral metal complex solids were washed with hexane and recrystallised from dichloromethane-hexane to provide good yields of these metal complexes. The reaction sequence is shown in Scheme 2.5.



Scheme 2.5. Schematic representation of the chiral Schiff base metal complexes.

2.3.3.7. Synthesis of nickel complex, 7

To a solution of ligand **L**¹ (0.352 g, 0.5 mmol), in acetonitrile (25 mL) was added $\text{Ni}(\text{ClO}_4)_2 \cdot 6\text{H}_2\text{O}$ (0.183 g, 0.5 mmol) and stirred for 10 hours at room temperature. The reaction mixture was filtered and the filtrate was kept for crystallization at room temperature. After a week, orange red crystals suitable for X-ray single crystal determination were obtained (Yield: 70%). The reaction sequence is shown in Scheme 2.6.



Scheme 2.6. Schematic representation of the chiral nickel complex **7**.

2.3.3.8. Characterization data for complexes, 1–7

Characterization data for nickel complex, 1

M. F.: $C_{32}H_{44}N_6O_2 Br_2Cl_2Ni \cdot 7H_2O$; M. W.: $960.24 \text{ g mol}^{-1}$; IR ($\nu \text{ cm}^{-1}$, KBr pellet): 3390, 3034, 2941, 1618, 1539, 1433, 1332; 1H NMR ($CDCl_3$, δ , ppm): 1.25 (s, 6H, CH_3), 1.64 (br, H_2O), 2.16 (d, 16H, $J = 7 \text{ Hz}$, CH_2), 2.4 (s, 4H, CH_2), 2.80 (s, 4H, CH_2), 3.06 (s, 4H, CH_2), 3.71 (s, 2H, CH), 7.21 - 7.26 (m, 4H, Ar-CH), 7.38 (s, 2H, HC=N); CD λ_{max} (mdeg) (CH_3OH): 410 (-1.63), 340 (-1.1), 249 (-8.96); UV-Vis (CH_3OH) [λ_{max}/nm ($\epsilon/dm^3 \text{ mol}^{-1} \text{ cm}^{-1}$)]: 414 (4533), 336 (5406), 249 (43746); CHN Analysis: Calcd.: C, 40.03; H, 6.09; N, 8.75%; Found: C, 40.10; H, 6.13; N 8.69%.

Characterization data for manganese complex, 2

M. F.: $C_{32}H_{42}N_6O_2 Br_2ClMn \cdot 3H_2O$; M. W.: $846.96 \text{ g mol}^{-1}$; IR ($\nu \text{ cm}^{-1}$, KBr pellet): 3400, 1633, 1543; CD λ_{max} (mdeg) (CH_3OH): 409 (-0.26), 310 (-4.032), 245 (-5.66); UV-Vis (CH_3OH) [λ_{max}/nm ($\epsilon/dm^3 \text{ mol}^{-1} \text{ cm}^{-1}$)]: 412 (52211), 350 (64550), 285 (146462), 241(360153); CHN Analysis: Calcd.: C, 45.38; H, 5.71; N, 9.92%; Found: C, 45.63; H, 5.34; N, 9.59%.

Characterization data for copper complex, 3

Yield: 80%; Colour: Brown; M. F.: $C_{32}H_{44}N_6O_2 Br_2Cl_2Cu \cdot 6H_2O$; M. W.: $947.08 \text{ g mol}^{-1}$; IR ($\nu \text{ cm}^{-1}$, KBr pellet): 3400, 1622, 1535; CD λ_{max} (mdeg) (CH_3OH): 393 (-4.45), 250 (-10.58); UV-Vis (CH_3OH) [λ_{max}/nm ($\epsilon/dm^3 \text{ mol}^{-1} \text{ cm}^{-1}$)]: 581(628), 373 (8753), 269 (20990), 230 (42812); CHN Analysis: Calcd.: C, 40.58; H, 5.96; N, 8.87%; Found: C, 39.41; H, 5.62; N, 9.03%.

Characterization data for cobalt complex, 4

Yield: 85%; Colour: Crystalline black; M. F.: $C_{32}H_{44}N_6O_2 Br_2Cl_2Co \cdot 3H_2O$; M. W.: $888.42 \text{ g mol}^{-1}$; IR ($\nu \text{ cm}^{-1}$, KBr pellet): 3402, 1635, 1537; CD λ_{max} (mdeg) (CH_3OH): 410 (-0.89), 346 (-0.49), 226 (-8.56); UV-Vis (CH_3OH) [λ_{max}/nm (ϵ/dm^3

mol⁻¹ cm⁻¹)]: 402 (4973), 254 (39535), 227 (39224); CHN Analysis: Calcd.: C, 43.26; H, 5.67; N, 9.46%; Found: C, 44.61; H, 6.19; N, 9.81%.

Characterization data for iron complex, 5

Yield: 70%; Colour: Brown; M. F.: C₃₂H₄₄N₆O₂ Br₂Cl₂Fe·3H₂O; M. W.: 885.34 g mol⁻¹; IR (ν cm⁻¹, KBr pellet): 3368, 1622, 1543; CD λ_{max} (mdeg) (CH₃OH): 427 (-0.098), 360 (-0.98), 303 (-2.07), 252 (-3.93), 205 (-2.27); UV-Vis (CH₃OH) [λ_{max}/nm (ε/dm³ mol⁻¹ cm⁻¹)]: 412 (4256), 350 (8164), 292 (10975), 240 (35540); CHN Analysis: Calcd.: C, 43.41; H, 5.69; N, 9.49%; Found: C, 43.57; H, 5.56; N, 9.62%.

Characterization data for zinc complex, 6

Yield: 75%; Colour: Yellow; M. F.: C₃₂H₄₄N₆O₂ Br₂Cl₂Zn·3H₂O; M. W.: 894.88 g mol⁻¹; IR (ν cm⁻¹, KBr pellet): 3414, 1635, 1535; CD λ_{max} (mdeg) (CH₃OH): 390(-3.143), 353 (2.42), 305 (-0.01), 246 (-6.05); UV-Vis (CH₃OH) [λ_{max}/nm (ε/dm³ mol⁻¹ cm⁻¹)]: 370 (11796), 266 (16810), 230 (54363); CHN Analysis: Calcd.: C, 42.95; H, 5.63; N, 9.39%; Found: C, 43.10; H, 5.72; N, 9.51%.

Characterization data for nickel complex, 7

M. F.: C₃₆H₅₀N₈O₁₀Br₂NiCl₂·2H₂O; M.W.: 1080.27 g mol⁻¹; IR (ν cm⁻¹, KBr pellet): 3472, 1628, 1548, 1093; CD λ_{max} (mdeg) (CH₃OH): 411 (-0.56), 343 (-0.56), 251 (-5.34); UV-Vis (CH₃OH) [λ_{max}/nm (ε/dm³ mol⁻¹ cm⁻¹)]: 412 (3845), 321(7103), 247 (37840); CHN Analysis: Calcd.: C, 40.03; H, 5.04; N, 10.37%; Found: C, 39.95; H, 5.17; N, 9.93%.

2.4. Results and discussion

Synthetic details of the chiral complexes **1–7** are given in the experimental section 2.3.3. The complexes show IR bands at around 3400 cm⁻¹ corresponding to the water molecules and also at around 1635 – 1618 cm⁻¹ due to C=N stretching vibration. Absence of aldehydic C=O stretch of 4-bromo-2-formyl-6-(4-methylpiperazin-1-ylmethyl)phenol (**A**) at 1680 cm⁻¹ confirms that the chiral Schiff base metal complexes were formed. The strong band at ~1540 cm⁻¹ is characteristic of the

phenolic C-O stretching band. The bands due to C=C stretching and bending modes appear at $\sim 2935\text{ cm}^{-1}$, $\sim 2700\text{ cm}^{-1}$ and a strong band at $\sim 1430\text{ cm}^{-1}$.

The CHN analytical data of the complexes match with the mononuclear composition $[\text{L}^1\text{M}]\text{X}_2 \cdot n\text{H}_2\text{O}$. The circular dichroism spectra of the ligand and complexes have bands at around 400(-0.3) nm, 310(-4) nm and a high intensity $\pi \rightarrow \pi^*$ transition band at near 250(-10) nm. These CD signals confirm that the compounds are chiral. The circular dichroism and UV-vis spectra of the ligand and complexes are shown in Figures 2.9 and 2.10.

2.4.1. Nickel complex $[\text{L}^1\text{Ni}] \cdot 2\text{HCl} \cdot 7\text{H}_2\text{O}$, **1**

The chiral nickel complex **1** was synthesized by the procedure given in section 2.3.3.4. The IR spectrum of the complex shows stretching broad band at 3390 cm^{-1} corresponding to the water molecule and other two strong stretching bands at 1618 , 1539 cm^{-1} corresponding to the C=N and phenolic C-O groups. The bands due to C=C stretching and bending modes appear at 2941 cm^{-1} , 2700 cm^{-1} and a strong band at 1433 cm^{-1} .

The electronic spectrum of the complex recorded in methanol shows three bands at 414 nm, 336 nm and 249 nm. The bands at 336 and 414 nm is due to the intra ligand $n \rightarrow \pi^*$ and ligand to metal charge transfer transitions. The band at 249 nm is due to $\pi \rightarrow \pi^*$ electronic transitions of the ligand.

Circular dichroism spectrum of the nickel complex recorded in methanol solution shows band at 410(-1.6). The band at 340(-1.1) nm is due to the intra ligand transitions and the high intensity $\pi \rightarrow \pi^*$ transition band at 249(-9.6) nm confirms the complex is chiral (Figure 2.9). The CHN analytical data agree with the mononuclear composition of $[\text{L}^1\text{Ni}] \cdot 2\text{HCl} \cdot 7\text{H}_2\text{O}$. The molecular structure of the nickel complex is established by X-ray crystal structure analysis.

X-ray crystallography of nickel complex, **1**

The complex **1** gave orange-red coloured single crystals suitable for X-ray structure determination by the slow evaporation of the reaction mixture (acetonitrile) at room temperature. The mononuclear nickel complex crystallizes in monoclinic $P2_1$ space group. The asymmetric unit consists of two crystallographically independent molecules. ORTEP diagram of the molecule with atom numbering is shown in Figure 2.1. The important crystallographic parameters are given in Table 2.1. The crystal structure of the chiral nickel complex **1** is stabilized by an intricate array of hydrogen bonding interactions that involve water molecules and chloride anions leading to the formation of alternate supramolecular aqua-chloro helices. The enantiopure ligand **L**¹ (Scheme 2.2) is prepared in a Schiff-base condensation reaction of two equivalents of 4-bromo-2-formyl-6-(4-methylpiperazin-1-ylmethyl)phenol and one equivalent of (R,R)-*trans*-1,2-cyclohexanediamine in acetonitrile. Reaction of hydrated Ni(II) chloride and optically pure ligand **L**¹ afforded the neutral complex $[\text{NiL}^1] \cdot 2\text{HCl} \cdot 7\text{H}_2\text{O}$ **1** in good yield (Scheme 2.3). The crystals of $[\text{NiL}^1] \cdot 2\text{HCl} \cdot 7\text{H}_2\text{O}$ **1** were characterized by elemental and spectral analyses including single crystal X-ray structure determination. The molecular structure of the Ni(II) complex is presented in Figure 2.1. The asymmetric unit consists of two crystallographically independent molecules. These two complex units are nearly identical as shown in Figure 2.1 (1A and 1B). The nickel atom in **1** is four-coordinated with two imino nitrogen and two phenolic oxygen atoms acting as N_2O_2 donors set (from the ligand **L**¹). The Ni-O (phenolic) bond distances are 1.838(4) and 1.839(4) Å and the Ni-N (imine) bond distances are 1.865(5) and 1.850(5) Å.

The coordination geometry around the nickel is nearly square planar. C(14), C(19), C(46) and C(51) are the chiral centers of the ligand **L**¹ (Figure 2.1). The most exciting feature of the present system is an interesting arrangement of water molecules and chloride anions, which are inter molecular water-chloride non-covalent interactions.

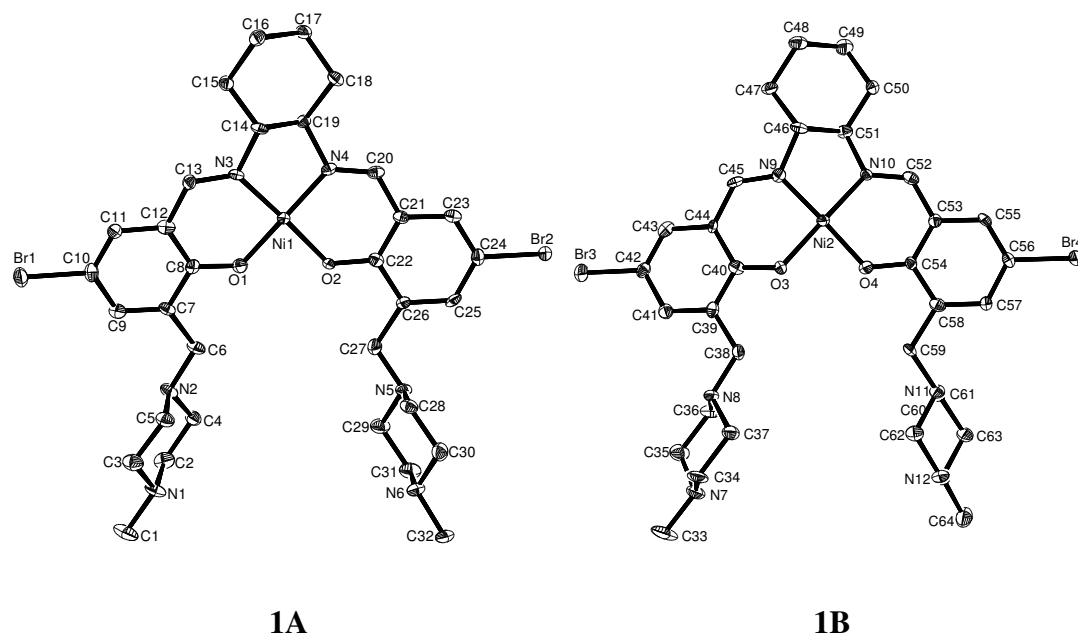


Figure 2.1. ORTEP diagram of the nickel complex **1** (individual molecules in the asymmetric unit of **1**). C(14), C(19), C(46) and C(51) are chiral centers. Thermal ellipsoids are at 50% probability level. Hydrogen atoms have been omitted for clarity.

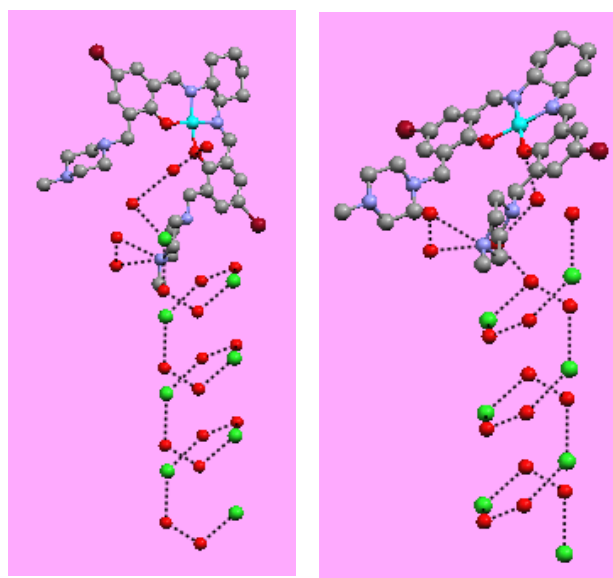


Figure 2.2. View illustrating aqua-chloro helices anchoring points (left: left-handed helix anchored by a $[\text{NiL}^1]$ in the asymmetric unit; right: right-handed helix anchored by the other $[\text{NiL}^1]$ complex in the asymmetric unit). Inter-connected water decamers have been omitted for clarity, except those involved in anchoring points by complex **1** (red: oxygen atoms; green: chloride anions, blue: nitrogens; and cyan: nickel ions).

We believe that, this is of great significance in current context of aqueous sea-salt aerosols²⁰ as well as water in mixed-component systems. Very recently, Chakravarty and co-workers have reported helical supramolecular host system with aquapores anchoring alternate helical water chains.²¹ Vittal *et al.* have shown the structure of a helical coordination polymer encapsulating a hydrogen-bonded helical stream of water molecules.²² The crystal lattice of the present compound **1** contains non-coordinated fourteen water molecules and four hydrochloric acid molecules, which are inter-connected through hydrogen bonding interactions leading to the formation of alternate aqua-chloro helical chains (Figure 2.3) anchored by chiral nickel complex [NiL¹] (Figure 2.2).

These alternate helices are inter-connected by a water decamer as shown in Figures 2.4 and 2.6. All water oxygen atoms and chloride anions, that are responsible for the formation of both left- and right-handed helices, are located in the asymmetric unit of **1**. O(17), O(18) water oxygen atoms and Cl(1) anion constitute the left-handed helical back bone. Similarly, O(11), O(12) water oxygen atoms and Cl(3) anion build the right-handed helical back bone (Figures 2.3 and 2.4). Interestingly, both left- and right-handed helices are connected by a common water decamer consisting of O(5), O(6), O(7), O(8), O(9), O(10), O(13), O(14), O(15) and O(16) water oxygen atoms (Figure 2.4). This water decamer can be described as consisting of a water tetramer (formed from O(8), O(9), O(10) and O(16) water oxygen atoms) and its two side-arm water trimers: O(5), O(6), O(7) and O(13), O(14) and O(15) water oxygens respectively.

The side arm of O(5), O(6), O(7) water trimer is associated with left handed helices and the other side arm (O(13), O(14) and O(15) water trimer) is linked with right handed helices. The helices run parallel to the crystallographic *b* axis, whereby the resulting helical layer (that consists of both left- and right-handed helices and water decamers) runs parallel to the crystallographic *c* axis as shown in Figures 2.5 and 2.6. The helices are anchored by the host complex [NiL¹] (Figure 2.2 and 2.6). The hydrogen bonding distances of whole supramolecular structure, that includes

helices, side-arms and water tetramer, are described in Table 2.3. O(1) and N(1) atoms (Figure 2.1 (1A)) are the anchoring points of one of the complexes in the asymmetric unit to the side-arms of the left-handed helix and associated water tetramer respectively. Similarly, O(3) and N(7) atoms of the other complex in the asymmetric unit (Figure 2.1 (1B)) connect to the side-arms of the right-handed helix and water tetramer respectively through hydrogen bonding interactions (Table 2.3 for relevant H-bond distances). The hydrogen atoms of the water molecules were not resolved in the crystal structure determination.

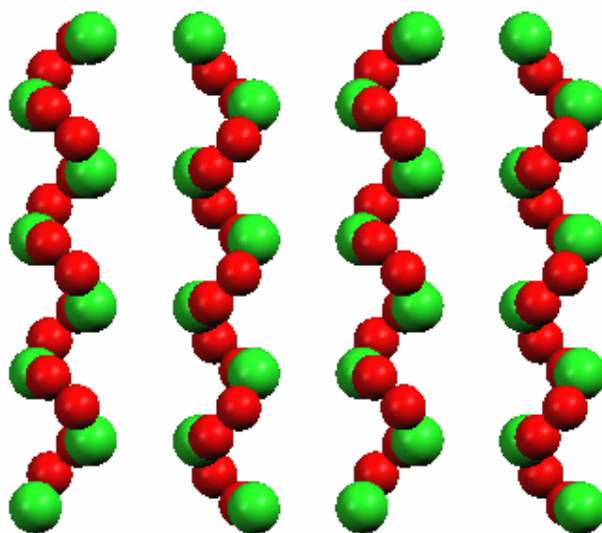


Figure 2.3. Alternate left-handed and right-handed aqua-chloro helices in the crystal lattice of **1** (inter-connected water decamers have been omitted for clarity). Space-filling plot (red: water and green: chloride anions).

It is noteworthy that the water molecules can be detected in the IR spectra of **1**. In addition to the formation of aqua-chloro helices in the crystal lattice of **1**, the complex $[\text{NiL}^1]$ undergoes $\text{C-H}\cdots\text{Br}$ hydrogen bonding interactions leading to the formation of both left- and right-handed helical arrangements (Figure 2.7). The complex of nickel(II) labelled with Ni(1) in the asymmetric unit is involved in the left-handed helix and the complex of nickel(II) labelled with Ni(2) is engaged forming right-handed helix.

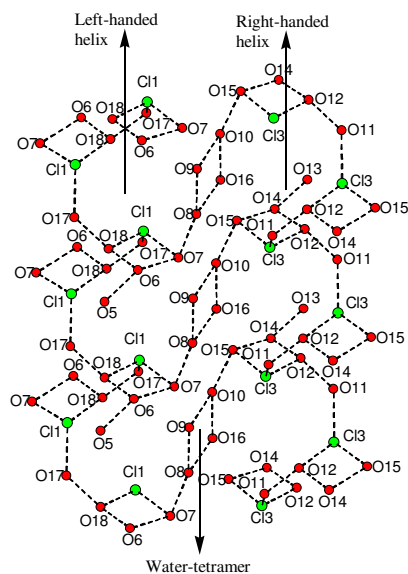


Figure 2.4. View illustrating alternate aqua-chloro helices with inter-connected water decamers in **1**. Ball and stick view with labels.

Interestingly, each nickel complex in the left-handed helix (formed by C–H·····Br hydrogen bonding interactions) is hydrogen bonded to a chloride anion (Cl(1)) that is, in turn, involved in forming left-handed aqua-chloro helix. Each nickel complex in the right-handed helix (formed by C–H·····Br hydrogen bonding interactions) is hydrogen bonded to a chloride anion (Cl(3)) that forms right-handed aqua-chloro helix (*vide supra*) as shown in Figure 2.7. Each nickel complex in the asymmetric unit undergoes C–H·····Br hydrogen bonding interactions. The Ni(1) complexes (it is a nickel(II) complex with the nickel ion labeled as Ni(1)) forms are linked by C(28)–H(28B)·····Br(2) hydrogen bonds forming a left-handed helix. Similarly, the Ni(2) complexes (it is a nickel(II) complex with the nickel ion labeled as Ni(2)) forms are linked by C(61)–H(61A)·····Br(4) hydrogen bonds forming a right-handed helix (Figure 2.7). The corresponding helical backbones are presented in Figure 2.8. The relevant hydrogen bonding parameters are: C(28)–H(28B)·····Br(2): 0.99, 2.81, 3.797(7), 172.8; C(61)–H(61A)·····Br(4): 0.99, 2.87, 3.858(7), 175.5.

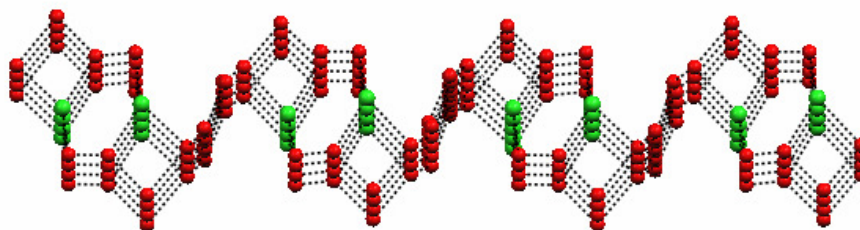


Figure 2.5. The helical layer running parallel to the crystallographic *c* axis in the crystal lattice of **1**. This view is looking down to the crystallographic *b* axis. (red: water and green: chloride anions).

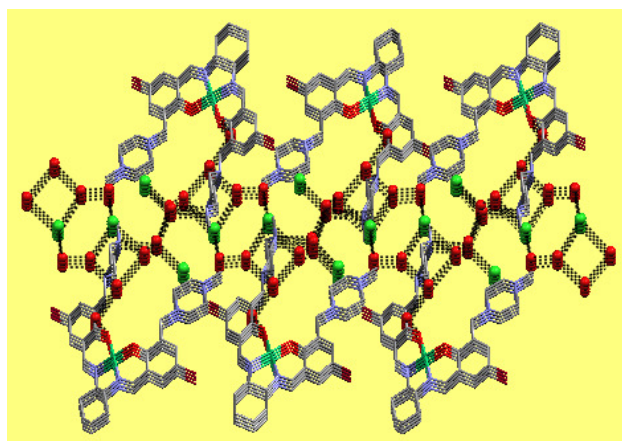


Figure 2.6. The helical layer running parallel to the crystallographic *c* axis. This view is looking down to the crystallographic *b* axis of nickel complex **1**.

The optical activity of the Ni(II) complex **1** is induced by the enantiopure ligand **L**¹ (Scheme 2.2). The UV-visible spectrum of the Ni(II) complex **1** is characterized by an intense band at 249 nm and two relatively weak peaks at 336 nm and 414 nm respectively. These are charge transfer transitions judging from their molar extinction coefficient values. The CD spectrum of the synthesized chiral ligand **L**¹ shows negative bands at around 340 and 266 nm. The CD spectrum of **1** as expected, exhibits negative bands, which are consistent with those in the electronic spectrum. A strong band at 3390 cm⁻¹ is observed in the IR spectra of **1**, that reflects the presence of hydrogen bonded water molecules in the crystal lattice of **1**. Selected bond lengths and bond angles are listed in Table 2.2.

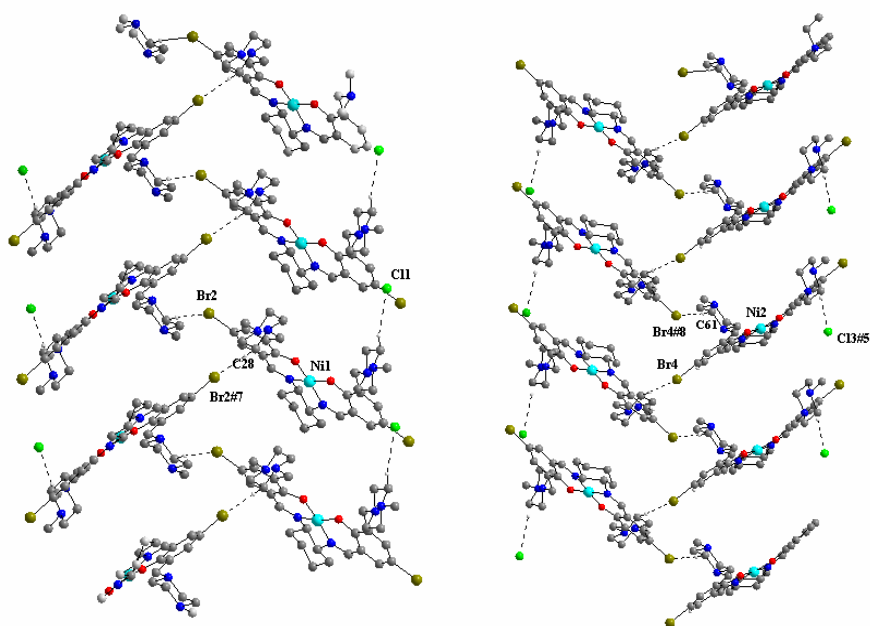


Figure 2.7. Left: the nickel complex with nickel labeled Ni(1) in the asymmetric unit undergoes C–H····Br hydrogen bonding interactions forming a left-handed helix. Right: the nickel complex with nickel labeled Ni(2) in the asymmetric unit undergoes C–H····Br hydrogen bonding interactions forming a right-handed helix in complex **1**.

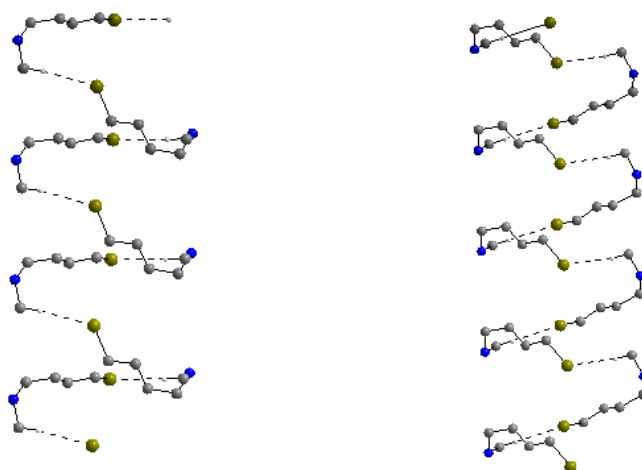


Figure 2.8. The $[\text{NiL}^1]$ complex forms inter molecular C–H····Br hydrogen bonding interactions, that leads to the formation of left- and right-handed helices.

Table 2.1. Crystallographic parameters of the mononuclear nickel complexes, **1** and **7**

Compound	[L ¹ Ni]·2HCl·7H ₂ O, 1	[L ¹ Ni](ClO ₄) ₂ ·2CH ₃ CN·2H ₂ O, 7
Empirical formula	C ₃₂ H ₅₈ N ₆ Br ₂ NiCl ₂ O ₉	C ₃₆ H ₅₄ N ₈ O ₁₂ Br ₂ NiCl ₂
<i>M</i>	960.24	1080.27
<i>T</i> /K	100(2)	273(2)
$\lambda/\text{\AA}$	0.71073	0.71073
Crystal system	Monoclinic	Monoclinic
Space group	<i>P</i> 2 ₁	<i>P</i> 2 ₁ / <i>c</i>
<i>a</i> /\AA	21.8997(10)	9.0262(6)
<i>b</i> /\AA	8.8129(4)	13.2339(8)
<i>c</i> /\AA	22.7230(10)	38.974(3)
$\beta/^\circ$	106.9510(10)	94.9420(10)
<i>U</i> /\AA ³ , <i>Z</i>	4195.0(3), 4	4638.2(5), 4
<i>D_c</i> /mg m ⁻³	1.495	1.530
μ/mm^{-1}	2.549	2.321
<i>F</i> (000)	1920	2168
Crystal size/mm	0.33 x 0.16 x 0.07	0.45 x 0.36 x 0.18
θ range /°	1.53 to 28.29	1.05 to 28.29
Limiting indices	-27 ≤ <i>h</i> ≤ 28, -11 ≤ <i>k</i> ≤ 11, -29 ≤ <i>l</i> ≤ 29	-11 ≤ <i>h</i> ≤ 11, -17 ≤ <i>k</i> ≤ 17, -50 ≤ <i>l</i> ≤ 49
Reflections collected	31325	52884
Reflections [<i>I</i> > 2σ(<i>I</i>)]	14174	10954
Data, parameters	14174, 937	10954, 505
Goodness-of-fit on <i>F</i> ²	0.966	0.942
Final <i>R</i> indices [<i>I</i> > 2σ(<i>I</i>)]	<i>R</i> 1 = 0.0448, <i>wR</i> 2 = 0.1090	<i>R</i> 1 = 0.0762, <i>wR</i> 2 = 0.2270
<i>R</i> indices (all data)	<i>R</i> 1 = 0.0618, <i>wR</i> 2 = 0.1130	<i>R</i> 1 = 0.1531, <i>wR</i> 2 = 0.2539

Table 2.2. Selected bond lengths (Å) and bond angles (°) of complex, **1**

Bond lengths			
Ni(1)-O(1)	1.838(4)	O(3)-C(40)	1.311(7)
Ni(1)-O(2)	1.839(4)	O(4)-C(54)	1.298(7)
Ni(2)-O(3)	1.849(4)	O(1)-C(8)	1.319(7)
Ni(2)-O(4)	1.838(4)	N(3)-C(13)	1.292(8)
Ni(1)-N(3)	1.865(5)	N(4)-C(20)	1.282(7)
Ni(1)-N(4)	1.850(5)	N(9)-C(46)	1.493(7)
Ni(2)-N(9)	1.839(5)	N(10)-C(52)	1.289(7)
Ni(2)-N(10)	1.858(5)	Br(1)-C(10)	1.915(6)
O(1)-C(8)	1.319(7)	Br(2)-C(24)	1.902(6)
O(2)-C(22)	1.310(7)	Br(3)-C(42)	1.877(6)
C(14)-N(3)	1.485(7)	Br(4)-C(56)	1.905(6)
N(4)-C(19)	1.500(6)	N(9)-C(46)	1.493(7)
Bond angles			
O(1)-Ni(1)-O(2)	83.54(18)	N(9)-Ni(2)-O(3)	94.3(2)
O(1)-Ni(1)-N(4)	173.6(2)	O(4)-Ni(2)-N(10)	94.96(19)
O(2)-Ni(1)-N(4)	94.92(19)	N(9)-Ni(2)-N(10)	86.7(2)
O(1)-Ni(1)-N(3)	95.1(2)	O(3)-Ni(2)-N(10)	178.80(19)
O(2)-Ni(1)-N(3)	173.5(2)	C(8)-O(1)-Ni(1)	127.4(4)
N(4)-Ni(1)-N(3)	87.1(2)	C(40)-O(3)-Ni(2)	127.2(4)
O(4)-Ni(2)-N(9)	177.5(2)	C(54)-O(4)-Ni(2)	127.1(4)
O(4)-Ni(2)-O(3)	84.02(18)	C(45)-N(9)-C(46)	122.4(5)
C(45)-N(9)-Ni(2)	126.3(4)	C(13)-N(3)-C(14)	121.4(5)
C(46)-N(9)-Ni(2)	111.3(4)	C(13)-N(3)-Ni(1)	127.0(4)
C(22)-O(2)-Ni(1)	126.1(4)	C(14)-N(3)-Ni(1)	111.4(4)

Table 2.3. Hydrogen bond distances (in Å) associated with aqua-chloro helices and their surroundings of complex, **1**(see Figures 2.4 and 2.6).

O(17)···O(18)#2	2.814(9)	O(11)···O(12)	2.722(9)
O(17)···Cl(1)#5	3.118(7)	O(11)···Cl(3)#2	3.147(6)
O(18)···Cl(1)#1	3.106(8)	O(12)···Cl(3)#5	3.163(7)
O(7)···Cl(1)#2	3.169(12)	O(12)···O(14)#2	2.776(10)
O(6)···O(18)#4	2.795(10)	O(14)···O(13)#3	2.913(9)
O(6)···O(5)#2	2.976(9)	O(14)···O(15)	2.961(11)
O(1)···O(5)	2.903(7)	O(15)···Cl(3)#6	3.261(9)
O(8)···O(9)	3.09(3)	O(3)···O(13)	2.862(7)
O(10)···O(16)#5	2.93(3)	O(8)···O(16)#5	2.787(15)
O(8)···O(7)	2.86(3)	O(10)···O(15)#5	2.90(2)
O(8)···N(1)	3.190(18)	O(10)···N(7)#5	3.19(2)
O(6)···O(7)	3.19(3)	O(10)···O(9)	3.06(2)
O(9)···N(1)	3.012(13)	O(16)···N(7)	2.890(11)
O(9)···Cl(2)	3.098(11)	O(10)···Cl(4)#6	3.072(11)
		O(16)···Cl(4)#3	3.117(8)
Symmetry codes: #1: x, y, z-1;		#2: x, 1+y, z; #3: x, y-1, z;	
#4: x, 1+y, 1+z;		#5: 2-x, 0.5+y, 1-z;	
#6: 2-x, y-0.5, 1-z.			

2.4.2. Manganese complex [L¹Mn(III)Cl]·3H₂O, **2**

The manganese complex was synthesized in good yields by the procedure given in section 2.3.3.5. The IR spectrum of the complex shows a broad band at around 3400 cm⁻¹ corresponding to the water molecule and other two strong stretching bands at around 1633, 1543 cm⁻¹ corresponding to the C=N and phenolic C-O groups. Circular dichroism spectra were recorded in methanol solution.

The CD spectra of the complex agreed reasonably well with the corresponding nickel complex. The bands at 409(-0.26), 310(-4.03) nm and high intensity band at 245(-5.66) confirms that the complex is chiral (Figure 2.9). The electronic spectra in methanol show band at 590 nm due to d-d transitions. The band at 412 nm is due to the ligand to metal charge transfer transition. An intra ligand n- π^* transitions band (shoulder) at 350 and band at 285 nm due to π - π^* electronic transitions of the ligand are also observed. The CHN analytical data of complex match with the mononuclear composition of $[L^1Mn(III)Cl]\cdot 3H_2O$.

2.4.3. Copper complex $[L^1Cu]Cl_2\cdot 6H_2O$, 3

The copper complex was synthesized by the procedure given in section 2.3.3.6. The IR spectrum of the complex shows a broad band at 4000 cm^{-1} due to water molecule and other two strong stretching bands at 1622, 1535 cm^{-1} corresponding to the C=N and phenolic C-O groups. The bands due to C=C stretching and bending modes appear at 2930 cm^{-1} and a strong band at 1431 cm^{-1} .

The electronic spectrum of the complex recorded in methanol solution shows three bands at 581 nm, 373 nm and 230 nm. The band at 581 nm is due to the d-d transitions and at 373 nm is due to the intraligand n- π^* transitions and the band at 230 nm is due to π - π^* electronic transitions of the ligand. The CD spectrum of the complex was recorded in methanol and it shows band at 394(-4.4) nm and a high intensity $\pi\rightarrow\pi^*$ transition band at 250(-10.5) nm (Figure 2.9). The elemental analytical data of the complex agree with the mononuclear composition of $[L^1Cu]Cl_2\cdot 6H_2O$.

2.4.4. Cobalt complex $[L^1Co]Cl_2\cdot 3H_2O$, 4

The chiral cobalt complex was synthesized in good yields by the procedure given in section 2.3.3.6. The IR spectrum of the complex shows a broad band at around 3402 cm^{-1} corresponding to the water molecule and other two strong stretching bands at around 1635, 1537 cm^{-1} corresponding to the C=N and phenolic C-O groups. Strong band appears for C=C at 1435 cm^{-1} .

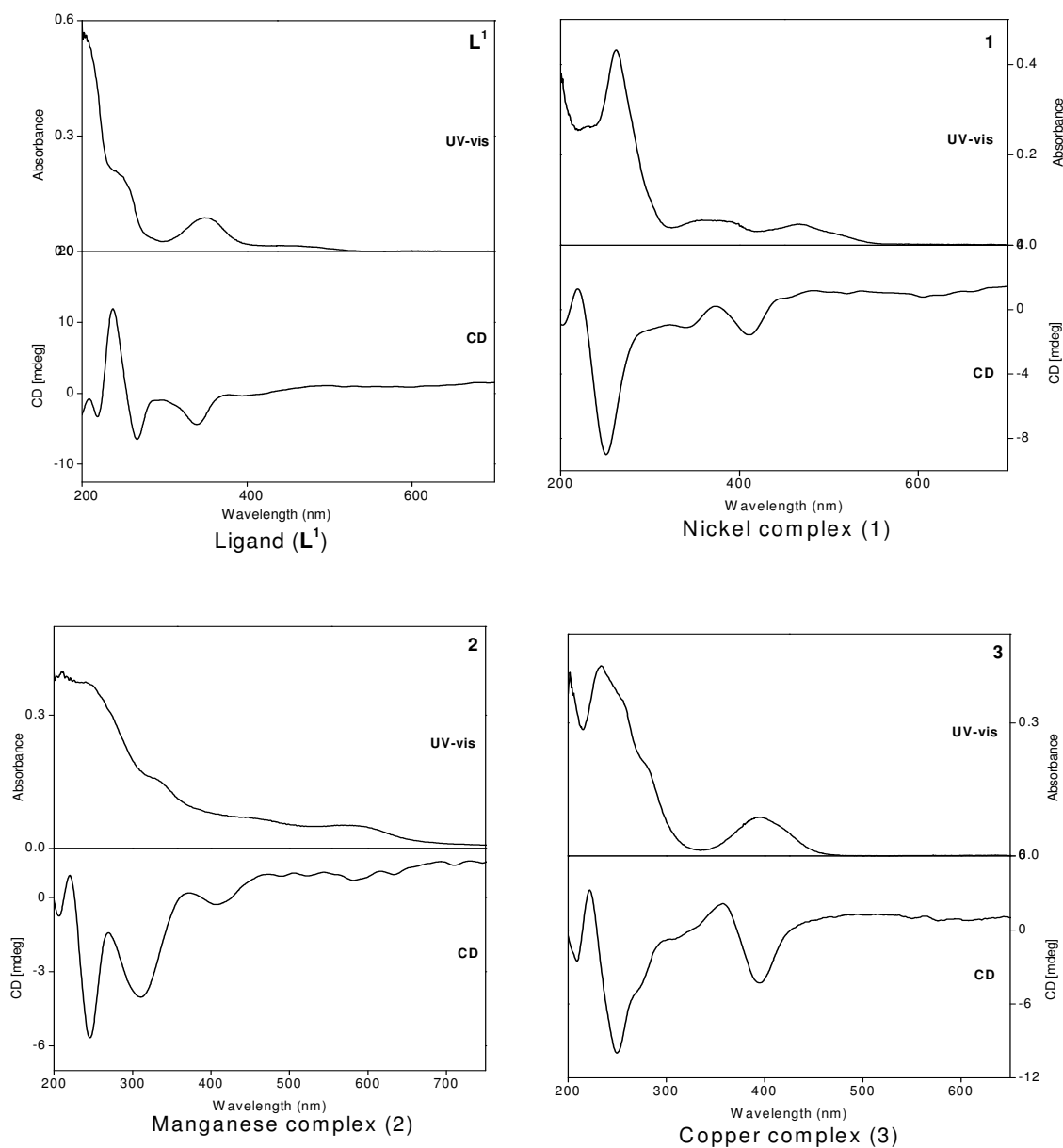


Figure 2.9. CD and UV-vis spectra of ligand L^1 and its Ni^{2+} , Mn^{3+} and Cu^{2+} complexes in MeOH solution (concentrations = $1 \times 10^{-4}M$ for CD and $1 \times 10^{-5}M$ for UV-vis spectroscopy).

Circular dichroism spectra of the cobalt complex recorded in methanol solution show bands at 410(-0.9), 346(-0.5) nm and 226(-8.5). These bands confirm the chirality of the complex (Figure 2.10). The electronic spectrum of the chiral cobalt complex recorded in methanol shows band at 402 nm due to ligand to metal charge

transfer transition and an intra ligand transitions band at 254 nm. The analytical data of the complex match with the mononuclear composition of $[L^1Co]Cl_2 \cdot 3H_2O$.

2.4.5. Iron complex $[L^1Fe]Cl_2 \cdot 3H_2O$, 5

The iron complex was synthesized in good yields by the procedure given in section 2.3.3.6. The IR spectrum of the complex shows a broad band at around 3402 cm^{-1} corresponding to the water molecules and other two strong stretching bands at around 1635 and 1537 cm^{-1} , corresponding to the C=N and phenolic C-O groups. Strong band appears for C=C at 1435 cm^{-1} . Circular dichroism spectra of the iron complex recorded in methanol solution show bands at $427(-0.1)$, $360(-0.98)$ and $252(-3.9)$ nm. These bands confirm that the complex is chiral (Figure 2.10). The electronic spectrum of the iron complex recorded in methanol shows a band at 412 nm due to ligand to metal charge transfer transition and an intra ligand transitions band at 350 nm. The analytical data of the complex match with the mononuclear composition of $[L^1Fe]Cl_2 \cdot 3H_2O$.

2.4.6. Zinc complex $[L^1Zn]Cl_2 \cdot 3H_2O$, 6

The zinc complex was synthesized by the procedure given in section 2.3.3.6. The IR spectrum of the complex shows broad band at 3414 cm^{-1} due to water molecules and other two strong stretching bands at 1635 , 1535 cm^{-1} corresponding to the C=N and phenolic C-O groups. The electronic spectrum of the complex recorded in methanol solution shows three bands at 370, 266 and 230 nm. The band at 370 nm is due to the intraligand $n-\pi^*$ transitions and the band at 230 nm is due to $\pi-\pi^*$ electronic transitions of the ligand. Circular dichroism spectrum of the complex recorded in methanol shows band at $390(-3.14)$ nm and the high intensity $\pi \rightarrow \pi^*$ transition band at $246(-6.05)$ nm confirming the chirality of the complex (Figure 2.10). The CHN analytical data of the complex agree well with the mononuclear composition of $[L^1Zn]Cl_2 \cdot 3H_2O$.

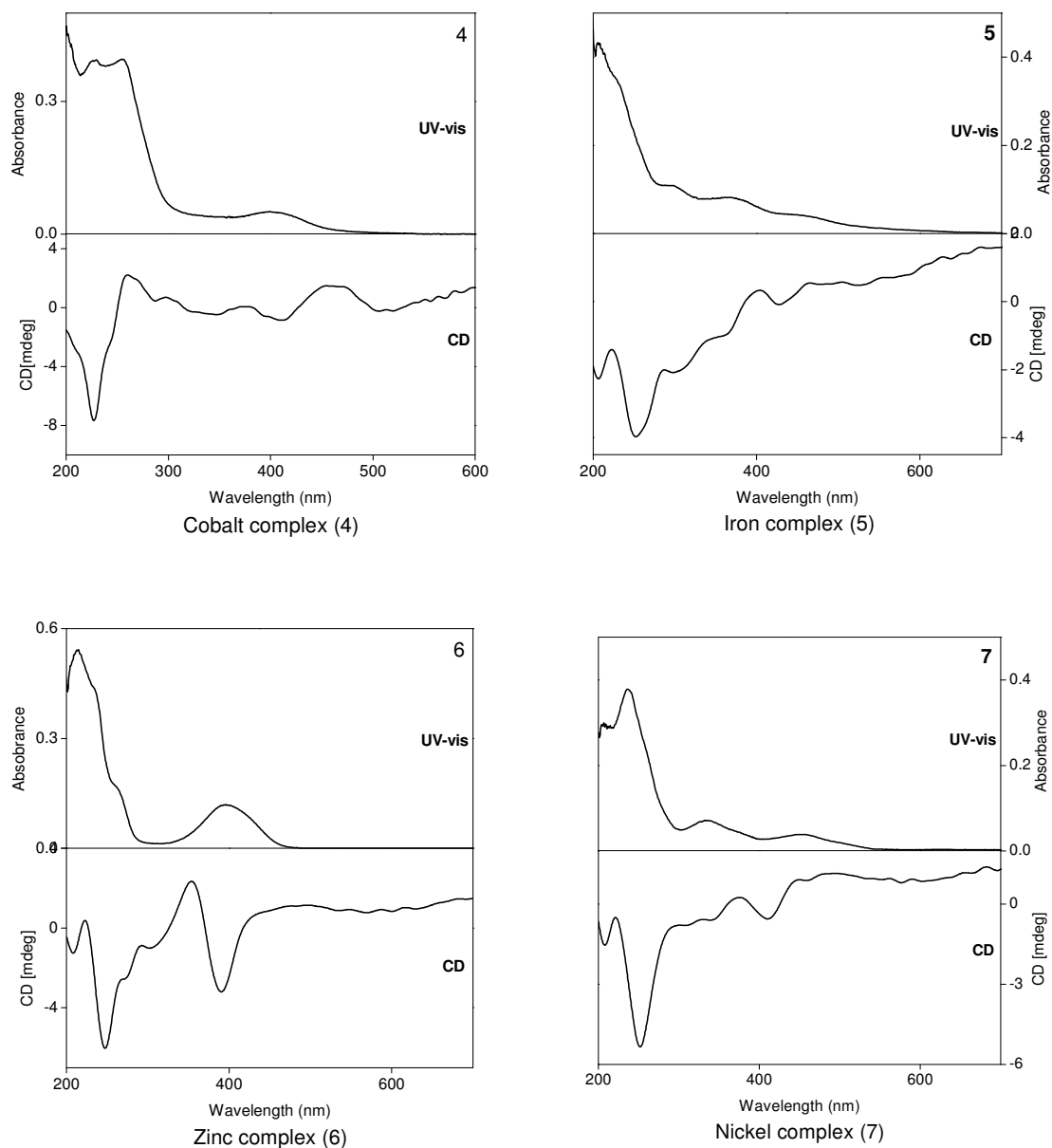


Figure 2.10. CD and UV-vis spectrum of the Co^{2+} , Fe^{2+} , Zn^{2+} and Ni^{2+} complexes in MeOH solution (concentrations = $1 \times 10^{-4}\text{M}$ for CD and $1 \times 10^{-5}\text{M}$ for UV-vis spectroscopy).

2.4.7. Nickel complex $[\text{L}^1\text{Ni}](\text{ClO}_4)_2 \cdot 2\text{CH}_3\text{CN} \cdot 2\text{H}_2\text{O}$, 7

The chiral nickel complex was synthesized by the procedure given in section 2.3.3.7. The IR spectrum of the nickel complex shows stretching bands at 1628 and 1548 cm^{-1} corresponding to the C=N and phenolic C-O groups. The strong band at

1093 cm^{-1} corresponds to the perchlorate anions. The electronic spectrum of the complex in methanol solution shows three bands at 412 nm, 321 nm and 247 nm. The bands at 321 and 412 nm are due to the intra ligand $n\text{-}\pi^*$ transitions and ligand to metal charge transfer transitions. The band at 247 nm is due to $\pi\text{-}\pi^*$ electronic transitions of the ligand.

The circular dichroism spectrum recorded in methanol solution shows bands at 411(-0.56) and 343(-0.56) nm due to the intra ligand transition and another high intensity $\pi\rightarrow\pi^*$ transition band at 251(-5.34) nm confirming the chirality of the complex (Figure 2.10). The CHN analytical data agree well with the mononuclear composition of $[\text{L}^1\text{Ni}](\text{ClO}_4)_2\cdot 2\text{CH}_3\text{CN}\cdot 2\text{H}_2\text{O}$. X-ray crystal structure establishes the molecular structure of the nickel complex, **7** as shown in Figure 2.11.

X-ray crystallography of nickel complex, **7**

The complex **7** gave orange-red coloured single crystals suitable for X-ray structure determination by on slow evaporation of the reaction mixture (acetonitrile) at room temperature. The mononuclear nickel complex crystallizes in monoclinic $P2_1/c$ space group. The ORTEP diagram of the molecule with atom numbering is shown in Figure 2.11. The important crystallographic parameters are given in Table 2.1. The molecule **7** consists of one nickel center, which is coordinated to two phenolic oxygens and two imino nitrogen atoms, thereby forming a tetra coordinate structure with N_2O_2 donor set having square planar geometry. In the molecule C(14) and C(19) are chiral centers. Two perchlorate ions act as counter anions. Two water molecules and two solvent CH_3CN molecules are also involved in the molecular structure. Selected bond lengths and bond angles are listed in Table 2.4. The average Ni(1)-O(1) and Ni(1)-O(2) bond distances are 1.850(4) and 1.849(4) Å. The average Ni(1)-N(3) and Ni(1)-N(4) bond distances are 1.847(6) and 1.850(5) Å. The average bond angles of the molecule are N(3)-Ni(1)-O(1) 94.7, N(3)-Ni(1)-O(2) 177.7, O(2)-Ni(1)-O(1) 84.41, O(1)-Ni(1)-N(4) 178.0, O(2)-Ni(1)-N(4) 94.8 and N(3)-Ni(1)-N(4) 86.1° respectively.

Table 2.4. Selected bond lengths (Å) and bond angles (°) of nickel complex, **7**

Bond lengths			
Ni(1)-O(1)	1.850(4)	O(1)-C(8)	1.319(7)
Ni(1)-O(2)	1.849(4)	O(2)-C(22)	1.306(7)
Ni(1)-N(3)	1.847(6)	C(1)-N(1)	1.496(9)
Ni(1)-N(4)	1.850(5)	N(6)-C(32)	1.470(8)
N(3)-C(13)	1.287(8)	Br(1)-C(10)	1.900(6)
N(3)-C(14)	1.460(9)	Br(2)-C(24)	1.899(6)
N(4)-C(19)	1.494(9)	C(33)-N(7)	1.073(10)
N(4)-C(20)	1.276(8)	C(35)-N(8)	1.120(10)
N(2)-C(6)	1.464(7)	N(6)-C(31)	1.445(8)
N(5)-C(28)	1.501(7)	N(6)-C(30)	1.479(8)
N(1)-C(2)	1.513(7)	C(14)-C(19)	1.250(11)
N(1)-C(3)	1.489(8)	C(17)-C(16)	1.343(13)
Bond angles			
N(3)-Ni(1)-O(1)	94.7(2)	O(1)-Ni(1)-N(4)	178.0(2)
N(3)-Ni(1)-O(2)	177.7(2)	O(2)-Ni(1)-N(4)	94.8(2)
O(2)-Ni(1)-O(1)	84.41(17)	N(3)-Ni(1)-N(4)	86.1(2)
C(8)-O(1)-Ni(1)	127.3(4)	C(19)-N(4)-Ni(1)	110.8(4)
C(22)-O(2)-Ni(1)	127.4(4)	C(20)-N(4)-Ni(1)	126.1(5)
N(3)-C(13)-C(12)	125.3(6)	C(13)-N(3)-Ni(1)	126.3(4)
N(4)-C(20)-C(21)	125.6(6)	C(14)-N(3)-Ni(1)	111.6(5)
C(14)-C(19)-N(4)	114.9(7)	N(2)-C(4)-C(2)	109.0(5)
C(18)-C(19)-N(4)	117.6(7)	N(5)-C(28)-C(30)	109.1(5)
N(3)-C(13)-C(12)	125.3(6)	C(9)-C(10)-Br(1)	119.1(4)
N(4)-C(20)-C(21)	125.6(6)	C(23)-C(24)-Br(2)	118.9(5)

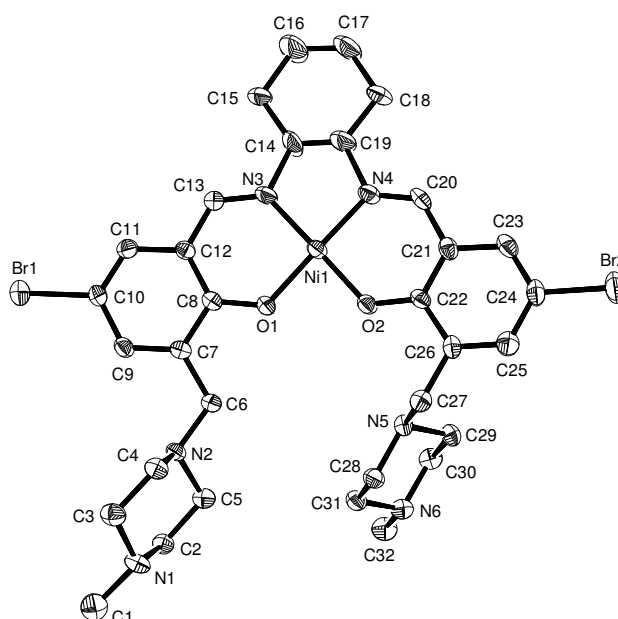


Figure 2.11. Thermal ellipsoid plot of the nickel complex **7**. C(14) and C(19) are chiral centers. Thermal ellipsoids are at 30% probability level. Hydrogen atoms have been omitted for clarity.

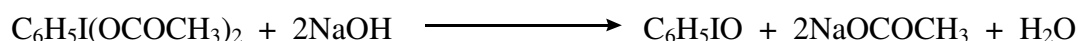
2.5. Catalysis

To examine the nature of the chiral complexes in the catalytic process, alkenes oxidation reactions were studied. The catalytic activities of the chiral Schiff base complexes were investigated for the epoxidation of alkenes by a terminal oxidant. The oxidations were carried out in CH_3CN using iodosylbenzene (PhIO) as the terminal oxidant at room temperature. In absence of the catalyst under similar reaction conditions, there is no reaction between oxidant and olefins.

The oxidation products of the olefins were confirmed by ^1H -NMR spectroscopy. The oxidation product yields and enantiomeric excess of the styrene were determined by gas chromatography (GC). The oxidation product yields and enantiomeric excess of the *cis*-stilbene and *trans*-stilbene were determined by HPLC analysis.

2.5.1. Synthesis of Iodosylbenzene (PhIO)

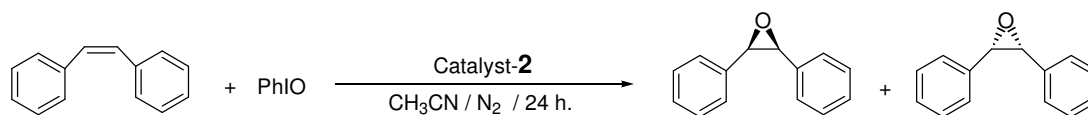
The iodosylbenzene (PhIO) used in the catalytic study as oxidant is prepared using a reported procedure.²³ Finely ground iodosylbenzene diacetate (32.2 g, 0.10 mol) is placed in a 250 mL beaker and 150 mL of 3N sodium hydroxide is added over a 5 minute period with vigorous stirring. The lumps of solid formed are triturated with a stirring rod or spatula for 15 minutes and the reaction mixture kept for an additional 45 minutes to complete the reaction. 100 mL of water is added, the mixture is stirred vigorously and the crude solid iodosobenzene is collected on a Büchner funnel, washed there with 200 mL of water and dried by maintaining suction. Final purification is effected by triturating the dried solid in 75 mL of chloroform in a beaker. The iodosylbenzene is separated by filtration and air-dried (Yield: 85%).



2.5.2. Epoxidation of *cis*-stilbene catalyzed by manganese complex, **2**

The chiral manganese catalyst **2** (0.022 g, 0.025 mmol) and *cis*-stilbene (0.180 g, 1 mmol) were dissolved in 5 mL acetonitrile. The reaction was initiated by the addition of iodosylbenzene (PhIO) (0.220 g, 1 mmol) and stirred at room temperature under nitrogen atmosphere for 24 hours.

After stirring, the mixture was concentrated in vacuum. Anhydrous ether (10 mL) added to the brown residue and the ether solution was carefully filtered. Then the ether was removed under reduced pressure and purified with column chromatography from hexane. The catalytic epoxidation reaction sequence of *cis*-stilbene is shown in Scheme 2.7.



Scheme 2.7. Schematic representation of catalytic epoxidation of *cis*-stilbene.

The product was confirmed by $^1\text{H-NMR}$ spectroscopy (*cis*-stilbene epoxide $\delta \sim 4.34$ in CDCl_3) of reported stilbene epoxide.²⁴ The methylene protons of diphenylethylene appeared as a singlet at $\delta \sim 5.45$ in CDCl_3 . HPLC analyses of *cis*-stilbene epoxide product was carried out on a Shimadzu SCL-10A instrument equipped with CHIRALCEL OD-H using Class-VP program (90:10 hexane / *i*-PrOH, 0.5 mL/min, 254 nm, retention times: 7.8 min for *cis*-stilbene; 10.50 min and 11.45 min for epoxides).

The HPLC analysis profile of the *cis*-stilbene epoxide catalyzed by **2** as a function of time is shown in Figure 2.12. HPLC analysis data showing yield and enantiomeric excess of *cis*-stilbene epoxide catalyzed by complex **2** as a function of time are given in Table 2.5 and Table 2.6 (entry 1). The manganese catalyst **2** is cheering for the epoxidation reactions of *cis*-stilbene yields up to 40% at room temperature with 74% of enantiomeric excess (Figure 2.12).

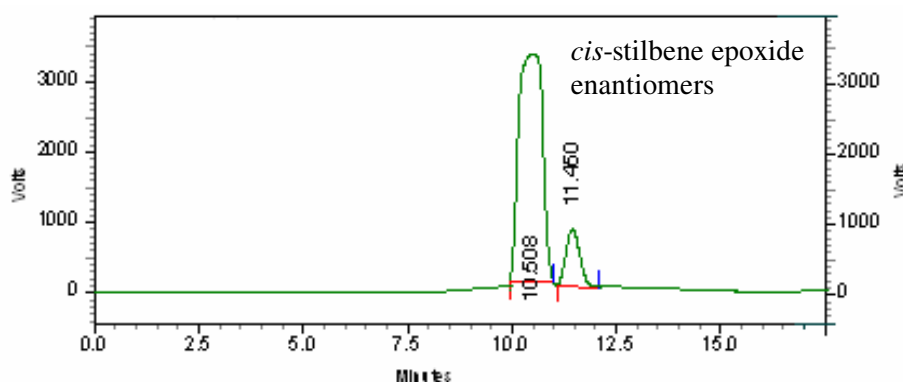


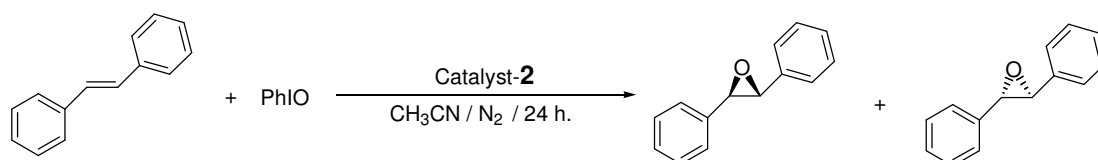
Figure 2.12. HPLC analysis profile of *cis*-stilbene epoxide catalyzed by complex **2**.

Table 2.5. HPLC analysis data of *cis*-stilbene epoxide, showing percentage of enantiomeric excess catalyzed by complex **2** as a function of time

Pk #	Retention Time	Area	Area %	Height	Height %
1	10.508	127135673	87.170	3230203	79.949
2	11.450	18712450	12.830	810126	20.051
Totals		145848123	100.000	4040329	100.000

2.5.3. Epoxidation of *trans*-stilbene catalyzed by manganese complex, **2**

The chiral manganese catalyst **2** (0.022 g, 0.025 mmol) and *trans*-stilbene (0.180 g, 1 mmol) were dissolved in 5 mL acetonitrile. The reaction was initiated by the addition of iodosylbenzene (PhIO) (0.220 g, 1 mmol) and stirred at room temperature under nitrogen atmosphere for 24 hours. After stirring, the mixture was concentrated in vacuum. Anhydrous ether (10 mL) added to the brown residue and the ether solution was carefully filtered. Then the ether was removed under reduced pressure and purified with column chromatography from hexane. The catalytic epoxidation reaction sequence of *trans*-stilbene is shown in Scheme 2.8.



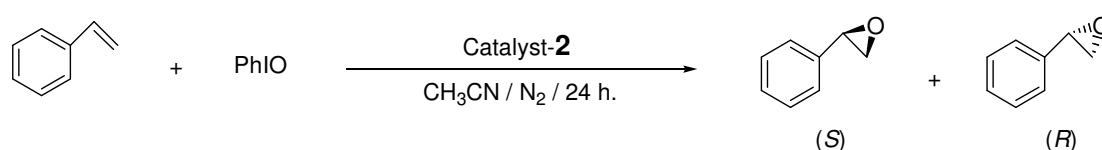
Scheme 2.8. Schematic representation catalytic epoxidation of *trans*-stilbene.

The product was confirmed by ¹H-NMR spectroscopy (*trans*-stilbene epoxide $\delta \sim 3.85$ in CDCl₃) of reported stilbene epoxide.²⁵ HPLC analyses of *trans*-stilbene epoxide product was carried out on a Shimadzu SCL-10A instrument equipped with CHIRALCEL OD-H using Class-VP program (90:10 hexane / *i*-PrOH, 0.5 mL/min, 254 nm, retention times: 9.18 min for *trans*-stilbene; 10.5 min and 11.45 min for epoxides). HPLC analysis data of yield and enantiomeric excess of *trans*-stilbene epoxide catalyzed by complex **2** as a function of time are given in Table 2.6 (entry 2). Epoxidation of *trans*-stilbene catalyzed by **2**, yields up to 20% at room temperature with 32% of enantiomeric excess.

2.5.4. Epoxidation of styrene catalyzed by manganese complex, **2**

Epoxidation of styrene by the chiral catalyst **2** with iodosylbenzene (PhIO) as oxidant were carried out by the following procedure: The chiral catalyst **2** (0.022 g, 0.025 mmol) and styrene (0.104 g, 1 mmol) were dissolved in 5 mL acetonitrile. The

reaction was initiated by the addition of iodosylbenzene (0.220 g, 1 mmol) and stirred at room temperature under nitrogen atmosphere for 24 hours. After completion of the reaction, the solvent was removed under reduced pressure. Anhydrous ether (10 mL) added to the brown residue and the ether solution was carefully filtered. Then the ether was removed under reduced pressure and purified using short silica gel column from hexane. The catalytic epoxidation reaction sequence of styrene is shown in Scheme 2.9.

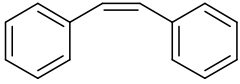
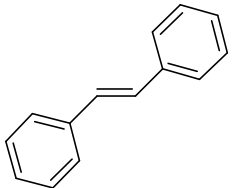
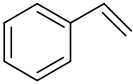
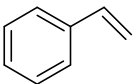
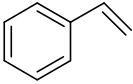
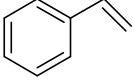
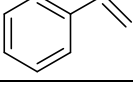


Scheme 2.9. Schematic representation of catalytic epoxidation of styrene.

The ¹H-NMR spectroscopy shows a set of three peaks with a doublet of doublet at ~ 3.85 ppm and two triplets ~ 2.6-3.2 ppm assigned to the product styrene epoxide, is comparable with that of reported styrene epoxide.²⁶ Gas chromatographic analyses were carried out on a Shimadzu GC 14B instrument equipped with a chiral capillary column (Supelco α -DEX 325, 30m length, 0.25mm id, 0.25 μ m film thickness) and a flame ionization detector (FID). Column temperature programmed at 90 °C, Injector and Detector temperatures programmed 200 °C with nitrogen as carrier gas.

Synthetic standards (Authentic samples) of the products were used to determine yields by comparison of peak area and retention time are shown in Figure 2.13. The retention time of authentic samples as follows: Styrene ~20 min; 1-phenyl acetaldehyde ~ 40 min; PhI ~ 56 min; acetophenone ~ 60 min; styrene epoxide ~ 63 and 65 min. The retention time and peak area of the catalytic reaction products were comparable with that of standard samples.

Table 2.6. Oxidation products ^a of olefins using PhIO catalyzed by **2**, **3**, **4** and **5**

Entry	Substrate	Catalyst	Epoxide Yield (%)	Epoxide e. e. (%)	1-Phenyl acetaldehyde Yield(%) ^c	Acetophenone Yield(%) ^c
1		Mn(III) 2	40 ^b	74 ^d	—	—
2		Mn(III) 2	20 ^b	32 ^d	—	—
3		Mn(III) 2	97 ^c	—	2	—
4 ^f		Mn(III) 2	95 ^c	6 ^e	—	—
5		Cu(II) 3	—	—	63	30
6		Co(II) 4	—	—	85	5
7		Fe(II) 5	—	—	97	—

^a Products confirmed by ¹H-NMR spectroscopy. ^b Based on substrate consumed and determined by chiral column (CHIRALCEL OD-H) HPLC analysis. ^c Based on substrate consumed and determined by chiral column GC analysis (Supelco α -DEX 325, 30m length, 0.25mm id, 0.25 μ m film thickness). ^d Enantiomeric excess of epoxides, determined by chiral column (CHIRALCEL OD-H) HPLC analysis. ^e Enantiomeric excess of epoxides, determined by chiral column GC analysis (Supelco α -DEX 325, 30m length, 0.25mm id, 0.25 μ m film thickness). ^f Reaction carried out at 0 °C.

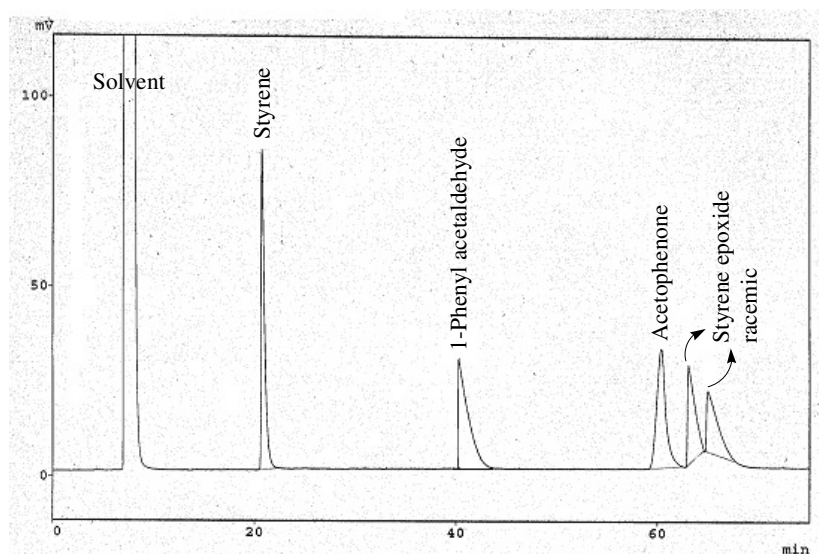


Figure 2.13. Gas chromatographic (GC) analysis profile of authentic samples.

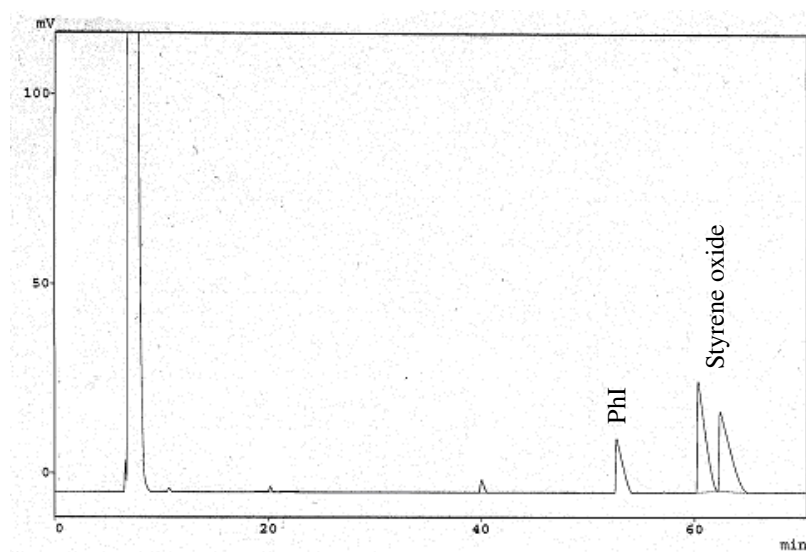


Figure 2.14. Representative gas chromatographic (GC) analysis of styrene epoxidation product catalyzed by manganese complex **2**.

The amount of epoxide formed and the enantiomeric excess of the epoxide catalyzed by complex **2** as a function of time as shown in Figure 2.14. The percentage of product yields and the enantiomeric excess of the epoxides are given in Table 2.6 (entries 3 and 4). The manganese catalyst **2** is encouraging for the epoxidation reactions of the styrene, yields up to 97% at room temperature.

The same procedure was followed for the catalytic activity of other complexes viz. Ni^{+2} , Cu^{+2} , Co^{+2} and Fe^{+2} (**1**, **3**, **4** and **5**) for the styrene oxidation reactions were also investigated. Catalysts, **3**, **4**, **5** are favour the oxidation of styrene to 1-phenylacetaldehyde as the major product and acetophenone as the side product. The percentages of product yields are given in Table 2.6 (entries 5-7). However; no epoxidation product was detected for these catalysts. Nickel complex is not catalytically active for the oxidation reaction of olefins.

2.6. Conclusions

New optically active chiral Schiff base metal complexes **1–7** were characterized by analytical and spectral methods. The nickel complexes **1** and **7** were structurally characterized by X-ray single crystal analysis. The coordination geometry around the metal centers in complexes **1** and **7** is square planar. Ligand **L**¹ and its metal complexes **1–7** exhibit circular dichroism confirming their chirality.

There is extensive hydrogen bonding in the molecular structure of **1**, which results in the simultaneous formation of supramolecular left- and right-handed aqua-chloro helices in the crystal lattice of chiral complex **1**. In complex **1** chirality is induced by the enantiopure ligand **L**¹; however, we have observed both handed aqua-chloro helices. This tells us that, the formation of alternative left- and right-handed aqua-chloro helices is not due to the chirality of the complex, but by the directional nature of the hydrogen bonds in the crystal lattice. It is unique that all water molecules and chloride anions, present in the crystal lattice of **1**, are exclusively involved in hydrogen bonding interactions. The nickel complex **1** seems to act as a template in the formation of such alternate aqua-chloro helices.

Catalytic activities of the chiral Schiff base complexes for the oxidation reactions of the styrene, *cis*-stilbene and *trans*-stilbene were carried out in CH_3CN using iodosylbenzene as the terminal oxidant at room temperature. The manganese catalyst **2** favours the epoxidation reactions of the alkenes. The catalytic activity of the other complexes viz. Cu^{+2} , Co^{+2} and Fe^{+2} (**3**, **4** and **5**) for the styrene oxidation reactions were also investigated. These catalysts favour oxidation of styrene to 1-

phenylacetaldehyde as the major product and acetophenone as the side product. No styrene epoxide product was detected for these catalysts. Manganese catalyst **2** is promising catalyst for styrene epoxidation, yields up to 97% at room temperature. Epoxidation of *trans*-stilbene catalyzed by complex **2**, yields up to 20% at room temperature with 32% of enantiomeric excess. Epoxidation of *cis*-stilbene catalyzed by **2**, yields up to 40% at room temperature with 74% of enantiomeric excess.

2.7. References

1. E. N. Jacobsen, "Asymmetric Catalysis Epoxidation of Unfunctionalized Olefins," in "Catalytic Asymmetric Synthesis" by I. Ojima, VCH, New York **1993**, Chap. 4.2, pp. 159-202. References are cited therein.
2. A. N. Collins, G. N. Sheldrake and J. Crosby (Eds.), Chirality in Industry, The commercial Manufacture and applications of optically Active Compounds, John Wiley, **1995**.
3. I. W. Ojima, *Catalytic Asymmetric Synthesis*, VCH, New York, **1993**.
4. (a) M. G. Finn and K. B. Sharpless, *J. Am. Chem. Soc.*, **1991**, 113, 113; (b) R. A. Johnson and K. B. Sharpless, in: B. Frost (Ed.) *Comprehensive Organic Synthesis*, Vol. 7, Oxidation, Pergamon Press, Oxford, **1992**, Chapter 3.2.
5. B. E. Rossiter, in: J. D. Morrison (Ed.), *Asymmetric Synthesis*, Academic Press, Orlando, **1985**, Vol. 5, p. 194.
6. Y. Naito, F. Tani, N. Ishihara and K. Maruyama, *Bull. Chem. Soc., Jpn.*, **1993**, 66, 158.
7. R. L. Halterman and S. T. Jan, *J. Org. Chem.*, **1991**, 56, 5253.
8. Y. Naito, N. Ishihara, F. Tani and K. Maruyama, *Chem. Lett.*, **1991**, 1933.
9. (a) Y. Naito, F. Tani, N. Ishihara and K. Maruyama, *J. Am. Chem. Soc.*, **1991**, 113, 6865; (b) J. T. Groves and R. S. Myers, *J. Am. Chem. Soc.*, **1993**, 115, 5791.
10. (a) J. T. Groves, W. J. Kruper, and Jr., R. C. Haushalter, *J. Am. Chem. Soc.*, **1980**, 102, 6375; (b) J. T. Groves, W. J. Kruper, Jr., T. E. Nemo and R. S. Myers, *J. Mol. Catal.*, **1980**, 7, 169.

11. (a) E. N. Jacobsen, in *Catalytic Asymmetric Synthesis.*, Ed. I. Ojima, VCH, **1993**, 159. (b) T. Katsuki, *Coordination. Chem. Rev.*, **1995**, 140, 189; (c) J. P. Collman; X. Zhang; V. J. Lee; E. S. Uffelman; and J. I. Brauman, *Science.*, **1993**, 261, 1404
12. (a) H. Yoon; T. R. Wagler; K. J. O'Connor; and C. J. Burrows, *J. Am. Chem. Soc.*, **1990**, 112, 4568; (b) R. Irie; Y. Ito; and T. Katsuki, *Tetrahedron Lett.*, **1991**, 32, 47, 6891.
13. Jonathan D. Crane, David E. Fenton, Jean Marc Latour and Arnold J. Smith, *J. Chem. Soc., Dalton trans.*, **1991**, 2979.
14. Jay F. Larrow and Eric N. Jacobsen, *J. Org. Chem.*, **1994**, 59, 1939.
15. SMART & SAINT Software Reference Manuals, Version 6.22, Bruker AXS Analytic X-Ray Systems, Inc., Madison, WI, **2000**.
16. G. M. Sheldrick, SADABS, Software for Empirical Absorption Correction, University of Göttingen, Germany, **2000**.
17. SHELXTL Reference Manual, Version 5.1, Bruker AXS, Analytic X-Ray Systems, Inc., WI, **1997**.
18. L. J. Farrugia, *J. Appl. Cryst.*, **1997**, 30, 567.
19. A. L. Spek, *Platon, Molecular Graphics Software*, University of Glasgow, UK, **2001**.
20. (a) NASA Facts, online, **1996**, FS-1996-08-11-LaRC; (b) C. W. Spicer, E. G. Chapman, B. J. Finlayson-Pitts, R. A. Plastring, J. M. Hubbe, J. D. Fast and C. M. Berkowitz, *Nature.*, **1998**, 394, 353; (c) K. L. Foster, R. A. Plastring, J. W. Bottenheim, P. B. Shepson, B. J. Finlayson-Pitts and C. W. Spicer, *Science.*, **2001**, 291, 471; (d) L. Lehr, M. T. Zanni, C. Frischkorn, R. Weinkauff and D. M. Neumark, *Science.*, **1999**, 284, 635; (e) C. Bassmann, U. Boesl, D. Yang, G. Drechsler and E. W. Schlag, *Int. J. Mass Spectrum. Ion Processes.*, **1996**, 159, 153; (f) E. M. Knipping, M. J. Lakin, K. L. Foster, P. Jungwirth, D. J. Tobias, R. B. Gerber, D. Dabdub and B. J. Finlayson-pitts, *Science.*, **2000**, 288, 301; (g) P. Jungwirth and D. J. Tobias, *J. Phys. Chem. B.*,

- 2000**, 104, 7702; (h) D. E. Smith and L. X. Dang, *J. Chem. Phys.*, **1994**, 100, 3757; (i) H. E. Dorset, R. O. Watts and S. S. Xantheas, *J. Phys. Chem. A.*, **1999**, 103, 3351; (j) I.-C. Yeh, L. Perera and M. L. Berkowitz, *Chem. Phys. Lett.*, **1997**, 264, 31; (k) R. W. Gora, S. Roszak and J. Leszczynski, *Chem. Phys. Lett.*, **2000**, 325, 7; (l) D. J. Tobias, P. Jungwirth and M. Parrinello, *J. Chem. Phys.*, **2001**, 114, 7036; (m) S. J. Stuart and B. J. Berne, *J. Phys. Chem. A.*, **1999**, 103, 10300; (n) M. K. Saha and I. Bernal, *Inorg. Chem. Commun.*, **2005**, 8, 871.
21. A. Mukherjee, M. K. Saha, M. Nethaji and A. R. Chakravarty, *Chem. Commun.*, **2004**, 716.
22. B. Sreenivasulu and J. J. Vittal, *Angew. Chem., Int. Ed.*, **2004**, 43, 5769.
23. H. Saltzman and J. G. Sharefkin, *Org. Synth.*, **1973**, Coll. Vol. V, 658.
24. K. Srinivasan, P. Michaud and J. K. Kochi, *J. Am. Chem. Soc.*, **1986**, 108, 2309.
25. D. Das and C.-P. Cheng, *J. Chem. Soc., Dalton Trans.*, **2000**, 1081.
26. R. I. Kureshy, N. H. Khan, S. H. R. Abdi, A. K. Bhatt and P. Iyer, *J. Mol. Catal.*, **1997**, 121, 25.
-

Chapter 3

Chiral Schiff base metal complexes derived from 4-methyl 2,6-di[(S)-(+)-1-phenylethyliminomethyl]phenol and relevant catalysis

3.1. Abstract

New chiral Schiff base ligand L^2 (L^2 = 4-methyl-2,6-di[(S)-(+)-1-phenylethyliminomethyl]phenol) and its complexes of first-row transition metals (Zn, Cu, Ni, Co, Fe and Mn) have been synthesized starting from 2,6-diformyl-4-methylphenol and S-(–)-1-phenylethylamine. Characterization of the ligand L^2 and its metal complexes **8–14** (M = Zn^{+2} , **8**; Cu^{+2} , **9**; Ni^{+2} , **10**; Co^{+2} , **11**; Fe^{+2} , **12**; Mn^{+2} , **13**; Cu^{+2} , **14**) were carried out by microanalysis, IR, UV/Vis, fluorescence and CD spectral studies. Structures of zinc complex **8** and copper complex **9** were determined by single crystal X-ray crystallographic methods. Chiral Zn(II) complex, $[ZnL^2Cl_2]$ **8** self-assembles *via* C–H \cdots Cl hydrogen bonding into supramolecular helices.

Ligand L^2 and the complexes **8–14**, exhibit circular dichroism and emission signals at room temperature. Of these complexes zinc complex **8** is highly fluorescent ($\lambda = 496$ nm, $\phi_{em} = 0.46$) in methanol solution. Crystal data for zinc complex **8**: Orthorhombic space group $P2_12_12_1$, $a = 9.614(2)$ Å, $b = 13.825(3)$ Å, $c = 18.667(3)$ Å, $V = 2481.1(8)$ Å³, $Z = 4$. Crystal data for copper complex **9**: Orthorhombic space group $P2_12_12_1$, $a = 16.9457(6)$ Å, $b = 18.1124(7)$ Å, $c = 30.9295(11)$ Å, $V = 9493.11(6)$ Å³, $Z = 8$. The coordination geometry around the metal center in both complexes is distorted-tetrahedral.

Catalytic activities of the chiral Schiff base complexes for the oxidation reactions of styrene, *cis*-stilbene and *trans*-stilbene were carried out in CH₃CN using iodosylbenzene (PhIO) as the terminal oxidant at room temperature. Epoxidation of

cis-stilbene catalyzed by **13**, yields up to 25% with 70% of enantiomeric excess at room temperature.

3.2. Introduction

Asymmetric epoxidation of alkenes is one of the important methods for the synthesis of chiral intermediates in the field of pharmaceuticals and agrochemicals.¹ The enantioselective preparation of epoxides is a challenging and important synthetic problem since these compounds are highly valuable chiral synthons. Of the numerous approaches, the most well known one is the Sharpless method.²

Commonly studied metal catalysts for the asymmetric epoxidation of unfunctionalized olefins are chiral metalloporphyrins and manganese-salen complexes. Among the most useful systems for the asymmetric epoxidation of non-functionlized olefins is the Jacobsen-Katsuki salen-Mn catalyzed reactions.³ Metalloporphyrins usually exhibit high turnover numbers and moderate enantioselectivities.⁴ Recently, several other types of metal catalysts for the asymmetric epoxidation of olefins have been reported. These include nickel complexes bearing cyclic or acyclic tetraaza multidentate ligands.⁵

There has been considerable interest on helical supramolecular architectures, particularly on helices from coordination compounds.⁶ In most of these helical structures, the building units, e.g., coordination compounds are linked via covalent bonds.⁷ Even though supramolecular architecture has largely capitalized on non-covalent (e.g., hydrogen bonding) interactions,⁸ hydrogen-bonded assemblies of coordination compounds that lead to helical structures have not been explored much. Supramolecular left-handed helix, formed by C–H...Cl hydrogen bonding interactions, using a chiral Zn(II) complex, [ZnL²Cl₂] **8** (L² = 4-methyl-2,6-di[(S)-(+)-1-phenylethyliminomethyl] phenol) as a building unit. Compound **8** exhibits both chirality and emissive properties. Coordination compounds with both circular dichroism and emission signals at room temperature are well documented in literature.⁹

Chiral Schiff base metal complexes are useful catalysts for selective organic transformation reactions. View of this aspect, we synthesized new chiral Schiff base ligand **L**² and its complexes with first-row transition metals (Zn, Cu, Ni, Co, Fe and Mn). Herein we discuss the characterization of the ligand **L**² and its metal complexes **8–14** and examined their catalytic activity towards the oxidation reactions of the styrene, *cis*-stilbene and *trans*-stilbene.

3.3. Experimental

3.3.1. Chemicals and reagents

All the chemicals used in this study were commercially available and used as received. 2,6-diformyl-4-methylphenol was synthesized starting from p-cresol using published procedure.¹⁰ S-(–)-1-phenylethylamine was purchased from Lancaster. HPLC grade solvents were used for spectral analysis. All metal salts were purchased commercially and used as received. All other solvents were purified and dried by the usual methods.¹¹ Iodobenzenediacetate, styrene, *cis*-stilbene and *trans*-stilbene were purchased from Aldrich chemicals. Iodosylbenzene was prepared according to literature procedure.²²

3.3.2. Physical measurements

Elemental analyses were carried out on a Perkin-Elmer 240C CHN analyzer. The ¹H-NMR spectra were recorded with a Bruker DRX-400 spectrometer using CDCl₃ as the solvent. Tetramethylsilane (TMS) was the internal standard. Infrared spectra were recorded on a Jasco Model 5300 FT-IR spectrophotometer. The spectra of the solid samples were recorded using KBr pellets. The UV-visible spectra were recorded with Shimadzu model UV-3101PC UV-vis spectrophotometer. The CD spectra were measured with a JASCO J-810 spectropolarimeter.

The pale yellow single crystal of zinc complex **8** was mounted on a glass fiber on CAD4 Nonius Enraf MACH 3 diffractometer, equipped with graphite monochromated Mo-K_α radiation ($\lambda = 0.71073 \text{ \AA}$). 25 carefully centered reflections were used to determine cell parameters. XTAL 3.5 version was employed for the data reduction.¹² The

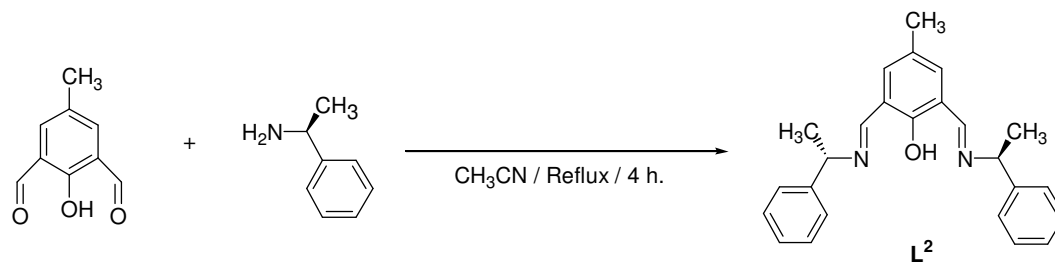
solution and refinement were carried out using SHELX-97.¹³ The X-ray intensity data for the copper **9** was measured at 100(2) K on a Bruker SMART APEX CCD area detector system equipped with a graphite monochromator and a Mo-K α fine-focus sealed tube ($\lambda = 0.71073\text{\AA}$) operated at 1500 W power (50 kV, 30 mA). The detector was placed at a distance of 4.995 cm from the crystal. The SMART software was used for intensity data acquisition and the SAINT-Plus software was used for data extraction. Data were corrected for absorption effects using the multi-scan technique (SADABS). The solution and refinement of the data were obtained using SHELXL-97¹⁴ program.

Optical rotation was measured with an AUTOPOL-II automatic polarimeter (readability $\pm 0.01^\circ$). Gas chromatographic analyses were carried out on a Shimadzu GC 14B instrument equipped with a stainless steel packed column (5 m, 5 % SE 30) and a chiral capillary column (Supelco α -DEX 325, 30m length, 0.25mm id, 0.25 μ m film thickness) and a flame ionization detector (FID). HPLC analyses of *cis*-stilbene epoxide and *trans*-stilbene epoxide products were carried out on a Shimadzu SCL-10A instrument equipped with CHIRALCEL OD-H using Class-VP program.

3.3.3. Synthesis

3.3.3.1. Synthesis of chiral Schiff base ligand, **L**²

To a solution of 2,6-diformyl-4-methylphenol (0.492 g, 3 mmol) in 20 mL of acetonitrile was added S-(–)-1-phenylethylamine (0.727 g, 6 mmol) in 5 mL of acetonitrile. The reaction mixture was refluxed for 4 hours. The solution was filtered, concentrated on rotary evaporator to dryness. The resulting chiral Schiff base ligand **L**² (4-methyl-2,6-di[(S)-(+)-1-phenylethyliminomethyl]phenol) is semi solid (Yield: 0.9 g, 81%). The reaction sequence is shown in Scheme 3.1.



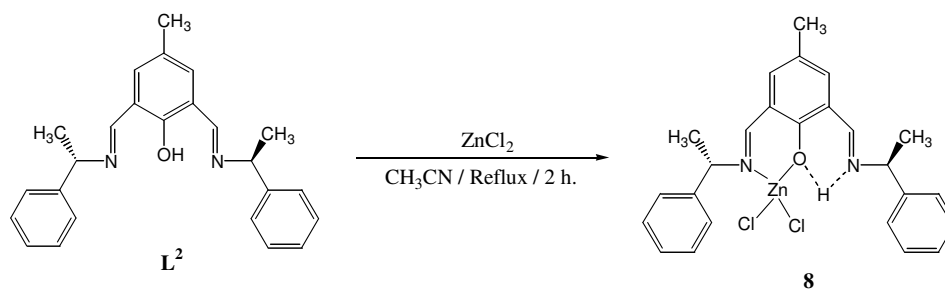
Scheme 3.1. Schematic representation of the chiral Schiff base ligand L^2 .

Characterization data for L^2

Optical rotation $[\alpha]_D^{25}$: + 116 (c 1, ethanol); M. F.: $C_{25}H_{26}N_2O$; M. W: 370.49 g mol⁻¹; IR (ν cm⁻¹, KBr pellet): 1641, 1598; ¹H NMR ($CDCl_3$): δ 1.63 (d, 6H, J = 5.86 Hz, CH_3), 2.29 (s, 3H, Ar- CH_3), 4.59 (q, 2H, J = 6.61 Hz, CH), 7.28 - 7.38 (m, 12H, Ar-CH), 8.64 (s, 2H, HC=N); CD λ_{max} (mdeg) (CH_3OH): 350 (+4.98), 244 (+24.03); CD λ_{max} (mdeg) (CH_3CN): 343 (+5.83), 265 (+25.75); UV-Vis (CH_3CN) [λ_{max}/nm ($\epsilon/dm^3 mol^{-1} cm^{-1}$): 350 (7000), 244 (34600); UV-Vis (CH_3OH) [λ_{max}/nm ($\epsilon/dm^3 mol^{-1} cm^{-1}$): 440(264), 350 (693), 244 (3645).

3.3.3.2. Synthesis of $[L^2ZnCl_2]$, **8**

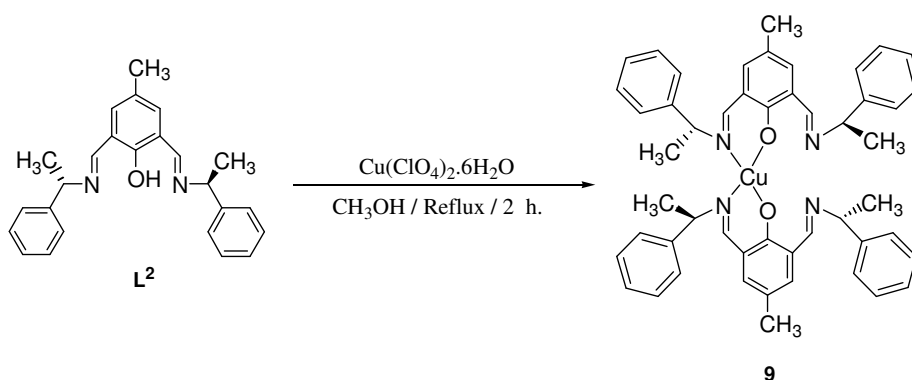
To a solution of 2,6-diformyl-4-methylphenol (2.46 g, 15 mmol) in 40 mL of acetonitrile was added S-(−)-1-phenylethylamine (3.63 g, 30 mmol) in 10 mL of acetonitrile. The reaction mixture was refluxed for 4 hours. To the resulting Schiff base, formed in situ, anhydrous $ZnCl_2$ (2.04 g, 15 mmol) was added and refluxed for another 2 hours. It was then filtered and the filtrate was kept in an open conical flask at room temperature for one week yielding 5.62g of pale yellow crystals of $[L^2ZnCl_2]$ **8** (Yield: 74%). The reaction sequence is shown in Scheme 3.2.



Scheme 3.2. Schematic representation of the chiral Schiff base zinc complex **8**.

3.3.3.3. Synthesis of $[L^2_2Cu](ClO_4)_2$, **9**

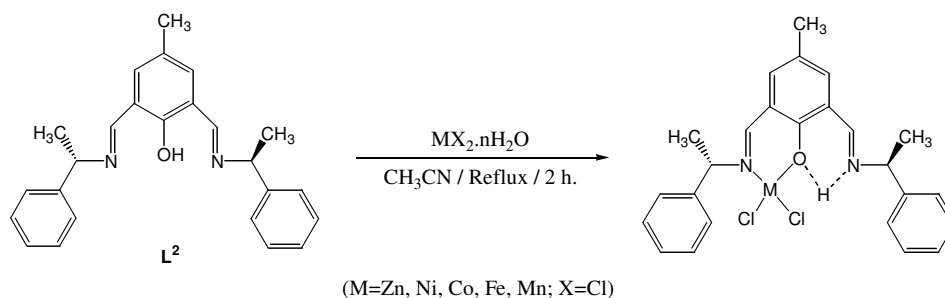
To a solution of 2,6-diformyl-4-methylphenol (0.164 g, 1 mmol) in 20 mL of methanol was added S-(–)-1-phenylethylamine (0.242 g, 2 mmol) in 10 mL of methanol. The reaction mixture was refluxed for 4 hours. To the resulting Schiff base, formed in situ, $Cu(ClO_4)_2 \cdot 6H_2O$ (0.370 g, 1 mmol) was added and refluxed for another 2 hours. The solvent evaporated using rotary evaporator. The resulting copper complex was recrystallized from methanol solution. Green single crystals were obtained by the slow evaporation at room temperature (Yield: 70%). The reaction sequence is shown in Scheme 3.3.



Scheme 3.3. Schematic representation of chiral Schiff base copper complex **2**.

3.3.3.4. General synthetic procedure for complexes, **10–14**

To a solution of 2,6-diformyl-4-methylphenol (0.164 g, 1 mmol) in 20 mL of acetonitrile was added S-(–)-1-phenylethylamine (0.242 g, 2 mmol) in 10 mL of acetonitrile. The reaction mixture was refluxed for 4 hours. To the resulting Schiff base, formed in situ, hydrated MX_2 ($M = Ni$, **10**; Co , **11**; Fe , **12**; Mn , **13** and Cu , **14**; $X = Cl$) (1 mmol) was added and refluxed for another 2 hours. The solvent was removed using rotary evaporator. The resulting metal complexes were washed with hexane and recrystallized from acetonitrile. The reaction sequence is shown in Scheme 3.4.



Scheme 3.4. Schematic representation of chiral Schiff base metal complexes.

3.3.3.5. Characterization data for complexes, 8–14

Characterization data for [L²ZnCl₂], 8

M. F.: C₂₅H₂₆N₂OZnCl₂; M. W.: 506.78 g mol⁻¹; IR (ν cm⁻¹, KBr pellet): 1660, 1628, 1547; ¹H NMR (CDCl₃) δ: 1.76 (d, 3H, J = 6.82 Hz, CH₃), 2.06 (d, 3H, J = 6.82 Hz, CH₃), 2.13 (s, 3H, Ar-CH₃), 4.58 (q, 2H, J = 6.84 Hz, CH), 7.16 - 7.48 (m, 12H, Ar-CH), 7.97 (s, 1H, HC=N), 8.18 (s, 1H, HC=N); CD λ_{max} (mdeg) (CH₃CN): 411 (+24.79), 302 (+0.51), 256 (+52.71), 217(-123.74); UV-Vis (CH₃CN) [λ_{max}/nm (ε/dm³ mol⁻¹ cm⁻¹): 414 (4400), 353 (6700), 243 (34500); UV-Vis (CH₃OH) [λ_{max}/nm (ε/dm³ mol⁻¹ cm⁻¹): 407(630), 361 (342), 247 (2515); CHN Analysis :Calcd.: C, 59.25; H, 5.17; N, 5.53%; Found: C, 59.26; H, 5.24; N, 5.47 %.

Characterization data for 9

M. F.: C₅₀H₅₂N₄O₁₀CuCl₂; M. W.: 1003.42 g mol⁻¹; IR (ν cm⁻¹, KBr pellet): 1649, 1548, 1091, 621; CD λ_{max} (mdeg) (CH₃OH): 406 (-1.91), 310 (-2.56), 250 (-6.04), 230 (3.79); UV-Vis (CH₃OH) [λ_{max}/nm (ε/dm³ mol⁻¹ cm⁻¹): 663 (1166), 408(1172), 246 (3765); CHN Analysis: Calcd.: C, 59.85; H, 5.22; N, 5.58%; Found: C, 59.92; H, 5.28; N, 5.63%.

Characterization data for 10

Yield: 75%; Colour: Pale green; M.F.: C₂₅H₂₆N₂ONiCl₂; M. W.: 500.09 g mol⁻¹; IR (ν cm⁻¹, KBr pellet): 3414, 1647, 1543; CD λ_{max} (mdeg) (CH₃OH): 493 (1.16), 310

(-1.06), 255 (-3.66), 221 (2.03), 208 (-2.41); UV-Vis (CH₃OH) [$\lambda_{\text{max}}/\text{nm}$ ($\epsilon/\text{dm}^3 \text{ mol}^{-1} \text{ cm}^{-1}$)]: 616 (360), 395 (826), 319 (359), 250 (3248); CHN Analysis: Calcd.: C, 60.04; H, 5.24; N, 5.60%; Found.: C, 60.13; H, 5.18; N, 5.64%.

Characterization data for 11

Yield: 80%; Colour: Brown; M. F.: C₂₅H₂₆N₂OCuCl₂; M. W.: 500.33 g mol⁻¹; IR ($\nu \text{ cm}^{-1}$, KBr pellet): 3468, 1649, 1545; CD λ_{max} (mdeg) (CH₃OH): 500 (1.10), 410 (-0.87), 275 (-2.82), 220 (-2.20); UV-Vis (CH₃OH) [$\lambda_{\text{max}}/\text{nm}$ ($\epsilon/\text{dm}^3 \text{ mol}^{-1} \text{ cm}^{-1}$)]: 407 (941), 358 (787), 245 (4810); CHN Analysis: Calcd.: C, 60.01; H, 5.24; N, 5.60%; Found.: C, 59.97; H, 5.33; N, 5.57%.

Characterization data for 12

Yield: 65%; Colour: Dark brown; M. F.: C₂₅H₂₆N₂OFeCl₂; M. W.: 497.24 g mol⁻¹; IR ($\nu \text{ cm}^{-1}$, KBr pellet): 3414, 1643, 1548; CD λ_{max} (mdeg) (CH₃OH): 711 (1.66), 463 (1.21), 353 (0.93), 280 (-0.58), 243 (1.64), 205 (-9.23); UV-Vis (CH₃OH) [$\lambda_{\text{max}}/\text{nm}$ ($\epsilon/\text{dm}^3 \text{ mol}^{-1} \text{ cm}^{-1}$)]: 523 (7013), 415 (366), 343 (779), 260 (2196), 244 (3059); CHN Analysis: Calcd.: C, 60.39; H, 5.27; N, 5.63%; Found.: C, 60.43; H, 5.35; N, 5.79%.

Characterization data for 13

Yield: 85%; Colour: Brown; M. F.: C₂₅H₂₆N₂OMnCl₂; M. W.: 496.33 g mol⁻¹; IR ($\nu \text{ cm}^{-1}$, KBr pellet): 3500, 1649, and 1541; CD λ_{max} (mdeg) (CH₃OH): 456 (1.66), 356 (0.7), 247 (1.44), 212 (-5.57); UV-Vis (CH₃OH) [$\lambda_{\text{max}}/\text{nm}$ ($\epsilon/\text{dm}^3 \text{ mol}^{-1} \text{ cm}^{-1}$)]: 436 (326), 351 (856), 245 (4247); CHN Analysis: Calcd.: C, 60.50; H, 5.28; N, 5.64%; Found.: C, 60.43; H, 5.31; N, 5.67%.

Characterization data for 14

Yield: 90%; Colour: Green; M. F.: C₂₅H₂₆N₂OCuCl₂; M. W.: 504.94 g mol⁻¹; IR ($\nu \text{ cm}^{-1}$, KBr pellet): 3485, 1630, 1548; CD λ_{max} (mdeg) (CH₃OH): 380 (-1.40), 270 (-4.03); UV-Vis (CH₃OH) [$\lambda_{\text{max}}/\text{nm}$ ($\epsilon/\text{dm}^3 \text{ mol}^{-1} \text{ cm}^{-1}$)]: 714 (4020), 367 (640), 257 (2610); CHN Analysis: Calcd.: C, 59.47; H, 5.19; N, 5.55%; Found.: C, 59.43; H, 5.17; N, 5.62%.

3.4. Results and discussion

Synthetic details of the chiral complexes **8–14** are given in the experimental section 3.3.3. In all the complexes, chiral source is 4-methyl-2,6-di[(S)-(+)-1-phenylethyliminomethyl]phenol) **L**². The IR spectrum of the ligand shows stretching bands at around 1641, 1598 cm⁻¹ corresponding to the C=N and the phenolic C-O groups respectively. The formation of chiral Schiff base ligand was confirmed by the absence of aldehydic C=O stretch of 2,6-diformyl-4-methylphenol at 1680 cm⁻¹. The CHN analytical data of the complexes match with the mononuclear compositions. The ligand **L**² and its metal complexes **8–14** are CD active.

3.4.1. Zinc complex [**L**²ZnCl₂], **8**

The optical activity of the zinc complex is induced by the chiral ligand **L**².¹⁹ The UV-visible spectrum of the zinc complex is characterized by an intense band at 243 nm and two peaks at 353 and 414 nm respectively as shown in Figure 3.1. The circular dichroism (CD) spectrum of the chiral ligand **L**² shows positive bands around 350 nm and 245 nm. The CD spectrum of **8**, as expected, exhibits positive bands (Figure 3.1).

The fluorescence properties of **L**² and [**L**²ZnCl₂] **8** examined in methanol and acetonitrile reveal that Zn²⁺ ion enhances the fluorescence. The fluorescence spectra of **L**² and [**L**²ZnCl₂] **8** in methanol and acetonitrile solutions are shown in Figure 3.2. There is significant band shift and increase in fluorescence intensity for [**L**²ZnCl₂] **8**. The maximum excitation of the zinc complex is at 414 nm, and the maximum emission is at 504 nm. The fluorescence intensity at 504 nm is *ca.* 12 times of that of the ligand at 580 nm (Figure 3.2). The emission band (at 580 nm) of the free ligand **L**² does not shift with its varying concentrations in MeCN solutions. On the other hand, the emission band of the complex [**L**²ZnCl₂] **8** is concentration dependent. The band maxima gradually shift to lower energy region with increasing concentrations. This shift could be due to the inter-molecular hydrogen bonding association of the complex [**L**²ZnCl₂] **8** (Figure 3.2) at relatively higher concentrations. The emission quantum

yield (ϕ_{em}) of the free ligand \mathbf{L}^2 at ambient temperature, using 1,6-diphenyl 1,3,5-hexatriene (dpht) in MeCN as standard, was found to be 0.0053 and that of the complex $[\text{ZnL}^2\text{Cl}_2]$ **8** at 0.051.

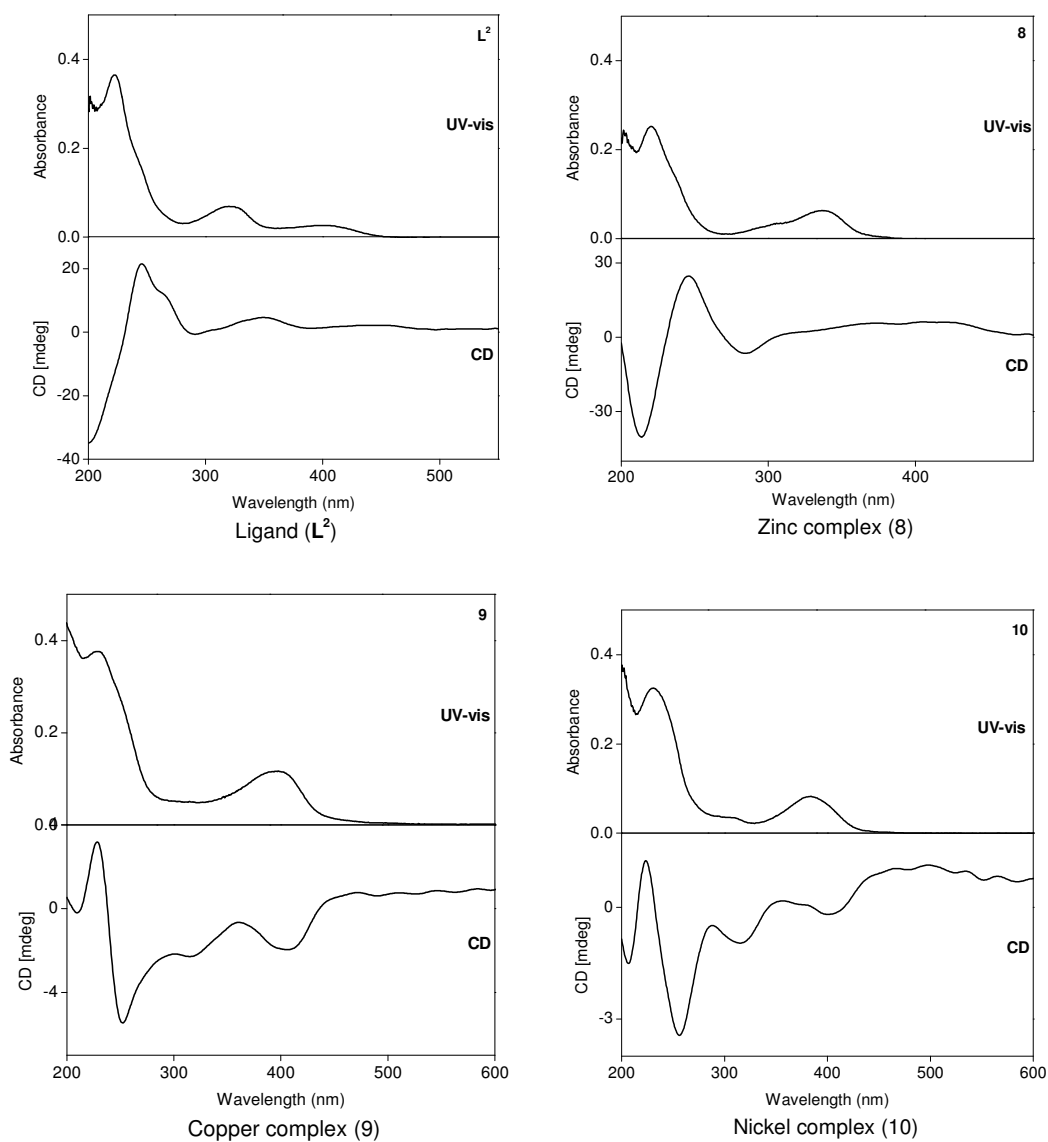


Figure 3.1. CD spectra and UV-vis spectra of ligand \mathbf{L}^2 and its Zn^{2+} , Cu^{2+} , Ni^{2+} complexes in MeOH solution (concentrations = $1 \times 10^{-4}\text{M}$ for CD and $1 \times 10^{-5}\text{M}$ for UV-vis each experiment).

The emission quantum yield (ϕ_{em}) of the free ligand L^2 at ambient temperature, using 1,6-diphenyl 1,3,5-hexatriene (dpht) in MeOH as standard, was found to be 0.0053 and that of the complex $[\text{ZnL}^2\text{Cl}_2]$ **8** is highly enhanced as $\phi_{\text{em}} = 0.46$ (Figure 3.2). The blue shift of the emission band (504 nm) in the complex **8** as compared to the emission band at 580 nm of free ligand L^2 is quite unexpected as one would expect the emission maximum of the free ligand L^2 to be at higher energy relative to the complex due to its relatively high-energy excitation band. This anomaly can be explained by the fact that excited states resulting from complexes of Zn(II) are typically ligand-centered (LC) owing to the inability of the d^{10} metal center to participate in low energy charge transfer or metal-centered transitions.²⁰

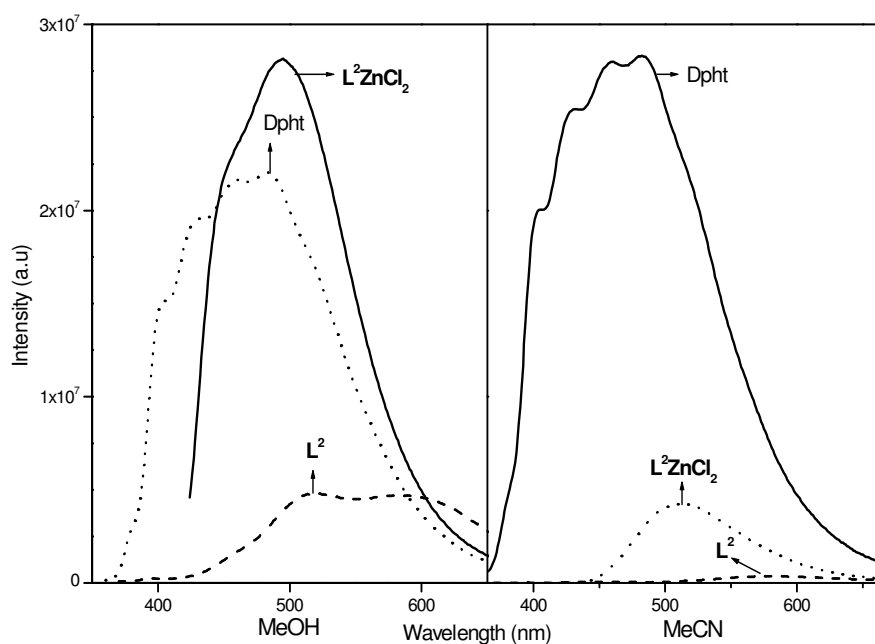


Figure 3.2. Fluorescence spectra of ligand L^2 , **8** and dpht (standard) at 298 K in (0.2 OD) Left : methanol and right: acetonitrile solutions.

Therefore, the emission from $[\text{ZnL}^2\text{Cl}_2]$ **8** is believed to arise from an excited state centered on the L^2 which contains a phenolic proton. It is well-established that the emissive organic phenol, e.g., 2,6-diformyl-4-methylphenol undergoes blue shift of its emission band (from 530 nm to 445 nm) on treatment with a base B (e.g.,

piperidine or triethylamine) and this observation is interpreted to support the existence of an equilibrium between undissociated phenol and a proton-transferred species of phenol with the formation of phenoxide anion and BH^+ cation.²¹

The same analogy can be extended to the present system, because the phenolic proton of the ligand L^2 (Scheme 3.1) gets deprotonated on complexation with Zn^{2+} and this proton is transferred to the adjacent imine nitrogen (of the same ligand L^2) with the formation of NH^+ . This proton transfer is also evidenced by IR spectral studies and crystal structure determination of complex $[\text{ZnL}^2\text{Cl}_2]$ **8**. Indeed, this proton is nicely located on uncoordinated imine nitrogen in the crystal structure of **8**.

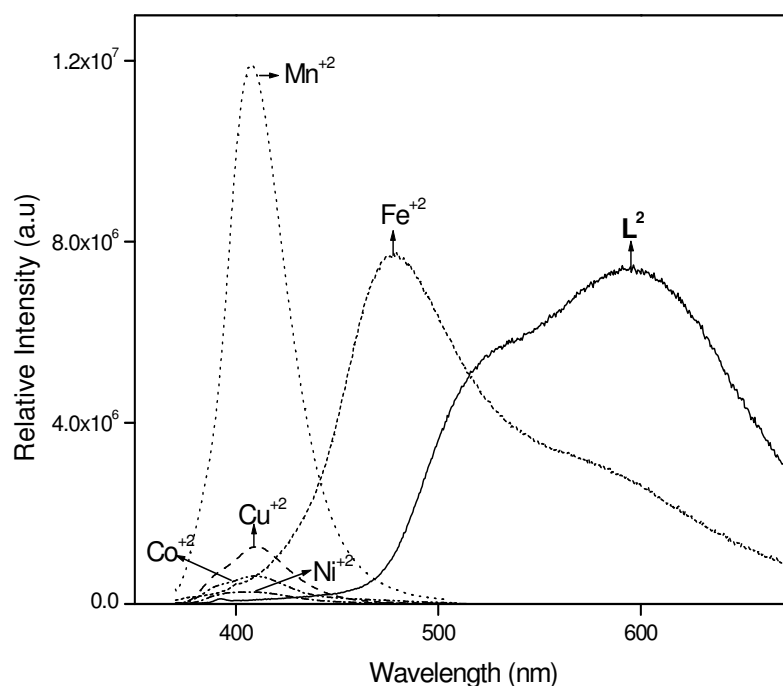


Figure 3.3. Emission spectra of ligand L^2 and Cu^{2+} , Ni^{2+} , Co^{2+} , Fe^{2+} , Mn^{2+} complexes in MeOH (concentrations = $1 \times 10^{-4}\text{M}$ for each experiment).

An emission experiment on the free ligand L^2 in presence of an added base, triethylamine in MeCN solution indicates the existence of an equilibrium between an undissociated L^2 and a proton transferred species of L^2 . The emission spectra of other metal complexes were shown in Figure 3.3.

X-ray crystallography of $[\text{L}^2\text{ZnCl}_2]$, **1**

The enantiopure ligand L^2 (Scheme 3.1) is prepared by Schiff-base condensation reaction of one equivalent of 2,6-diformyl-4-methyl phenol with two equivalents of (S)-(-)-1-phenylethylamine in acetonitrile. Reaction of Zn(II) chloride and optically pure ligand L^2 afforded the neutral complex $[\text{Zn}^{\text{II}}\text{L}^2\text{Cl}_2]$ **8** in good yield (Scheme 3.2). Crystals of $[\text{ZnL}^2\text{Cl}_2]$ **8** were characterized by elemental and spectral analyses. Single crystal X-ray structure determination data are given in Table 3.1. Bond lengths, bond angles are given in Table 3.2. The molecular structure of the Zn(II) complex **8** is presented in Figure 3.4.

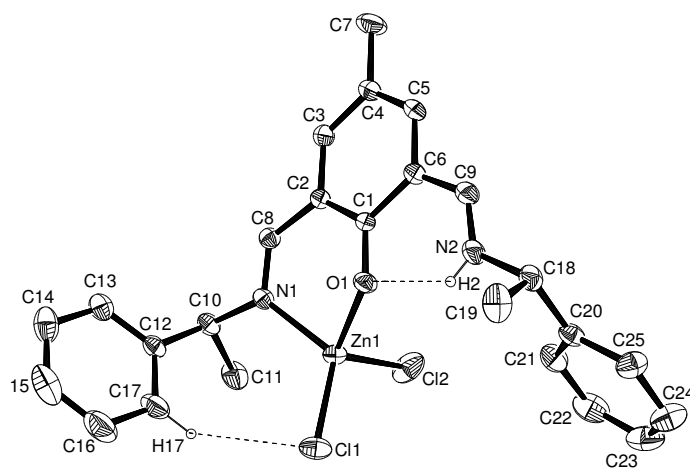


Figure 3.4. Thermal ellipsoid plot of the structure of $[\text{ZnL}^2\text{Cl}_2]$ **8**. C(18) and C(10) are chiral centers. Thermal ellipsoids are at 40% probability level. Hydrogen atoms have been omitted for clarity. Hydrogen atoms, involved in the intra-molecular hydrogen bonding interactions, are shown.

The zinc atom in **8** is four-coordinated with N(1), O(1) donors (from the ligand L^2) and two chloride ligands, in a distorted tetrahedral geometry. The chiral ligand L^2 (Chiral centers are C(18) and C(10)) has two arms with two donor nitrogen atoms. One nitrogen N(1) of one arm is coordinated to zinc and the nitrogen N(2) of the other arm remains uncoordinated. This is because the phenolic hydroxyl O(1) gets deprotonated and N(2) gets protonated during complexation. This is also evidenced in

the IR spectrum of the complex, in which the hydroxyl stretching of the free ligand **L**² at $\sim 3400\text{ cm}^{-1}$ is not observed. This kind of proton transfer is known in literature.¹⁵ There are two intra-molecular hydrogen bonds: N(2)–H(2)····O(1) (2.615(5)) and C(17)–H(17)····Cl(1) (3.533(7)). Complex **8** self-assembles *via* hydrogen bonding into supramolecular helices. It is the C(13)–H(13)····Cl(2) intermolecular hydrogen bond (3.665(6) Å in length) that drives the formation of the helix as shown in Figure 3.5.

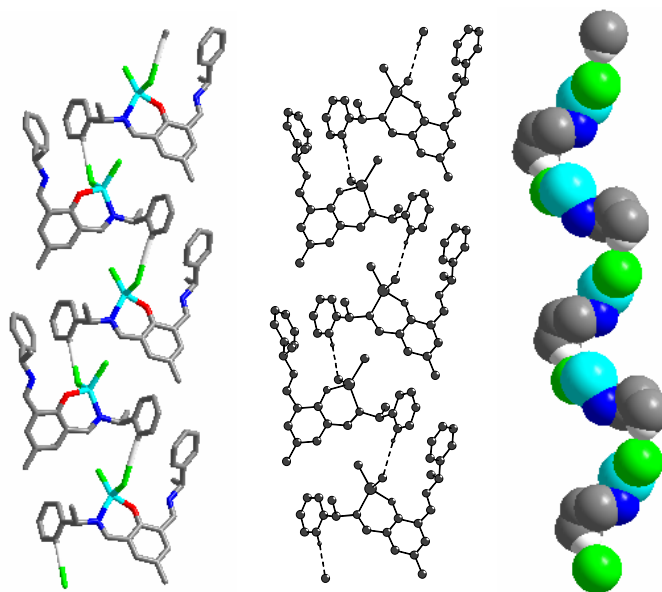


Figure 3.5. Intermolecular C–H····Cl hydrogen bonded interactions between adjacent molecules that leads to the formation of hydrogen bonded helices in $[\text{ZnL}^2\text{Cl}_2]$ **8**. Left: ball and stick presentation, middle: wire-frame presentation and right: space-filling plot (helical backbone). All the hydrogen atoms except those involved in hydrogen bonding have been omitted for clarity. Colour: red: oxygen; blue: nitrogen; green: Chlorine; cyan: zinc; gray: carbon.

A systematic investigation of C–H····Cl hydrogen bonding interactions, using inorganic supramolecular synthons, has recently been reported.⁸ The hydrogen bonding parameters of the C–H····Cl bond (present work) are quite comparable to those of C–H····Cl bonds in other reported systems.^{16,17} The path of the helix (Figure 3.5) can be traced by following the hydrogen bonds counter clockwise around the two-fold screw axis of the helix. At the molecular level, the crystal contains a single enantiomer of the complex **8**.

Table 3.1. Crystallographic parameters of the mononuclear zinc **8** and copper **9**

Compound	[L ² ZnCl ₂], 8	[L ² Cu](ClO ₄) ₂ , 9
Empirical formula	C ₂₅ H ₂₆ N ₂ OCl ₂ Zn	C ₅₀ H ₅₂ N ₄ O ₁₀ Cl ₂ Cu
<i>M</i>	506.75	1003.42
<i>T</i> /K	293(2)	100(2)
$\lambda/\text{\AA}$	0.71073/3197	0.71073
Crystal system	Orthorhombic	Orthorhombic
Space group	<i>P</i> 2 ₁ 2 ₁ 2 ₁	<i>P</i> 2 ₁ 2 ₁ 2 ₁
<i>a</i> /\AA	9.614(2)	16.9457(6)
<i>b</i> /\AA	13.825(3)	18.1124(7)
<i>c</i> /\AA	18.667(3)	30.9295(11)
<i>U</i> /\AA ³ , <i>Z</i>	2481.1(8), 4	9493.1(6), 8
<i>D_c</i> /mg m ⁻³	1.357	1.401
μ/mm^{-1}	1.224	0.636
<i>F</i> (000)	1048	4168
Crystal size/mm	0.62 x 0.60 x 0.60	0.21 x 0.40 x 0.06
θ range /°	1.83 to 27.45	1.30 to 28.26
Limiting indices	0 ≤ <i>h</i> ≤ 12, 0 ≤ <i>k</i> ≤ 17, 0 ≤ <i>l</i> ≤ 24	-21 ≤ <i>h</i> ≤ 22, -20 ≤ <i>k</i> ≤ 23, -40 ≤ <i>l</i> ≤ 38
Reflections collected	3197	60245
Reflections [<i>I</i> > 2σ(<i>I</i>)]	3197	22058
Data, parameters	3197, 284	22058, 1207
Goodness-of-fit on <i>F</i> ²	1.065	1.037
Final <i>R</i> indices [<i>I</i> > 2σ(<i>I</i>)]	<i>R</i> 1 = 0.0352, <i>wR</i> 2 = 0.0743	<i>R</i> 1 = 0.0793, <i>wR</i> 2 = 0.1567
<i>R</i> indices (all data)	<i>R</i> 1 = 0.0580, <i>wR</i> 2 = 0.0907	<i>R</i> 1 = 0.1305, <i>wR</i> 2 = 0.1794

Table 3.2. Selected bond lengths (Å) and bond angles (°) of zinc complex, **8**

Bond lengths			
Zn(1)-O(1)	1.984(3)	C(2)-C(3)	1.384(6)
Zn(1)-N(1)	2.036(3)	C(2)-C(8)	1.462(6)
Zn(1)-Cl(1)	2.2137(13)	C(3)-C(4)	1.388(7)
Zn(1)-Cl(2)	2.2149(16)	C(4)-C(5)	1.360(7)
O(1)-C(1)	1.298(5)	C(4)-C(7)	1.499(7)
N(2)-C(9)	1.259(6)	C(5)-C(6)	1.388(6)
N(2)-C(18)	1.465(6)	C(6)-C(9)	1.419(6)
N(1)-C(8)	1.271(5)	C(10)-C(12)	1.513(7)
N(1)-C(10)	1.498(5)	C(10)-C(11)	1.539(7)
C(1)-C(2)	1.411(6)	C(12)-C(13)	1.371(7)
C(1)-C(6)	1.446(6)	C(12)-C(17)	1.383(7)
C(13)-C(14)	1.385(8)	C(14)-C(15)	1.353(10)
Bond angles			
O(1)-Zn(1)-N(1)	92.17(13)	C(8)-N(1)-Zn(1)	119.4(3)
O(1)-Zn(1)-Cl(1)	110.15(9)	C(10)-N(1)-Zn(1)	124.4(3)
N(1)-Zn(1)-Cl(1)	122.67(11)	O(1)-C(1)-C(2)	123.7(3)
O(1)-Zn(1)-Cl(2)	108.32(11)	O(1)-C(1)-C(6)	120.1(4)
N(1)-Zn(1)-Cl(2)	109.18(11)	N(1)-C(8)-C(2)	127.1(4)
Cl(1)-Zn(1)-Cl(2)	112.04(6)	N(2)-C(9)-C(6)	126.1(4)
C(1)-O(1)-Zn(1)	120.1(3)	N(1)-C(10)-C(12)	110.2(4)
C(9)-N(2)-C(18)	128.3(4)	N(1)-C(10)-C(11)	107.9(4)
C(8)-N(1)-C(10)	115.5(4)	C(2)-C(1)-C(6)	116.2(4)
N(2)-C(18)-C(20)	111.7(4)	C(12)-C(10)-C(11)	113.8(4)
N(2)-C(18)-C(19)	107.8(4)	C(20)-C(18)-C(19)	112.8(5)

This local chirality translates throughout the crystal into the formation of only left-handed helices at the supramolecular level (Figure 3.5). Three zinc complex fragments form one helix turn in **8** with a pitch of 13.825 Å. The absolute configuration of the compound molecule was successfully determined by refining the Flack parameter [0.017(19)].¹⁸ The important crystallographic parameters are given in Table 3.1. Selected bond lengths and bond angles are listed in Table 3.2.

3.4.2. Copper complex $[\text{L}_2\text{Cu}](\text{ClO}_4)_2$, **9**

The chiral copper complex was synthesized in methanol in good yields by the procedure given in section 3.3.3.3 (Scheme 3.3). The IR spectrum of the complex $[\text{L}_2\text{Cu}](\text{ClO}_4)_2$ shows strong bands at around 1091 and 621 cm^{-1} corresponding to the perchlorate anions and other two strong stretching bands at around 1649, 1548 cm^{-1} corresponding to the C=N and phenolic C-O groups.

Circular dichroism spectrum of the complex in methanol solution is shown in Figure 3.1. Bands appear at 406(-1.91), 310(-2.56) nm and the high intensity $\pi \rightarrow \pi^*$ transition band at 250(-6.04). Appearance of these signals confirms that the complex is chiral. The electronic spectrum of the chiral copper complex in methanol exhibits three bands in the range of 220-900 nm. The broad band at 663 nm is due to d-d electronic transitions, the strong band at 408 nm is due to ligand to metal charge transfer transition and an intra ligand transition band appears at 246 nm. The analytical data of the complex match with the mononuclear composition of $[\text{L}_2\text{Cu}](\text{ClO}_4)_2$ **9**. The complex was well studied by single crystal X-ray structure determination.

X-ray crystallography of $[\text{L}_2\text{Cu}](\text{ClO}_4)_2$, **9**

The mononuclear copper complex crystallizes in orthorhombic $P2_12_12_1$ space group. The asymmetric unit consists of two crystallographically independent molecules and four perchlorate anions in the molecular structure of **9**. The ORTEP diagram of the copper complex with atom numbering scheme is shown in Figure 3.6

(9A and 9B). The important crystallographic parameters are given in Table 3.1. The copper atoms in each molecule (9A and 9B) are four coordinated with two phenolic oxygens and two imine nitrogens, from two ligands, in a distorted tetrahedral geometry. The chiral ligand L^2 in molecule, 9A (chiral centers are C(7), C(18), C(32) and C(43)) and in molecule, 9B (chiral centers are C(57), C(68), C(82) and C(93)) has two arms with two donor nitrogen atoms. Nitrogen atoms N(1) and N(3) of one arm is coordinated to copper and the nitrogens N(2) and N(4) of the other arm remain uncoordinated in molecule, 9A. Nitrogen atoms N(5) and N(7) of one arm is coordinated to copper and the nitrogen N(6) and N(8) of the other arm remain uncoordinated in molecule, 9B.

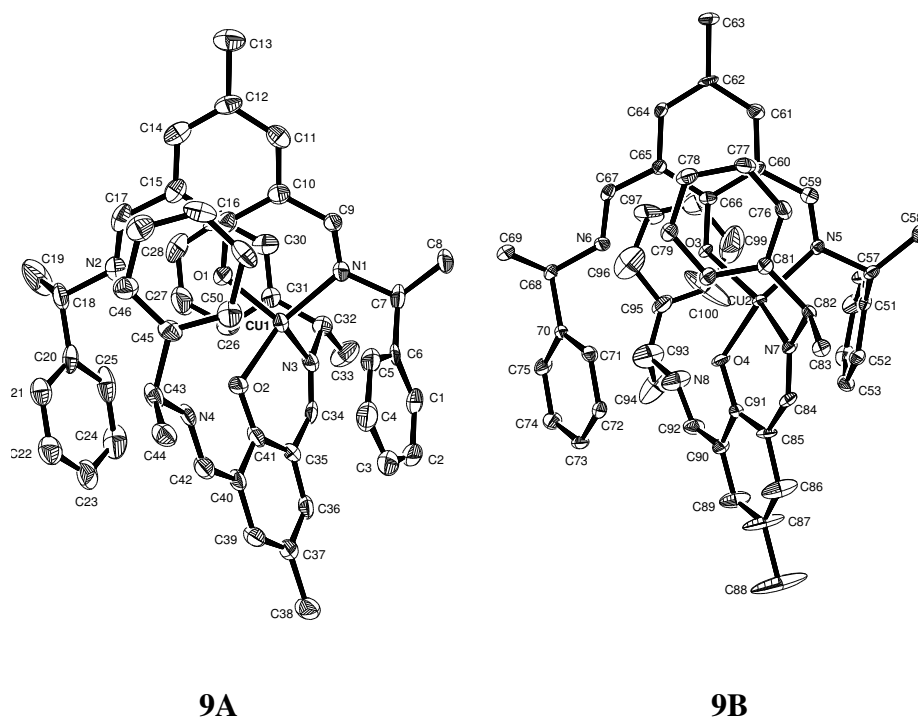


Figure 3.6. ORTEP diagram of the copper complex **9** (Individual molecules in the asymmetric unit of **9**). Chiral centers C(7), C(18), C(32), C(43) in 9A and C(57), C(68), C(82), C(93) are in 9B. Thermal ellipsoids are at 30% probability level. Hydrogen atoms have been omitted for clarity.

Table 3.3. Selected bond lengths (Å) and bond angles (°) of copper complex, **9**

Bond lengths			
Cu(2)-O(3)	1.925(4)	O(1)-C(16)	1.306(7)
Cu(2)-N(5)	1.948(5)	Cl(1)-O(6)	1.425(5)
Cu(2)-N(7)	1.972(4)	Cl(1)-O(8)	1.427(4)
Cu(2)-O(4)	1.900(4)	Cl(1)-O(5)	1.442(5)
Cu(1)-O(2)	1.902(4)	O(10)-Cl(2)	1.383(5)
Cu(1)-N(3)	1.946(5)	Cl(2)-O(11)	1.385(7)
Cu(1)-N(1)	1.975(5)	Cl(2)-O(9)	1.376(6)
Cu(1)-O(1)	1.897(4)	N(2)-C(17)	1.278(8)
O(2)-C(41)	1.308(7)	N(2)-C(18)	1.485(7)
N(1)-C(9)	1.273(7)	O(3)-C(66)	1.309(6)
N(1)-C(7)	1.487(7)	O(4)-C(91)	1.320(7)
Bond angles			
O(1)-Cu(1)-O(2)	88.60(17)	O(4)-Cu(2)-O(3)	91.12(16)
O(1)-Cu(1)-N(3)	146.7(2)	O(4)-Cu(2)-N(5)	149.8(2)
O(2)-Cu(1)-N(3)	92.50(18)	O(3)-Cu(2)-N(5)	93.10(18)
O(1)-Cu(1)-N(1)	94.06(19)	O(4)-Cu(2)-N(7)	92.77(18)
O(2)-Cu(1)-N(1)	142.64(19)	O(3)-Cu(2)-N(7)	148.12(18)
N(3)-Cu(1)-N(1)	104.7(2)	N(5)-Cu(2)-N(7)	99.15(19)
C(66)-O(3)-Cu(2)	123.0(4)	C(7)-N(1)-Cu(1)	113.9(4)
C(91)-O(4)-Cu(2)	124.0(4)	C(59)-N(5)-Cu(2)	123.8(4)
C(9)-N(1)-Cu(1)	123.5(4)	C(57)-N(5)-Cu(2)	113.2(3)
C(41)-O(2)-Cu(1)	122.4(3)	C(9)-N(1)-C(7)	121.9(5)
C(16)-O(1)-Cu(1)	127.2(4)	C(59)-N(5)-C(57)	122.7(5)

The phenolic groups are gets deprotonated and free arm of the imine-nitrogen are gets protonated. This suggests that they are securely bound in the second cavity of the coordination site by intra molecular hydrogen bonding to the nitrogen atoms. The free arms of the imine-N are far to coordinate with second metal. This is due to the fact that phenolic hydroxyl group gets deprotonated O(1) and O(2) in molecule, 9A and O(3) and O(3) in molecule, 9B during complexation. This is also evidenced in the IR spectrum of the complex, in which the hydroxyl stretching of the free ligand L^2 at $\sim 3400\text{ cm}^{-1}$ is not observed. Nearly the two ligands are structurally perpendicular to each other in the complex. Selected bond lengths and bond angles are given in Table 3.3. The average bond distances of the molecule, 9A (Figure 3.6) are Cu(1)-O(1)(phenolic) 1.897(4) Å, Cu(1)-O(2)(phenolic) 1.902(4) Å, Cu(1)-N(1)(imine) 1.975(5) Å and Cu(1)-N(3)(imine) 1.946(5) Å. In molecule, 9B (Figure 3.6) Cu(2)-O(3)(phenolic) 1.925(4) Å, Cu(2)-O(4)(phenolic) 1.900(4) Å, Cu(2)-N(5)(imine) 1.948(5) Å and Cu(2)-N(7)(imine) 1.972(4) Å bond lengths are slightly deviated. The average bond angles of the molecule, 9A are between O(1)-Cu(1)-N(1) 94.06(19)°, O(2)-Cu(1)-N(1) 142.64(19)°, O(1)-Cu(1)-N(3) 146.7(2)° and O(2)-Cu(1)-N(3) 92.50(18)° respectively. In the molecule, 9B bond angles are between O(3)-Cu(2)-N(5) 93.10(18)°, O(4)-Cu(2)-N(5) 149.8(2)°, O(3)-Cu(2)-N(7) 148.12(18)° and O(4)-Cu(2)-N(7) 92.77(18)° respectively.

3.4.3. Nickel complex [L^2NiCl_2], 10

The nickel complex was synthesized by the procedure given in section 3.3.3.4. and recrystallized from acetonitrile. The IR spectrum of the complex shows band at 3414 cm^{-1} corresponding to hydroxyl group and other two strong stretching bands at 1647, 1543 cm^{-1} corresponding to the C=N and phenolic C-O groups. The electronic spectrum of the complex in methanol solution shows bands at 616, 395, 319 and 250 nm. The broad band at 616 nm is due to d-d electronic transitions, the band at 395 nm is due to the ligand to metal charge transfer transition and the band at 319 nm is due to the intraligand $n-\pi^*$ transitions. The band at 250 nm is due to $\pi-\pi^*$ electronic

transitions of the ligand. CD spectrum of the complex recorded in methanol shows bands at 493, 310 and the high intensity $\pi \rightarrow \pi^*$ transition bands at 255, 221 and 208 nm. These bands confirm that the complex is chiral (Figure 3.1). The elemental analytical data of the complex agree with the mononuclear composition of $[L^2NiCl_2]$.

3.4.4. Cobalt complex $[L^2CoCl_2]$, 11

The chiral cobalt complex **11** was synthesized in good yields by the procedure given in section 3.3.3.4. The IR spectrum of the complex $[L^2CoCl_2]$ shows stretching broad band at around 3468 cm^{-1} corresponding to the hydroxyl group and other two strong stretching bands at around $1649, 1545\text{ cm}^{-1}$ corresponding to the C=N and phenolic C-O groups. Circular dichroism spectra of the cobalt complex recorded in methanol solution show bands at 500(1.10), 410(-0.87), 275(-2.82) and 220(-2.20). Appearance of these bands confirms that the complex is chiral (Figure 3.7). The electronic spectrum of the chiral cobalt complex recorded in methanol shows bands at 407 nm due to the ligand to metal charge transfer transitions and at 358 nm due to the intraligand $n \rightarrow \pi^*$ interactions. The band at 245 nm is due to $\pi \rightarrow \pi^*$ electronic transitions of the ligand. The analytical data match with the mononuclear composition of $[L^2CoCl_2]$.

3.4.5. Iron complex $[L^2FeCl_2]$, 12

This complex was synthesized in good yields by the procedure given in section 3.3.3.4. The IR spectrum of the complex $[L^2FeCl_2]$ shows stretching broad band at around 3414 cm^{-1} corresponding to the hydroxyl group and other two strong stretching bands at around $1643, 1548\text{ cm}^{-1}$ corresponding to the C=N and phenolic C-O groups. Circular dichroism spectrum of the iron complex recorded in methanol solution shows bands at 463(1.21), 280(-0.58), 243(1.64) and a high intensity band at 205(-9.23) nm. These bands confirm that the complex is chiral. The electronic spectrum of the iron complex in methanol solution shows broad band at 663 nm due

to d-d electronic transitions. Ligand to metal charge transfer transition band at 415 nm and an intra ligand transitions band at 343 nm are observed.

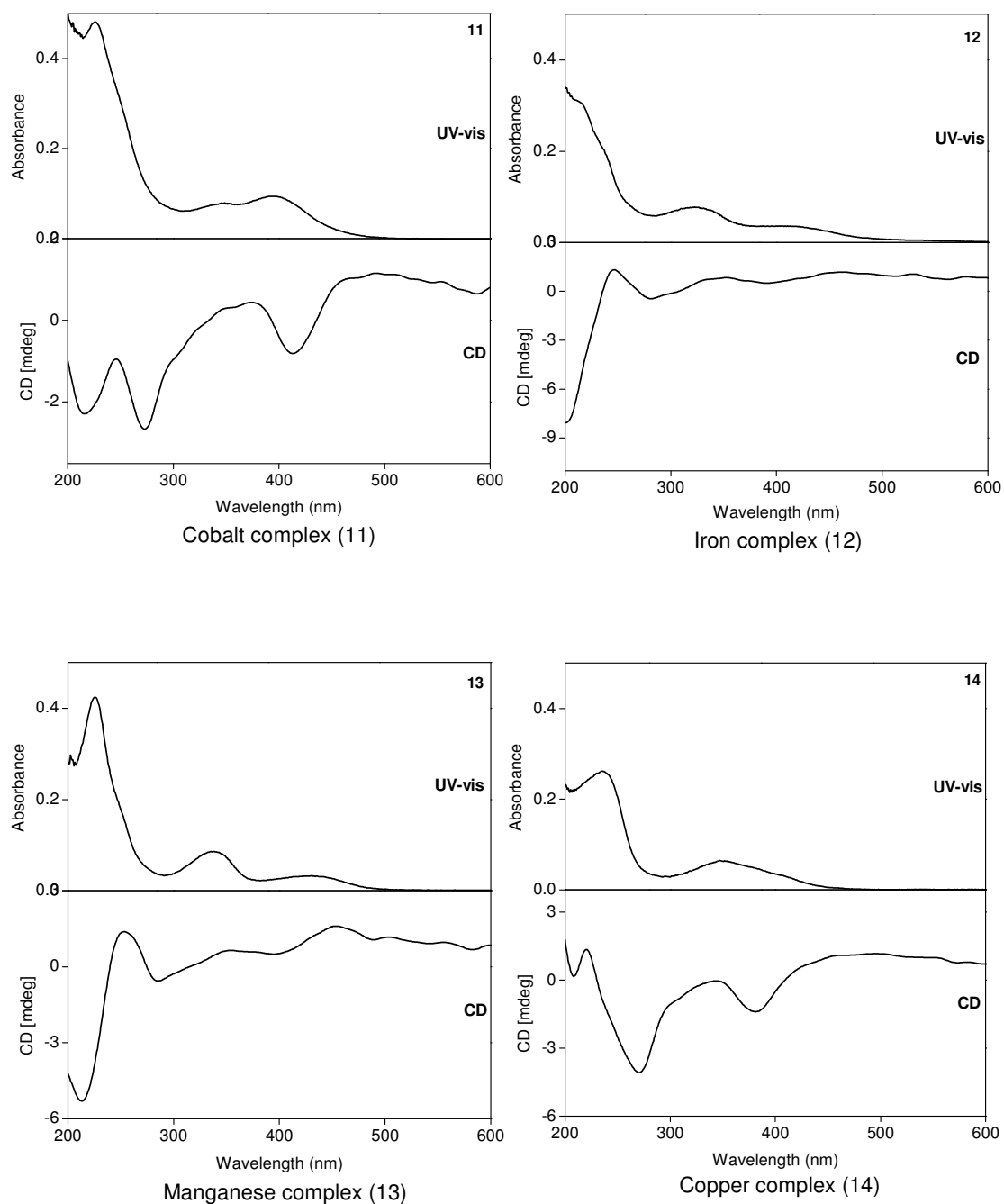


Figure 3.7. CD and UV-vis spectra of the Co^{2+} , Fe^{2+} , Mn^{2+} and Cu^{+2} complexes in MeOH solution (concentrations = $1 \times 10^{-4}\text{M}$ for CD and $1 \times 10^{-5}\text{M}$ for UV-vis each experiment).

The band at 244 nm is due to $\pi\text{-}\pi^*$ electronic transitions of the ligand (Figure 3.7). The analytical data of the complex match with the mononuclear composition of $[\text{L}^2\text{FeCl}_2]$.

3.4.6. Manganese complex $[\text{L}^2\text{MnCl}_2]$, **13**

The manganese complex **13** was synthesized in good yields by the procedure given in section 3.3.3.4. The IR spectrum of the complex $[\text{L}^2\text{MnCl}_2]$ shows stretching broad band at around 3500 cm^{-1} corresponding to the hydroxyl group and other two strong stretching bands at around $1649, 1541\text{ cm}^{-1}$ corresponding to the C=N and phenolic C-O groups. Circular dichroism spectra was recorded in methanol solution. The CD spectra of the complex agreed well with the corresponding zinc complex. Bands appear at $456(1.66), 356(0.7), 247(1.44)\text{ nm}$ and the high intensity $\pi\rightarrow\pi^*$ transition bands at $212(-5.57)\text{ nm}$. The electronic spectrum of the manganese complex recorded in methanol shows bands at 436 nm due to ligand to metal charge transfer transition and intra ligand $n\text{-}\pi^*$ transition bands at 351 and 245 nm (Figure 3.7). The analytical data match with the mononuclear composition of $[\text{L}^2\text{MnCl}_2]$.

3.4.7. Copper complex $[\text{L}^2\text{CuCl}_2]$, **14**

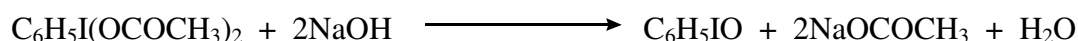
The copper complex **14** was synthesized by the procedure given in section 3.3.3.4. The copper complex was recrystallised from acetonitrile. The IR spectrum of the copper complex shows hydroxyl stretching broad band at 3484 cm^{-1} and other two strong stretching bands at $1630, 1548\text{ cm}^{-1}$ corresponding to the C=N and phenolic C-O groups. The electronic spectrum of the complex in methanol solutions shows band at 714 nm due to the d-d electronic transitions. The band at 367 nm is due to the intraligand $n\text{-}\pi^*$ and the band at 257 nm is due to $\pi\text{-}\pi^*$ electronic transitions of the ligand. CD spectrum of the complex was recorded in methanol solutions. The charge transfer region of the spectra shows band at $380(-1.40)\text{ nm}$ and the high intensity $\pi\rightarrow\pi^*$ transition band at $270(-4.03)\text{ nm}$ confirming that the complex is chiral (Figure 3.7). The analytical data of the complex agree with the mononuclear composition of $[\text{L}^2\text{CuCl}_2]$.

3.5. Catalysis

To examine the nature of the chiral complexes in the catalytic process, we studied the alkenes oxidation reactions. The oxidations were carried out in CH₃CN using iodosylbenzene (PhIO) as the terminal oxidant at room temperature for 24 hours. In absence of the catalyst under similar reaction conditions, there is no reaction between oxidant and olefins.

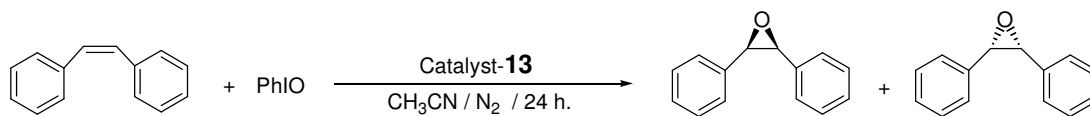
3.5.1. Synthesis of Iodosylbenzene (PhIO)

The iodosylbenzene (PhIO) used in the catalytic study as oxidant is prepared using a reported procedure.²² Finely ground iodosylbenzene diacetate (32.2 g, 0.10 mol) is placed in a 250 mL beaker and 150 mL of 3N sodium hydroxide is added over a 5 minute period with vigorous stirring. The lumps of solid that formed are triturated with a stirring rod or spatula for 15 minutes and the reaction mixture stands for an additional 45 minutes to complete the reaction. 100 mL of water is added, the mixture is stirred vigorously and the crude solid iodosobenzene is collected on a Büchner funnel, washed there with 200 mL of water and dried by maintaining suction. Final purification is effected by triturating the dried solid in 75 mL of chloroform in a beaker. The iodosylbenzene is separated by filtration and air-dried (Yield: 85%).



3.5.2. Epoxidation of *cis*-stilbene catalyzed by manganese complex, 13

The chiral manganese catalyst **13** (0.025 g, 0.05 mmol) and *cis*-stilbene (0.180 g, 1 mmol) were dissolved in 5 mL acetonitrile. The reaction was initiated by the addition of iodosylbenzene (PhIO) (0.220 g, 1 mmol) and stirred at room temperature under nitrogen atmosphere for 24 hours. After stirring, the mixture was concentrated in vacuum. Anhydrous ether (10 mL) added to the brown residue and the ether solution was carefully filtered. Then the ether was removed under reduced pressure and purified with column chromatography from hexane. The catalytic epoxidation reaction sequence of *cis*-stilbene is shown in Scheme 3.5.



Scheme 3.5. Schematic representation of catalytic epoxidation of *cis*-stilbene.

The product was confirmed by ¹H-NMR spectrum (*cis*-stilbene epoxide $\delta \sim 4.35$ in CDCl₃) of reported stilbene epoxide.²³ HPLC analyses of *cis*-stilbene epoxide product was carried out on a Shimadzu SCL-10A instrument equipped with CHIRALCEL OD-H using Class-VP program (90:10 hexane / *i*-PrOH, 0.5 mL/min, 254 nm, retention times: 7.8 min for *cis*-stilbene; 10.55 min and 11.52 min for epoxides).

The HPLC analysis profile of the *cis*-stilbene epoxide catalyzed by **13** is shown in Figure 3.8. HPLC analysis data percentage of enantiomeric excess of *cis*-stilbene epoxide catalyzed by complex **13** as a function of time are given in Table 3.4 and Table 3.5 (entry 1). Epoxidation of *cis*-stilbene catalyzed by **13**, yields up to 25% with 70% of enantiomeric excess at room temperature.

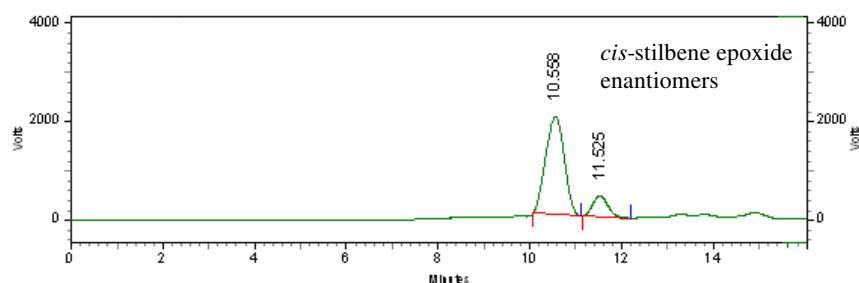


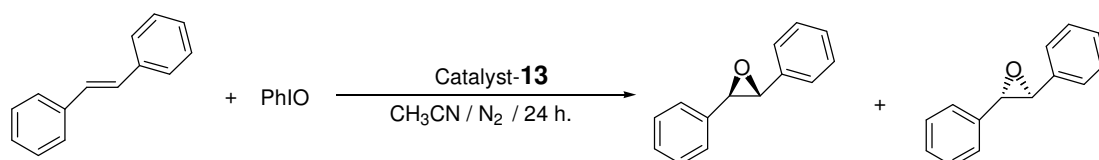
Figure 3.8. HPLC analysis profile of *cis*-stilbene epoxide catalyzed by complex **13**.

Table 3.4. HPLC analysis data of *cis*-stilbene epoxide, showing percentage of enantiomeric excess catalyzed by complex **13** as a function of time

Pk #	Retention Time	Area	Area %	Height	Height %
1	10.558	56181269	85.022	1987757	82.475
2	11.525	9896957	14.978	422363	17.525
Totals		66078226	100.000	2410120	100.000

3.5.3. Epoxidation of *trans*-stilbene catalyzed by manganese complex, **13**

The chiral manganese catalyst **13** (0.025 g, 0.025 mmol) and *trans*-stilbene (0.180 g, 1 mmol) were dissolved in 5 mL acetonitrile. The reaction was initiated by the addition of iodosylbenzene (PhIO) (0.220 g, 1 mmol) and stirred at room temperature under nitrogen atmosphere for 24 hours. After stirring, the mixture was concentrated in vacuum. Anhydrous ether (10 mL) added to the brown residue and the ether solution was carefully filtered. Then the ether was removed under reduced pressure and purified with column chromatography from hexane. The catalytic epoxidation reaction of *trans*-stilbene is shown in Scheme 3.6.

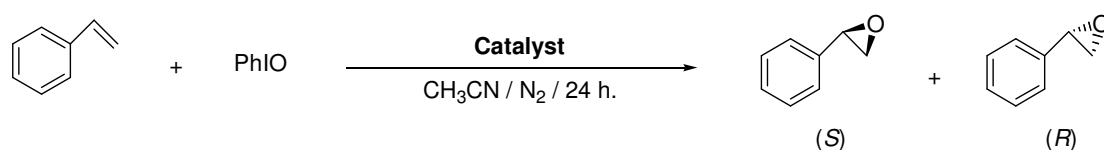


Scheme 3.6. Schematic representation catalytic epoxidation of *trans*-stilbene.

The product was confirmed by ¹H-NMR spectrum (*trans*-stilbene epoxide δ ~ 3.86 in CDCl₃) of reported stilbene epoxide.²⁴ HPLC analyses of *trans*-stilbene epoxide product was carried out on a Shimadzu SCL-10A instrument equipped with CHIRALCEL OD-H using Class-VP program (90:10 hexane / *i*-PrOH, 0.5 mL/min, 254 nm, retention times: 9.18 min for *trans*-stilbene; 10.6 min and 11.55 min for epoxides). HPLC analysis percentage of enantiomeric excess of *trans*-stilbene epoxide catalyzed by complex **13** as a function of time are given in Table 3.5 (entry 2).

3.5.4. Oxidation of styrene catalyzed by chiral complexes **9**, **10**, **11**, **12** and **13**

All the oxidation reactions of styrene were carried out by the same procedure. The catalytic reaction sequence is shown in Scheme 3.7. The oxidation of styrene by the chiral catalysts of manganese **13**, copper **9**, nickel **10**, cobalt **11**, and iron **12** with iodosylbenzene (PhIO) as oxidant were carried out by the following procedure.



Scheme 3.7. Schematic representation of catalytic epoxidation of styrene.

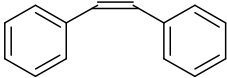
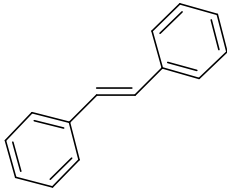
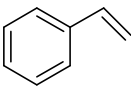
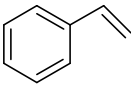
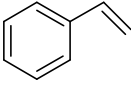
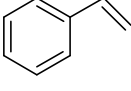
The chiral catalyst (0.05 mmol) and styrene (0.104 g, 1 mmol) were dissolved in 5 mL acetonitrile. The reaction was initiated by the addition of iodosylbenzene (0.220 g, 1 mmol) and stirred at room temperature under nitrogen atmosphere for 24 hours.

After completion of the reaction, solvent was removed under reduced pressure. Anhydrous ether (10 mL) was added to the brown residue and the ether solution was carefully filtered. Then, the ether was removed under reduced pressure and purified using short silica gel column from hexane. The products of the styrene were confirmed by ¹H-NMR spectroscopy (styrene epoxide $\delta \sim 3.84$ in CDCl₃). The oxidation product yields and enantiomeric excess of styrene were determined by gas chromatography (GC). The gas chromatographic profile of authentic samples are shown in Chapter 2 (Figure 2.13). The amount of epoxide formed on epoxidation of styrene and the enantiomeric excess of the epoxide catalyzed by copper complex **9** as a function of time are shown in Figure 3.9.

The percentages of product yields and of the epoxides are given in Table 3.5 (entries 3-6). Copper(II) **9** and cobalt(II) **11** catalysts are encouraging epoxidation reactions Table 3.5 (entries 4 and 5), Iron(II) **12** catalyst is favours the oxidation of

styrene to 1-phenylacetaldehyde as major product and acetophenone as a side product. No oxidation product was detected by the Mn(II) **13** and Ni(II) **10** complexes for the styrene.

Table 3.5. Oxidation products ^a of olefins by PhIO catalyzed by **13**, **9**, **11** and **12**

Entry	Substrate	Catalyst	Epoxide Yield (%)	Epoxide e. e. (%)	1-Phenyl acetaldehyde Yield(%) ^c	Acetophenone Yield(%) ^c
1		Mn(II) 13	25 ^b	70 ^d	—	—
2		Mn(II) 13	5 ^b	35 ^d	—	—
3		Mn(II) 13	No reaction	—	—	—
4		Cu(II) 9	26 ^c	—	32	34
5		Co(II) 11	23 ^c	—	26	38
6		Fe(II) 12	—	—	65	34

^a Products confirmed by ¹H-NMR spectroscopy. ^b Based on substrate consumed and determined by chiral column (CHIRALCEL OD-H) HPLC analysis. ^c Based on substrate consumed and determined by chiral column GC analysis (Supelco α -DEX 325, 30m length, 0.25mm id, 0.25 μ m film thickness). ^d Enantiomeric excess of epoxides, determined by chiral column (CHIRALCEL OD-H) HPLC analysis.

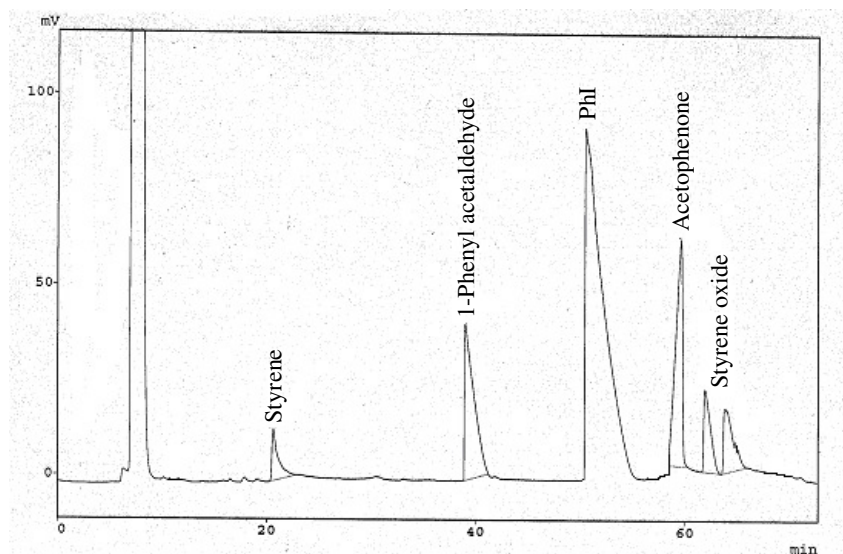
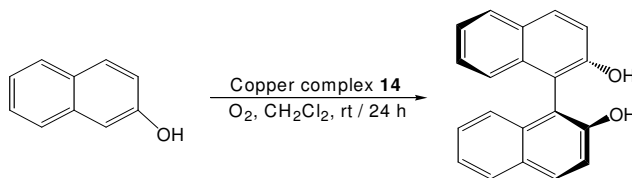


Figure 3.9. Gas chromatographic (GC) analysis of styrene oxidation products catalyzed by copper complex **9**.

3.5.5. Catalytic oxidative coupling reaction of β -naphthol

The chiral copper catalyst **14** (0.025 g, 0.05 mmol) and 2-naphthol (0.144 g, 1 mmol) were dissolved in 15 mL dichloromethane. The reaction was initiated by passing molecular oxygen and stirred at room temperature for 24 hours.

After completion of the reaction, solvent was removed under reduced pressure. Anhydrous ether (10 mL) was added to the residue and the ether solution was carefully filtered. Then, the product BINOL (see Scheme 3.8) was purified using silica gel column from hexane-ethylacetate (Yield: 65%). The product was confirmed by ^1H -NMR spectroscopy.



Scheme 3.8. Catalytic oxidative coupling of β -naphthol catalyzed by **14**.

3.6. Conclusions

New chiral Schiff base metal complexes were synthesized and characterized by microanalysis, UV-vis, IR, CD and fluorescence spectral studies. X-ray structure determination of the $[\text{ZnL}^2\text{Cl}_2]$ **8**, self-assembles *via* hydrogen bonding interactions into supramolecular helices. It is observed that in the crystal structure of **8**, the phenolic groups are deprotonated and free arm of the imine-nitrogen gets protonated. This perhaps suggests that protons are securely bound in the second cavity of the coordination site by intra-molecular hydrogen bonding to the nitrogen atoms. The uncoordinated arm of the ligand plays an important role in forming mononuclear complex. The X-ray crystal structure determination of the copper complex **9** revealed the formation of mononuclear complex with two ligand molecules L^2 binding to the metal center. All the complexes **8–14** show chirality (proved by circular dichroism) and exhibit remarkable emission properties at room temperature. Among these metal complexes, zinc complex **8** is highly fluorescent in methanol solution.

The copper **9** and cobalt **11** catalysts favour for the epoxidation reactions of the styrene. Epoxidation reaction of the *cis*-stilbene catalyzed by manganese complex **13**, yields up to 25% at room temperature with 70% of enantiomeric excess. Interestingly, copper complex **14** is catalytically active for the oxidative coupling of β -naphthol.

3.7. References

1. R. A. Sheldon and J. K. Kochi, *Metal-Catalysed Oxidation of Organic Compounds*. Academic Press, New York, **1981**.
2. Y. Gao, R. M. Hanson, J. M. Klunder, S. Y. Ko, H. Masamune, and K. B. Sharpless, *J. Am. Chem. Soc.* **1987**, 109, 5765.
3. (a) E. N. Jacobsen, in *Catalytic Asymmetric Synthesis*, Ed. I. Ojima, VCH, **1993**, 159. (b) T. Katsuki, *Coordination. Chem. Rev.* **1995**, 140, 189. (c) J. P. Collman; X. Zhang; V. J. Lee; E. S. Uffelman; and J. I. Brauman, *Science*, **1993**, 261, 1404.

4. (a) J. P. Collman; V. J. Lee; C. J. Kellen-Yuen; X. Zhang; J. A. Ibers; and J. I. Brauman, *J. Am. Chem. Soc.* **1995**, 117, 692. (b) R. L. Halterman; and S-T. Jan, *J. Org. Chem.* **1991**, 56, 5253. (c) S. O'Malley, and T. Kodadek, *J. Chem. Soc.* **1989**, 111, 9116.
5. (a) H. Yoon; T. R. Wagler; K. J. O'Connor; and C. J. Burrows, *J. Am. Chem. Soc.* **1990**, 112, 4568. (b) R. Irie; Y. Ito; and T. Katsuki, *Tetrahedron Lett.* **1991**, 32, 47, 6891.
6. (a) Abrahams, B. F.; Batten, S. R.; Hamit, H.; Hoskins, B. F.; Robson, R. *J. Chem. Soc., Chem. Commun.* **1996**, 1313. (b) Piguet, C.; Bernardinelli, G.; Hopfgartner, G. *Chem. Rev.* **1997**, 97, 2005. (c) Aspinall, H. C.; Bickley, J. F.; Dwyer, J. L. M.; Greeves, N.; Steiner, A. *Angew. Chem., Int. Ed. Engl.* **2000**, 39, 2858.
7. (a) Erxleben, A. *Inorg. Chem.* **2001**, 40, 412. (b) Nomiya, K.; Takahashi, S.; Noguchi, R. *J. Chem. Soc., Dalton Trans.* **2000**, 1343. (c) Niklas, N.; Hampel, F.; Alsfasser, R. *J. Chem. Soc., Chem. Commun.* **2003**, 1586. (d) Withersby, M. A.; Blake, A. J.; Champness, N. R.; Hubberstey, P.; Li, W.-S.; Schroeder, M.; *Angew. Chem., Int. Ed. Engl.* **1997**, 36, 2327. (e) Whang, D.; Heo, J.; Kim, C.-A.; Kim, K. *J. Chem. Soc., Chem. Commun.* **1997**, 2361. (f) Ranford, J. D.; Vittal, J. J.; Wu, D.; Yang, X. *Angew. Chem., Int. Ed. Engl.* **1999**, 38, 3498. (g) Ezuhara, T.; Endo, K.; Aoyama, Y. *J. Am. Chem. Soc.* **1999**, 121, 3279. (h) Ellis, W. E.; Schmitz, M.; Arif, A. A.; Stang, P. J. *Inorg. Chem.* **2000**, 39, 2547. (i) Siemeling, U.; Scheppelmann, I.; Neumann, B.; Stammler, A.; Stammler, H.-G.; Frelek, J. *J. Chem. Soc., Chem. Commun.* **2003**, 2236.
8. For example, Hanessian, S.; Gomtsyan, A.; Simard, M.; Roelens, S. *J. Am. Chem. Soc.* **1994**, 116, 4495.
9. (a) Canary, J. W.; Allen, C. S.; Castagnetto, J. M.; Wang, Y. *J. Am. Chem. Soc.* **1995**, 117, 8484. (b) Castagnetto, J. M.; Canary, J. W. *J. Chem. Soc., Chem. Commun.* **1998**, 203. (c) Ziegler, M.; von Zelewsky, A. *Coord. Chem. Rev.* **1998**, 177, 257. (d) Browne, W. R.; Hesek, D.; Gallagher, J. F.; O'Connor, C. M.; Killeen, J. S.; Aoki, F.; Ishida, H.; Inoue, Y.; Villani, C.; Vos, J. G. *J. Chem. Soc., Dalton Trans.* **2003**, 2597. (e) Browne, W. R.;

- O'Connor, C. M.; Villani, C.; Vos, J. G. *Inorg. Chem.* **2001**, *40*, 5461. (f) Fletcher, N. C.; Keene, F. R.; Viebrock, H.; von Zelewsky, A. *Inorg. Chem.* **1997**, *36*, 1113.
10. Gagne, R. R.; Spiro, C. L.; Smith, T. J.; Hamann, C. A.; Thies, W. R.; Shiemke, A. K. *J. Am. Chem. Soc.* **1981**, *103*, 4073.
11. (a) A. I. Vogel, *Textbook of Practical Organic Chemistry*, 4th Ed. ELBS and Longman, **1978**; (b) D. D. Perrin, W. L. F. Armarego, D. R. Perrin, *Purification of Laboratory Chemicals*, Pergamon Press, London, **1966**.
12. XTAL 3.5, Users Manual, eds S. R. Hall, G. S. D. King and J. M. Stewart, University of Western Australia, Perth, **1995**.
13. G. M. Sheldrick, SHELXS 86, SHELXL 93, Program for Crystal Structure Solution and Refinement, University of Gottingen, **1993**; SHELX-97, Program for Crystal Structure Solution and Refinement, University of Gottingen, Germany, **1997**.
14. Sheldrick, G. M. *SHELXS97 - Program for Crystal Structure Solution*; University of Gottingen, **1997**; Sheldrick, G. M. *SHELXL97 - Program for Crystal Structure Refinement*; University of Gottingen, **1997**.
15. Pizzala, H.; Carles, M.; Stone, W. E. E.; Thevand, A. *J. Chem. Soc., perkin trans. 2*. **2000**, 935.
16. Balamurugan, V.; Hundal, M. S.; Mukherjee, R. *Chem. Eur. J.* **2004**, *10*, 1683.
17. (a) Xuan, R.; Hu, W.; Yang, Z.; Xuan, R. *Acta Cryst.* **2003**, *C59*, m112. (b) Vembu, N.; Nallu, M.; Garrison, J.; Youngs, W. J. *Acta Cryst.* **2003**, *E59*, o939. (c) Braga, D.; Draper, S. M.; Champeil, E.; Grepioni, F. *J. Organomet. Chem.* **1999**, *573*, 73.
18. Flack, H. D. *Acta Cryst.* **1983**, *A39*, 876.
19. von Zelewsky, A.; Mamula, O. *J. Chem. Soc., Dalton Trans.* **2000**, 219.
20. (a) Dollberg, C. L.; Turro, C. *Inorg. Chem.* **2001**, *40*, 2484. (b) Roundhill, D. M. *Photochemistry and Photophysics of Metal Complexes: Modern Inorganic Chemistry Series*; Fackler, J. P., Ed.; Plenum Press: New York, **1994**; pp 56.
21. (a) Mukherjee, S. *Indian J. Chem.* **1987**, *26A*, 1002. (b) Das, R.; Mitra, S.; Mukherjee, S. *Bull. Chem. Soc. Jpn.* **1993**, *66*, 2492.
22. H. Saltzman and J. G. Sharefkin, *Org. Synth.*, **1973**, Coll. Vol. V, 658.
23. K. Srinivasan, P. Michaud and J. K. Kochi, *J. Am. Chem. Soc.*, **1986**, *108*, 2309.
24. D. Das and C.-P. Cheng, *J. Chem. Soc., Dalton Trans.*, **2000**, 1081.
-

Chapter 4

Synthesis of some optically active binuclear metal complexes and their catalytic activities towards organic oxidation

4.1. Abstract

New chiral Schiff base ligand L^3 (L^3 = 1,4-bis[3-(1-phenylethyliminomethyl)-2-hydroxy-5-bromobenzyl]piperazine) and its complexes **15–20** ($M = Mn^{+2}$, **15**; Cu^{+2} , **16**; Co^{+2} , **17**; Ni^{+2} , **18**; Fe^{+2} , **19**; Zn^{+2} , **20**) have been synthesized starting from one equivalents of 6,6'-piperazine-1,4-diyl dimethylenebis(4-bromo-2-formylphenol) and two equivalents of (S)-(-)-1-phenylethylamine. Characterization of the ligand L^3 and its metal complexes **15–20** were carried out by microanalysis, IR, UV/Vis-, and CD spectral studies. Structure of the ligand L^3 was determined by single crystal X-ray crystallographic methods. Crystal data for ligand L^3 : Orthorhombic space group $P2_12_12_1$, $a = 13.7894(8)$ Å, $b = 14.3556(8)$ Å, $c = 17.3043(10)$ Å, $V = 3425.5(3)$ Å³, $Z = 4$. Ligand L^3 and its complexes **15–20**, exhibits circular dichroism signals at room temperature.

To examine the nature of the chiral complexes in the catalytic process, we have studied the catalytic activities of the chiral Schiff base complexes towards the oxidation reactions of the styrene, *cis*-stilbene and *trans*-stilbene. The reactions were carried out in CH_3CN using iodosylbenzene (PhIO) as the terminal oxidant at room temperature. Quantification of the styrene epoxidation products was determined by gas chromatography (GC). The quantification of the *cis*-stilbene and *trans*-stilbene products was determined by HPLC. Epoxidation of *cis*-stilbene catalyzed by complex **15**, yields up to 40% at room temperature with 46% of enantiomeric excess.

4.2. Introduction

The design of catalysts that ensure high enantioselectivity in the epoxidation of un-functionalized alkenes constitutes one of the most significant importance in the asymmetric synthesis.¹ The major advances in this field have been achieved with complexes of chiral porphyrins², with the systems of Jacobsen³ and Katsuki *et al.*⁴, based on chiral Mn(III) Schiff base complexes using NaOCl as oxidant. A series of achiral bimetallic Mn(III) complexes were synthesized and characterized from the monomanganese complex Mn(III)LCl. The catalytic activity of the complexes shows that the second metal ion shows down formation of the active intermediate Mn(IV)=O and reduces the efficiency of the transfer of oxygen atom to the alkene.⁵ Mononuclear, as well as dinuclear metal centers, are commonly found in the active site of various oxygenase⁶ and the information on key structural features and factors governing oxygenase activity is rapidly increasing.⁷ Amongst various catalysts developed so far for enantioselective epoxidation, chiral metalloporphyrins⁸ and macrocyclic ligands are of special interest.⁹ Recently Katsuki have reported an efficient catalytic system for the epoxidation of several kinds of olefins with moderate to high enantioselectivity depending on the substitution degree of double bond using iodosylbenzene, NaOCl, H₂O₂ and periodates as terminal oxidant.¹⁰ Kureshy *et al.* have also reported various chiral catalysts for the asymmetric epoxidation reactions of olefins.¹¹

Natural L-Amino acids would be ideal chiral sources, as they are inexpensive and readily available from natural materials. The asymmetric epoxidation catalyzed by chiral salen-Mn complexes is one of the most intensively studied reactions with the results showing that the size and configuration of the C3 and C3' groups on the salen structure play very important roles on directivity or chiral induction.¹² As a result, this is a suitable reaction for evaluating amino acid-Schiff-base groups, which are incorporated at the C3 and C3' positions of the Katsuki salen-Mn catalysts.¹³ L-Amino acids as inexpensive and readily available natural products showed significant chiral induction and stereo-directing abilities. The mononuclear new chiral Mn(III)-Schiff

base complexes with L-Amino acid ethyl esters were found to be highly effective catalysts for the enantioselective epoxidation of conjugated olefins while the corresponding binuclear Mn(III) complexes showed lower enantioselectivity.¹⁴

In the present work, chiral Schiff base metal complexes are useful catalysts for selective organic transformation reactions. View of this aspect we synthesized new chiral schiff base ligand **L³** and its complexes with first-row transition metals (Mn, Cu, Co, Ni, Fe and Zn). Herein we discuss the structural characterization of the ligand **L³** and its metal complexes **15–20** and their catalytic activity towards asymmetric epoxidation of un-functionalized olefins.

4.3. Experimental

4.3.1. Chemicals and reagents

All the chemicals used in this study were commercially available and used as received. The chemicals and the sources are as follows: 5- bromosalicylaldehyde and piperazine were purchased from Lancaster (England) for the preparation of 6, 6'-piperazine-1,4-diylldimethylenebis(4-bromo-2-formylphenol).

S-(–)-1-phenylethylamine was purchased from Lancaster, CDCl₃ was obtained from Acros (India). All metal salts were purchased commercially and used as received. HPLC grade solvents were used for spectral analyses. All other solvents were purified and dried by the usual methods.¹⁵ Iodobenzenediacetate, styrene, *cis*-stilbene and *trans*-stilbene were purchased from Aldrich chemicals. Iodosylbenzene was prepared according to literature procedure.¹⁶

4.3.2. Physical measurements

Elemental analyses were carried out on a Perkin-Elmer 240C CHN analyzer. The ¹H-NMR spectra were recorded with a Bruker DRX-400 spectrometer using CDCl₃ as the solvent. Tetramethylsilane (TMS) was the internal standard. Infrared spectra were recorded on a Jasco Model 5300 FT-IR spectrophotometer. The spectra of the solid samples were recorded using KBr pellets. The UV-visible spectra were recorded with Shimadzu model UV-3101PC UV-vis spectrophotometer. The CD spectra were measured with a JASCO J-810 spectropolarimeter. The X-ray intensity

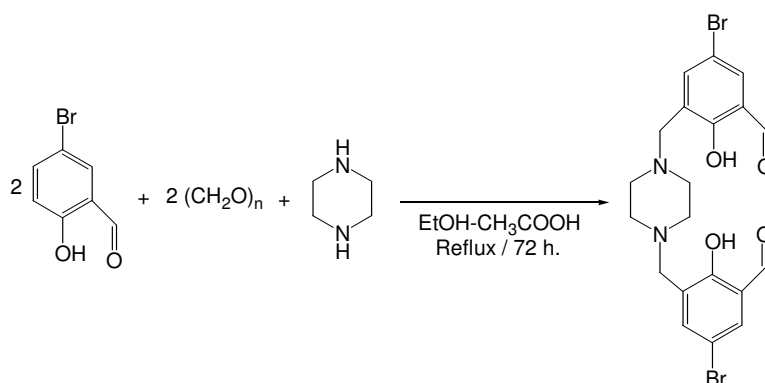
data for the ligand **L**³ was measured on a Bruker SMART APEX CCD area detector system equipped with a graphite monochromator and a Mo-K α fine-focus sealed tube ($\lambda = 0.71073 \text{ \AA}$) operated at 1500 W power (50 kV, 30 mA). The detector was placed at a distance of 4.995 cm from the crystal. Data were corrected for absorption effects using the multi-scan technique (SADABS). The SMART software was used for intensity data acquisition and the SAINT-Plus software was used for data extraction. The solution and refinement of the data were done using SHELXL-97¹⁷ program. Optical rotation was measured with an AUTOPOL-IV automatic polarimeter (readability $\pm 0.01^\circ$).

Gas chromatographic analyses were carried out on a Shimadzu GC 14B instrument equipped with a stainless steel packed column (5 m, 5 % SE 30) and a chiral capillary column (Supelco α -DEX 325, 30m length, 0.25mm id, 0.25 μ m film thickness) and a flame ionization detector (FID). HPLC analyses of *cis*-stilbene epoxide and *trans*-stilbene epoxide products were carried out on a Shimadzu SCL-10A instrument equipped with CHIRALCEL OD-H using Class-VP program.

4.3.3. Synthesis

4.3.3.1. 6,6'-piperazine-1,4-diyl dimethylenebis(4-bromo-2-formylphenol)

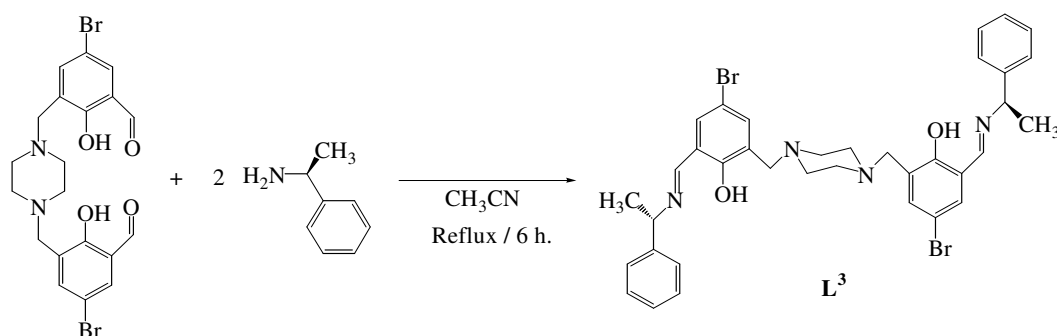
A mixture of piperazine (2.2 g, 0.025 mol), paraformaldehyde (1.8 g, 0.06 mol) and 5-bromosalicylaldehyde (10.2 g, 0.05 mol) in ethanol-acetic acid solutions (100 mL 4:1 v/v) was refluxed for 72 hours and neutralized with a saturated solution of sodium carbonate after cooling to room temperature. Ethanol was removed by distillation and the product was further purified by silica gel column chromatography using chloroform-light petroleum (1:4 v/v) as the eluent (Yield: 90%). M. W.: 512.20 g mol⁻¹; M. P.: 217 °C; ¹H-NMR (CDCl₃): δ 1.8 (m, 8H, piperazine CH₂), 3.6 (m, 4H, benzylic CH₂), 7.0-7.4 (d, 4H, aromatic CH) and 9.85 (s, 2H, CHO); IR (KBr): 3450 (phenolic OH), 2840-2940 (N-CH₂), 1670 (CHO) and 1450 cm⁻¹ (aromatic skeleton). (This is the modified procedure from the literature procedure¹⁸). The reaction sequence is shown in Scheme 4.1.



Scheme 4.1. Schematic representation of the Mannich reaction.

4.3.3.2. Synthesis of chiral ligand **L**³ (1,4-bis[3-(1-phenylethyliminomethyl)-2-hydroxy-5-bromo benzyl]piperazine)

To a solution of 6,6'-piperazine-1,4-diyl dimethylene bis(4-bromo-2-formylphenol) (0.256 g, 0.5 mmol) in acetonitrile (25 mL) was added (S)-(-)-1-phenylethylamine (0.121 g, 1 mmol). The reaction mixture was refluxed for 6 hours. The reaction mixture was then concentrated using rotary evaporator. The resulting yellow solid was recrystallized from acetonitrile solution. Yellow crystals of the desired chiral ligand **L**³ suitable for X-ray single crystal analysis were obtained after ten days at room temperature (Yield: 80%). The reaction sequence is shown in Scheme 4.2.



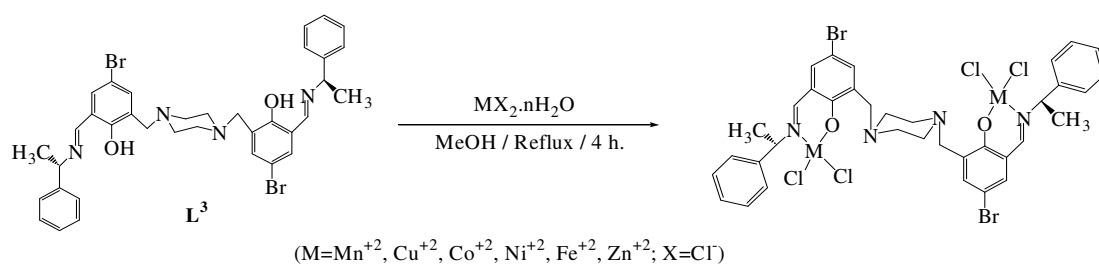
Scheme 4.2. Synthetic scheme for the chiral Schiff base ligand **L**³.

Characterization data for L³

Optical rotation $[\alpha]_D^{25}$: + 435.61 (c 1, chloroform); M. F.: C₃₆H₃₈Br₂N₄O₂; M. W.: 718.52 g mol⁻¹; IR (ν cm⁻¹, KBr pellet): 3057, 3016, 2939, 2885, 2818, 1630, 1620, 1575, 1446, 1373, 1294, 1124, 864, 752, 696; ¹H NMR (CDCl₃): δ 1.62(d, 6H, CH₃), 2.61 (s, 8H, piperazine), 3.62 (q, 4H, CH₂), 4.55 (q, 2H, CH), 7.24 - 7.48 (m, 14H, Ar-CH), 8.33 (s, 2H, HC=N), 13.75 (br, 2H, phenolic C-OH); CD λ_{max} (mdeg) (CH₃OH): 422 (+0.94), 330 (+3.31), 257 (+5.55), 227 (+2.38); UV-Vis (CH₃OH) [λ_{max}/nm (ε/dm³ mol⁻¹ cm⁻¹): 415(509), 331 (1510), 253 (4612), 219 (11083); CHN Analysis: Calcd.: C, 60.18; H, 5.33; N, 7.80%; Found.: C, 60.24; H, 5.26; N, 8.10%.

4.3.3.3. General synthetic procedure for complexes, 15–20

To a solution of 1,4-bis[3-(1-phenylethyliminomethyl)-2-hydroxy-5-bromo benzyl]piperazine **L³** (0.360 g, 0.5 mmol) in 25 mL of methanol was added MX₂·nH₂O (M = Mn, **15**; Cu, **16**; Co, **17**; Ni, **18**; Fe, **19**; Zn, **20**; X = Cl; n=0-6) (1 mmol) and refluxed for 4 hours. The solvent was removed by using rotary evaporator. The resulting metal complexes were washed with diethylether and recrystallized from methanol. The reaction sequence is shown in Scheme 4.3.



Scheme 4.3. Schematic representation of acyclic chiral Schiff base metal complexes.

4.3.3.4. Characterization data for complexes, 15–20

Characterization data for $[L^3Mn_2Cl_4] \cdot 2H_2O$, 15

Yield: 75%; Colour: Brown; M. F.: $C_{36}H_{38}Br_2N_4O_2Mn_2Cl_4 \cdot 2H_2O$; M. W.: 1006.24 g mol⁻¹; IR (ν cm⁻¹, KBr pellet): 3449, 3040, 2937, 2816, 1630, 1541, 1448, 1292, 1124, 1026, 972, 864, 752, 698; CD λ_{max} (mdeg) (CH₃CN): 473 (+0.68), 330 (+2.13), 257 (+3.65), 217 (-2.40); UV-Vis (CH₃OH) [λ_{max}/nm (ε/dm³ mol⁻¹ cm⁻¹)]: 400 (348), 335 (763), 250 (2384), 217 (5080); CHN Analysis: Calcd.: C, 42.97; H, 4.21; N, 5.57%; Found.: C, 43.06; H, 4.18; N, 5.64%.

Characterization data for $[L^3Cu_2Cl_4] \cdot 2H_2O$, 16

Yield: 70%; Colour: Dark green; M. F.: $C_{36}H_{38}Br_2N_4O_2Cu_2Cl_4 \cdot 2H_2O$; M. W.: 1023.45 g mol⁻¹; IR (ν cm⁻¹, KBr pellet): 3426, 3032, 2918, 1622, 1541, 1456, 1280, 1209, 1028, 761, 698; CD λ_{max} (mdeg) (CH₃OH): 358 (-1.91), 307 (-1.16), 287 (-0.85), 232 (+4.80); UV-Vis (CH₃OH) [λ_{max}/nm (ε/dm³ mol⁻¹ cm⁻¹)]: 695 (69), 400 (523), 354 (998), 266 (3077), 244 (4984); CHN Analysis: Calcd.: C, 42.25; H, 4.14; N, 5.47%; Found: C, 42.38; H, 4.22; N, 5.56%.

Characterization data for $[L^3Co_2Cl_4] \cdot 2H_2O$, 17

Yield: 80%; Colour: Dark brown; M. F.: $C_{36}H_{38}Br_2N_4O_2Co_2Cl_4 \cdot 2H_2O$; M. W.: 1014.23 g mol⁻¹; IR (ν cm⁻¹, KBr pellet): 3435, 3032, 2957, 1647, 1618, 1541, 1456, 1199, 873, 1020, 761, 698; CD λ_{max} (mdeg) (CH₃OH): 398 (+2.11), 337 (+1.73), 257 (+5.0), 210 (-7.19); UV-Vis (CH₃OH) [λ_{max}/nm (ε/dm³ mol⁻¹ cm⁻¹)]: 382 (1258), 340 (1256), 219 (8245); CHN Analysis: Calcd.: C, 42.63; H, 4.17; N, 5.52%; Found.: C, 42.54; H, 4.10; N, 5.64%.

Characterization data for $[L^3Ni_2Cl_4] \cdot 4H_2O$, 18

Yield: 73%; Colour: Pale green; M. F.: $C_{36}H_{38}Br_2N_4O_2Ni_2Cl_4 \cdot 4H_2O$; M. W.: 1049.78 g mol⁻¹; IR (ν cm⁻¹, KBr pellet): 3468, 2957, 1635, 1541, 1456, 1203, 1026, 765, 698; CD λ_{max} (mdeg) (CH₃OH): 325 (+1.18), 260 (+2.63); UV-Vis (CH₃OH) [λ_{max}/nm

($\epsilon/\text{dm}^3 \text{ mol}^{-1} \text{ cm}^{-1}$): 403 (931), 345 (687); CHN Analysis: Calcd.: C, 41.19; H, 4.42; N, 5.34%; Found.: C, 41.27; H, 4.33; N, 5.50%.

Characterization data for $[\text{L}^3\text{Fe}_2\text{Cl}_4]\cdot 2\text{H}_2\text{O}$, **19**

Yield: 67%; Colour: Black; M. F.: $\text{C}_{36}\text{H}_{38}\text{Br}_2\text{N}_4\text{O}_2\text{Fe}_2\text{Cl}_4\cdot 2\text{H}_2\text{O}$; M. W.: 1008.05 g mol^{-1} ; IR ($\nu \text{ cm}^{-1}$, KBr pellet): 3395, 2914, 1633, 1616, 1456, 1317, 761, 698; CD λ_{max} (mdeg) (CH_3OH): 543 (+1.64), 378 (+0.66), 281 (+0.76), 221 (-0.65); UV-Vis (CH_3OH) [$\lambda_{\text{max}}/\text{nm}$ ($\epsilon/\text{dm}^3 \text{ mol}^{-1} \text{ cm}^{-1}$)]: 427 (589), 330 (1264), 288 (2014), 212 (8721); CHN Analysis: Calcd.: C, 42.89; H, 4.20; N, 5.56%; Found.: C, 42.75; H, 4.23; N, 5.67%.

Characterization data for $[\text{L}^3\text{Zn}_2\text{Cl}_4]\cdot 2\text{H}_2\text{O}$, **20**

Yield: 70%; Colour: Yellow; M. F.: $\text{C}_{36}\text{H}_{38}\text{Br}_2\text{N}_4\text{O}_2\text{Zn}_2\text{Cl}_4\cdot 2\text{H}_2\text{O}$; M. W.: 1027.14 g mol^{-1} ; IR ($\nu \text{ cm}^{-1}$, KBr pellet): 3445, 2936, 1651, 1548, 1481, 1456, 1271, 1238, 1213, 1033, 877, 756, 698, 621, 515; CD λ_{max} (mdeg) (CH_3OH): 331 (+3.28), 255 (+5.43), 229 (-1.89), 212 (-4.33); UV-Vis (CH_3OH) [$\lambda_{\text{max}}/\text{nm}$ ($\epsilon/\text{dm}^3 \text{ mol}^{-1} \text{ cm}^{-1}$)]: 380 (1614), 231 (7425); CHN Analysis: Calcd.: C, 42.10; H, 4.12; N, 5.45%; Found.: C, 41.97; H, 4.16; N, 5.56%.

4.4. Results and discussion

Synthetic details of the chiral Schiff base ligand L^3 and its metal complexes **15–20** are given in the experimental section 4.3.3. In all the complexes chiral source is 1,4-bis[3-(1-phenylethyliminomethyl)-2-hydroxy-5-bromobenzyl]piperazine L^3 . The IR spectrum of the ligand shows stretching bands at around 1630, 1446 cm^{-1} corresponding to the C=N and the phenolic C-O groups respectively. The formation of chiral Schiff base ligand was confirmed by the absence of aldehydic C=O stretch of 6, 6'-piperazine-1,4-diyl dimethylene bis(4-bromo-2-formylphenol) at 1670 cm^{-1} . The CHN analytical data of the complexes match with the binuclear compositions. The ligand L^3 and its metal complexes **15–20** are CD active.

4.4.1. Chiral ligand, L^3

The circular dichroism (CD) spectrum of the chiral ligand L^3 shows positive bands around 330 nm, 257 nm and 227 nm. The appearance of the CD bands confirms that the compound is chiral as shown in Figure 4.2. The UV-visible spectrum of the ligand is characterized by an intense band at 253 nm and two peaks at 331 and 415 nm respectively.

X-ray crystallography of chiral ligand, L^3

The enantiopure ligand L^3 is prepared in good yields by Schiff-base condensation reaction of one equivalent of 6, 6'-piperazine-1, 4-diyl dimethylene bis(4-bromo-2-formylphenol) with two equivalents of (S)-(-)-1-phenylethylamine in acetonitrile solution (Scheme 4.2). Crystals of L^3 were characterized by elemental and spectral analyses. Single crystal X-ray structure determination data are given in Table 4.1. Selected bond lengths and bond angles are given in Table 4.2. The molecular structure of the ligand L^3 is presented in Figure 4.1. In crystal structure of L^3 , the phenolic protons are involving in intra-molecular hydrogen bonding O–H \cdots N interactions with the imine nitrogens. Two intra-molecular hydrogen bonds: O(1)–H(1) \cdots N(1) (2.578(5)) and O(2)–H(2) \cdots N(2) (2.594(5)).

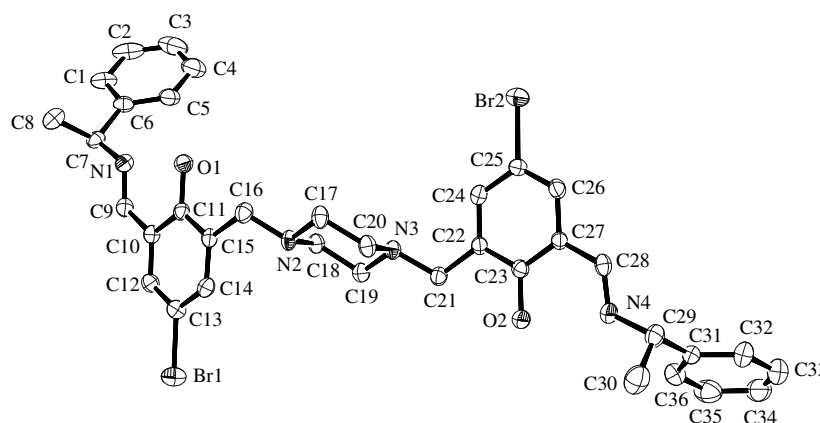


Figure 4.1. Thermal ellipsoid plot of the structure of ligand L^3 . C(7) and C(29) are chiral centers. Thermal ellipsoids are at 30% probability level. Hydrogen atoms have been omitted for clarity.

Table 4.1. Crystallographic parameters of the chiral Schiff base ligand, **L**³

Compound	Chiral ligand, L ³
Empirical formula	C ₃₆ H ₃₈ Br ₂ N ₄ O ₂
<i>M</i>	718.52
<i>T</i> /K	293(2) K
$\lambda/\text{\AA}$	0.71073
Crystal system	Orthorhombic
Space group	<i>P</i> 2 ₁ 2 ₁ 2 ₁
<i>a</i> /\AA	13.7894(8)
<i>b</i> /\AA	14.3556(8)
<i>c</i> /\AA	17.3043(10)
<i>U</i> /\AA ³ , <i>Z</i>	3425.5(3), 4
<i>D</i> _c /mg m ⁻³	1.393
μ/mm^{-1}	2.403
<i>F</i> (000)	1472
Crystal size/mm	0.36 x 0.16 x 0.14
θ range /°	1.84 to 28.28
Limiting indices	-17 ≤ <i>h</i> ≤ 18, -16 ≤ <i>k</i> ≤ 18, -22 ≤ <i>l</i> ≤ 21
Reflections collected	21833
Reflections [<i>I</i> > 2σ(<i>I</i>)]	7963
Data, parameters	7963, 398
Goodness-of-fit on <i>F</i> ²	0.949
Final <i>R</i> indices [<i>I</i> > 2σ(<i>I</i>)]	<i>R</i> 1 = 0.0458, <i>wR</i> 2 = 0.0727
<i>R</i> indices (all data)	<i>R</i> 1 = 0.1293, <i>wR</i> 2 = 0.0902

Table 4.2. Selected bond lengths (Å) and bond angles (°) of ligand, **L**³

Bond lengths			
N(1)-C(7)	1.453(5)	N(1)-C(9)	1.278(5)
N(2)-C(16)	1.450(4)	N(2)-C(17)	1.465(5)
N(2)-C(18)	1.464(4)	O(1)-C(11)	1.349(4)
O(2)-C(23)	1.351(4)	C(19)-N(3)	1.443(4)
N(3)-C(21)	1.454(4)	N(3)-C(20)	1.457(4)
C(29)-N(4)	1.467(5)	C(28)-N(4)	1.269(4)
Br(1)-C(13)	1.896(4)	Br(2)-C(25)	1.921(4)
C(22)-C(24)	1.381(5)	C(22)-C(23)	1.393(5)
C(22)-C(21)	1.502(5)	C(3)-C(4)	1.348(9)
C(3)-C(2)	1.372(9)	C(27)-C(26)	1.384(5)
C(7)-C(8)	1.518(5)	C(7)-C(6)	1.526(6)
C(29)-C(30)	1.512(6)	C(29)-C(31)	1.502(6)
Bond angles			
C(9)-N(1)-C(7)	119.7(4)	N(1)-C(7)-C(8)	108.2(3)
N(1)-C(7)-C(6)	110.5(4)	N(1)-C(9)-C(10)	122.5(4)
C(16)-N(2)-C(17)	110.4(3)	C(16)-N(2)-C(18)	111.8(3)
C(18)-N(2)-C(17)	108.9(3)	C(19)-N(3)-C(20)	109.1(3)
C(19)-N(3)-C(21)	112.3(3)	C(21)-N(3)-C(20)	110.5(3)
C(28)-N(4)-C(29)	118.3(4)	N(4)-C(28)-C(27)	121.9(4)
N(4)-C(29)-C(30)	107.3(4)	N(4)-C(29)-C(31)	111.2(3)
N(3)-C(21)-C(22)	113.1(3)	O(2)-C(23)-C(22)	117.7(3)
O(2)-C(23)-C(27)	121.6(4)	C(14)-C(13)-Br(1)	120.0(3)
C(24)-C(25)-Br(2)	117.8(3)	N(3)-C(19)-C(18)	110.0(3)
N(2)-C(17)-C(20)	110.4(3)	N(3)-C(20)-C(17)	111.5(3)

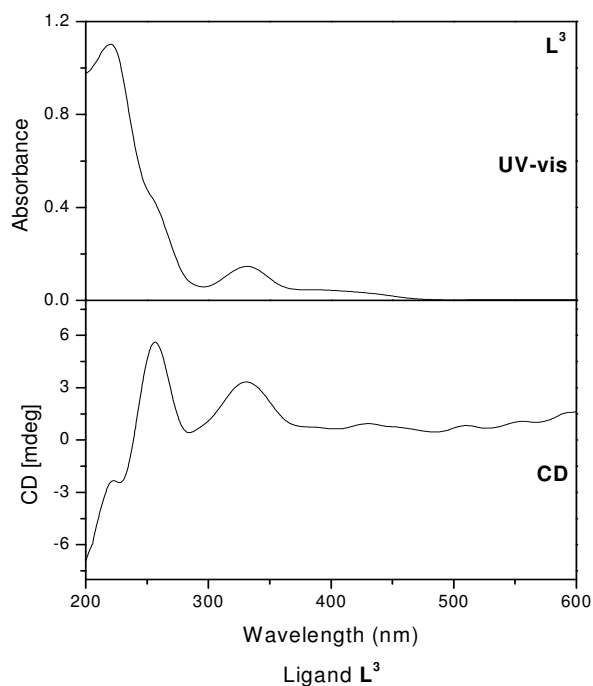


Figure 4.2. CD and UV-vis spectra of ligand L^3 in MeOH solutions (concentrations = 1×10^{-4} M for CD and 1×10^{-5} M for UV-vis).

4.4.2. Manganese complex $[L^3Mn_2Cl_4] \cdot 2H_2O$, **15**

The acyclic chiral binuclear manganese complex **15** was synthesized in good yields by the procedure given in section 4.3.3.3. The IR spectrum of the complex shows a broad band at around 3449 cm^{-1} corresponding to the water molecule and other two strong stretching bands at around 1630 and 1541 cm^{-1} corresponding to the C=N and phenolic C-O groups. Circular dichroism spectra were recorded in methanol solutions. The CD spectra of the complex show bands at $473(+0.68)$, $330(+2.13)$ nm and a high intensity band at $257(+3.65)$, which confirm that the complex is chiral (Figure 4.3). The electronic spectrum in methanol appears band at 400 nm due to the ligand to metal charge transfer transition. An intra ligand $n-\pi^*$ transitions band at 335 nm and another band at 250 nm due to $\pi-\pi^*$ electronic transitions of the ligand are also observed. The analytical data of the complex match with the binuclear composition of $[L^3Mn_2Cl_4] \cdot 2H_2O$.

4.4.3. Copper complex $[\text{L}^3\text{Cu}_2\text{Cl}_4]\cdot 2\text{H}_2\text{O}$, **16**

The chiral copper complex was synthesized by the procedure given in section 4.3.3.3. The binuclear copper(II) complex formation was evident from the C=N stretching vibration frequency observed at 1622 cm^{-1} which is lower than the C=N frequency (at 1630 cm^{-1}) observed for the free ligand L^3 . Moderately strong band at 1541 cm^{-1} appear for the complex corresponding to the phenolic C-O stretching vibrations. A broad band at 3426 cm^{-1} suggests the presence of lattice water. The electronic and the circular dichroism spectrum of the complex is measured in methanol solution (Figure 4.3). The complex exhibits d-d transitions band at 695 nm and the band at 355 nm is due to the charge-transfer band from phenolic oxygen to the vacant d-orbital of the copper(II). Two high intensity bands also appear at 266 nm and 244 nm. The circular dichroism spectrum of the copper complex shows the charge transfer transitions band at 358 (-1.91) and the band at 307 (-1.16) nm is due to the

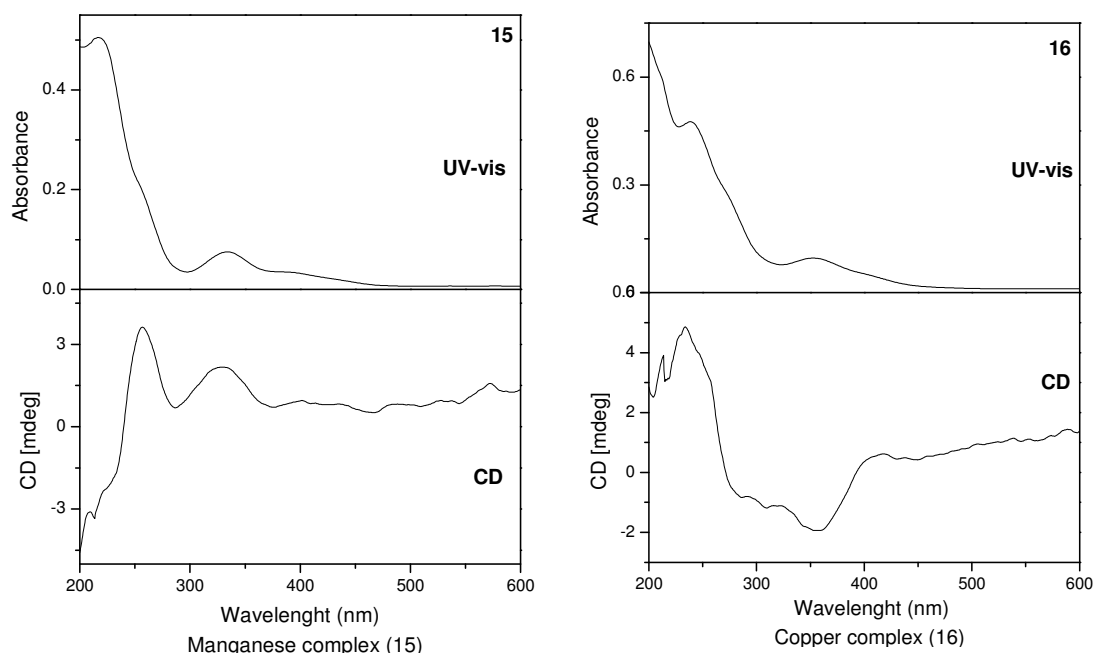


Figure 4.3. CD and UV-vis spectra of binuclear manganese **15** and copper **16** complexes recorded in MeOH solutions (concentrations = $1 \times 10^{-4}\text{M}$ for CD and $1 \times 10^{-5}\text{M}$ for UV-vis).

intra ligand transitions. These bands confirm that the complex is chiral. The CHN analytical data agree with the binuclear composition of $[L^3Cu_2Cl_4] \cdot 2H_2O$.

4.4.4. Cobalt complex $[L^3Co_2Cl_4] \cdot 2H_2O$, 17

The binuclear cobalt complex was synthesized in good yields by the procedure given in section 4.3.3.3. The IR spectrum of the complex shows a broad band at around 3435 cm^{-1} corresponding to the water molecule and other two strong stretching bands at around 1647 , 1541 cm^{-1} corresponding to the C=N and phenolic C-O groups. Strong band appears for C=C at 1456 cm^{-1} . Circular dichroism spectra of the cobalt complex recorded in methanol solution shows bands at 398 (+2.11), 337 (+1.73) and 257 (+5.0) nm. These bands confirm the chirality of the complex (Figure 4.4). The electronic spectrum of the chiral cobalt complex shows band at 382 nm due to the ligand to metal charge transfer transition and an intra ligand transitions band at 340 nm. The analytical data of complex match with the binuclear composition of $[L^3Co_2Cl_4] \cdot 2H_2O$.

4.4.5. Nickel complex $[L^3Ni_2Cl_4] \cdot 4H_2O$, 18

The chiral binuclear nickel complex was synthesized in good yields by the procedure given in section 4.3.3.3. The IR spectrum of the complex shows strong stretching band at around 1635 cm^{-1} corresponding to the C=N group and the phenolic C-O band appear at 1541 cm^{-1} . Strong band appears for C=C at 1456 cm^{-1} and a broad band at around 3468 cm^{-1} corresponding to the water molecules. The electronic and the circular dichroism spectra of the complex were recorded in methanol solutions (Figure 4.4). The electronic spectrum of the complex shows band at 403 nm due to the ligand to metal charge transfer transitions and a band observed at 345 nm corresponds to intra ligand transitions. The circular dichroism spectrum shows two positive bands at 325 (+1.18) and 260 (+2.63) nm. These bands confirm that the complex is chiral. The analytical data of complex match with the binuclear composition of $[L^3Ni_2Cl_4] \cdot 4H_2O$.

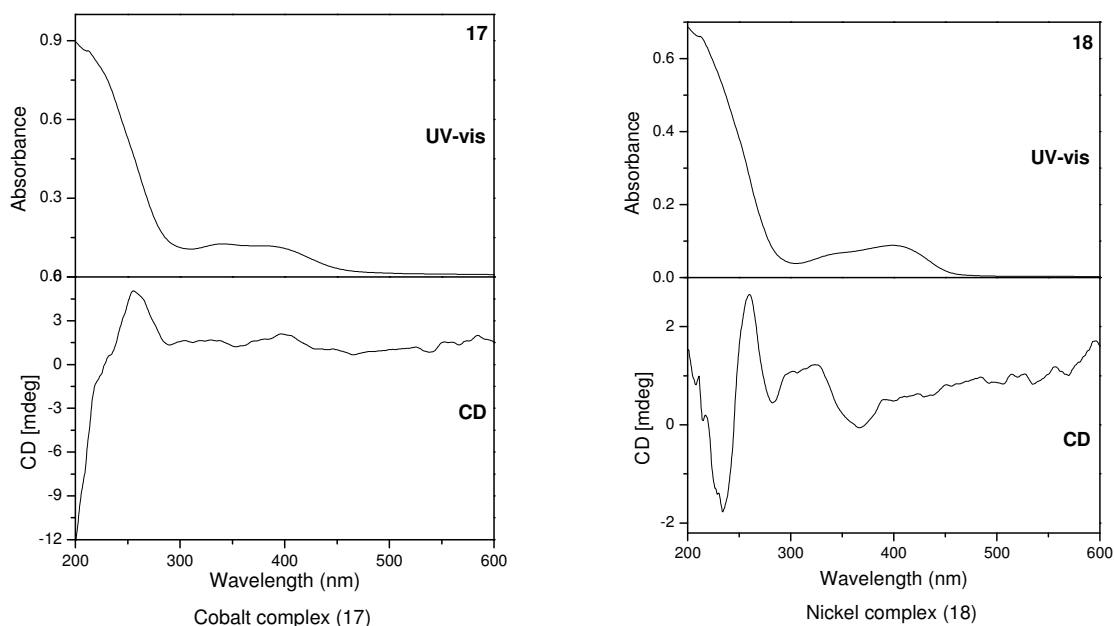


Figure 4.4. CD and UV-vis spectra of cobalt **17** and nickel **18** complexes recorded in MeOH solutions (concentrations = 1×10^{-4} M for CD and 1×10^{-5} M for UV-vis).

4.4.6. Iron complex $[L^3Fe_2Cl_4] \cdot 2H_2O$, **19**

The iron complex was synthesized in good yields by the procedure given in section 4.3.3.3. The IR spectrum of the complex shows strong stretching band at around 1633 cm^{-1} corresponding to the C=N groups and band appears for C=C at 1456 cm^{-1} . Circular dichroism spectrum of the iron complex recorded in methanol solution shows bands at 543 (+1.64), 378 (+0.66) and 281 (+0.76) nm. Appearance of these bands confirms that the complex is chiral (Figure 4.5). The electronic spectrum of the complex shows bands at 427 nm due to the ligand to metal charge transfer transitions and at 330 nm due to the intra ligand $n-\pi^*$ transitions. The band at 288 nm is due to $\pi-\pi^*$ electronic transitions of the ligand. The analytical data match with the binuclear composition of $[L^3Fe_2Cl_4] \cdot 2H_2O$.

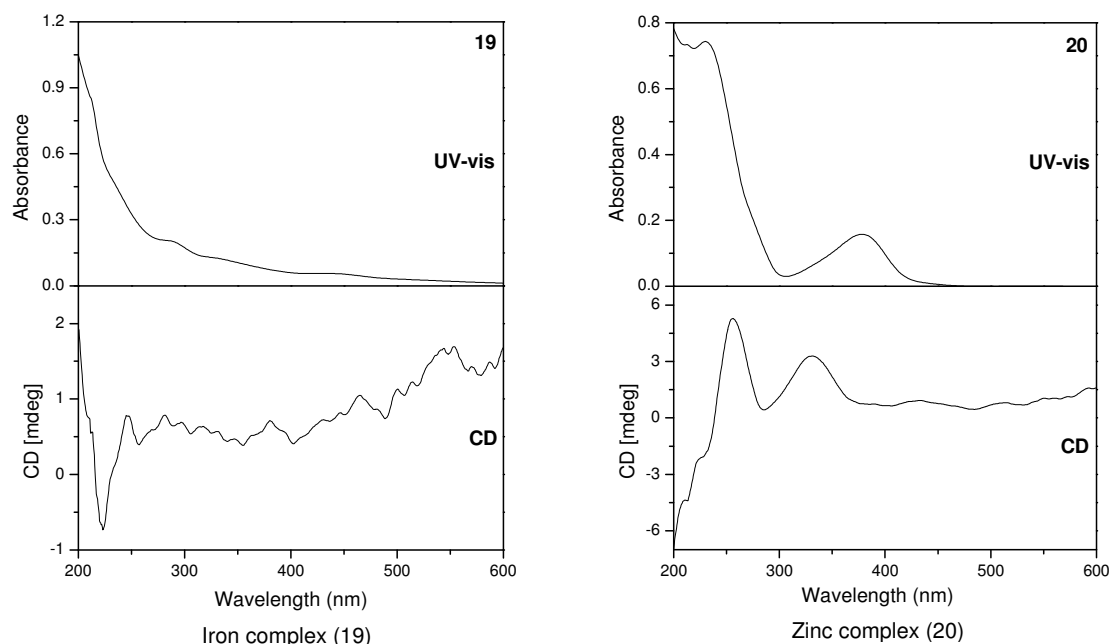


Figure 4.5. CD and UV-vis spectra of iron **19** and zinc **20** complexes recorded in MeOH solution (concentrations = 1×10^{-4} M for CD and 1×10^{-5} M for UV-vis).

4.4.7. Zinc complex $[L^3Zn_2Cl_4] \cdot 2H_2O$, **20**

Zinc complex was synthesized in good yields by the procedure given in section 4.3.3.3. The IR spectrum of the complex shows two strong stretching bands at around 1651 and 1548 cm^{-1} corresponding to the C=N and phenolic C-O groups. Circular dichroism spectrum of the complex recorded in methanol solution shows bands at 331 ($+3.28$) and a high intensity band at 255 ($+5.43$) nm. These bands confirm that the complex is chiral as shown in Figure 4.5. The electronic spectrum of the zinc complex in methanol solution shows broad band at 380 nm due to the ligand to metal charge transfer transitions and a band at 231 nm due to $\pi-\pi^*$ electronic transitions of the ligand. The analytical data of the complex match with the binuclear composition of $[L^3Zn_2Cl_4] \cdot 2H_2O$.

4.5. Catalysis

To examine the activity of the chiral complexes in the catalytic process, the alkenes oxidation reactions were studied. The epoxidation reactions were carried out in CH₃CN using iodosylbenzene (PhIO) as the terminal oxidant at room temperature. The oxidation reactions were run for 24 hours. In absence of the catalyst under similar reaction conditions, there is no reaction between oxidant and olefins.

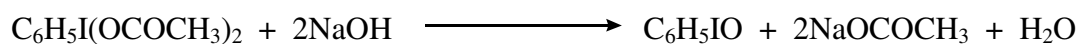
The gas chromatographic analyses of authentic samples are given in Chapter 2 (Figure 2.13). The products were confirmed by ¹H-NMR spectroscopy. The oxidation product yields and enantiomeric excess in the case of styrene were determined by gas chromatography (GC). The oxidation product yields and enantiomeric excess of the *cis*-stilbene and *trans*-stilbene were determined by HPLC analyses.

The amount of epoxide formed on epoxidation of *trans*- and *cis*-stilbene and the enantiomeric excess of the stilbene epoxide catalyzed by manganese complex **15** as a function of time are shown in Figures 4.6 and 4.7. The amount of epoxide formed on epoxidation of styrene and the enantiomeric excess of the epoxide catalyzed by cobalt complex **17** as a function of time are shown in Figure 4.8. The percentage of epoxide yields and the enantiomeric excess of the epoxides are given in Table 4.4. Manganese catalyst **15** is encouraging for the epoxidation reactions of the styrene (yield 98%) and for the *trans*-stilbene epoxidation giving up to 20% of enantiomeric excess and for the *cis*-stilbene epoxidation yielding up to 40% at room temperature with 46% of enantiomeric excess.

4.5.1. Synthesis of Iodosylbenzene (PhIO)

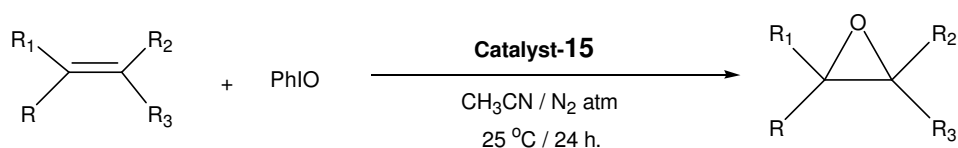
The iodosylbenzene (PhIO) used in the catalytic study as oxidant is prepared using a reported procedure.¹⁶ Finely ground iodosylbenzene diacetate (32.2 g, 0.10 mol) is placed in a 250 mL beaker and 150 mL of 3N sodium hydroxide is added over a 5 minute period with vigorous stirring. The lumps of solid that formed are triturated with a stirring rod or spatula for 15 minutes and the reaction mixture stands for an additional 45 minutes to complete the reaction. 100 mL of water is added, the mixture is stirred vigorously and the crude solid iodosobenzene is collected on a Büchner

funnel, washed there with 200 mL of water and dried by maintaining suction. Final purification is effected by triturating the dried solid in 75 mL of chloroform in a beaker. The iodosylbenzene is separated by filtration and air-dried (Yield: 85%).



4.5.2. Epoxidation of *cis* / *trans*-stilbene catalyzed by manganese complex, **15**

The chiral manganese catalyst **15** (0.025 g, 0.025 mmol) and *cis* / *trans*-stilbene (0.180 g, 1 mmol) were dissolved in 5 mL acetonitrile. The reaction was initiated by the addition of iodosylbenzene (PhIO) (0.220 g, 1 mmol) and stirred at room temperature under nitrogen atmosphere for 24 hours. The general reaction sequence is shown in Scheme 4.4. After stirring, the mixture was concentrated in vacuum. Anhydrous ether (10 mL) added to the brown residue and the ether solution was carefully filtered. Then the ether was removed under reduced pressure and purified with column chromatography from hexane.



Scheme 4.4. Schematic representation of catalytic epoxidation reaction.

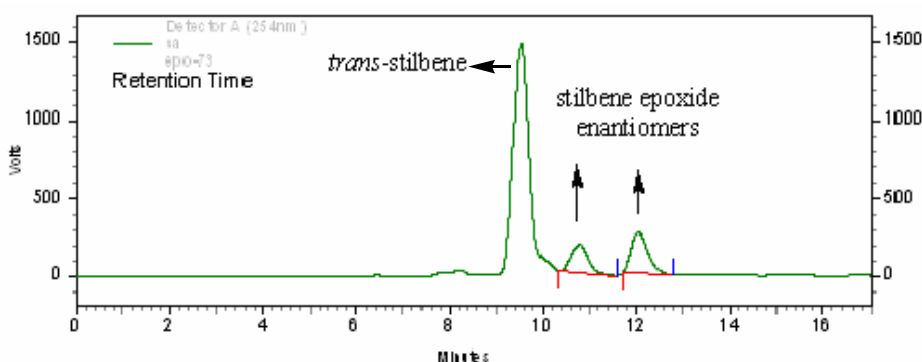


Figure 4.6. HPLC analysis of *trans*-stilbene epoxide enantiomers catalyzed by complex **15**.

The HPLC analysis profile of the *trans*-stilbene epoxide catalyzed by **15** is shown in Figure 4.6 and data percentage yields of enantiomeric excess are given in Table 4.4 (entry 2). The HPLC analysis profile of the *cis*-stilbene epoxide catalyzed by **15** is shown in Figure 4.7. HPLC analyses data percentage of enantiomeric excess of *cis*-stilbene epoxide catalyzed by complex **15** as a function of time are given in Table 4.3 and 4.4 (entry 1).

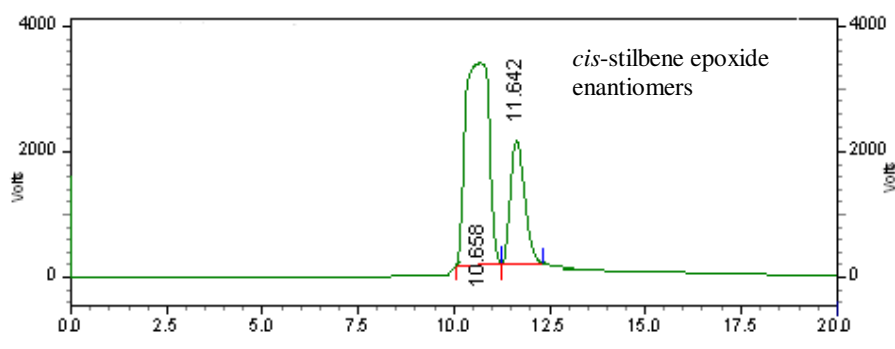


Figure 4.7. HPLC analysis profile of *cis*-stilbene epoxide catalyzed by complex **15**.

Table 4.3. HPLC analysis data percentage of enantiomeric excess catalyzed by complex **15** as a function of time

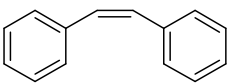
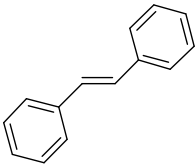
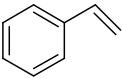
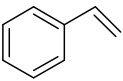
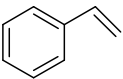
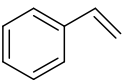
Pk #	Retention Time	Area	Area %	Height	Height %
1	10.658	137554919	72.996	3197331	62.131
2	11.642	50886532	27.004	1948801	37.869
Totals		188441451	100.000	5146132	100.000

4.5.3. Epoxidation of styrene catalyzed by chiral complexes **15**, **16**, **17** and **19**

All the reactions were carried out by the same procedure. Oxidations of styrene by the chiral complexes, manganese **15**, copper **16**, cobalt **7** and iron **19** with iodosylbenzene (PhIO) as oxidant were carried out by the following procedure:

The chiral catalyst (0.025 mmol) and styrene (0.104 g, 1 mmol) were dissolved in 5 mL acetonitrile. The reaction was initiated by the addition of iodosylbenzene (0.220 g, 1 mmol) and stirred at room temperature under nitrogen atmosphere for 24 hours (Scheme 4.5). After completion of the reaction, the solvent was removed under reduced pressure.

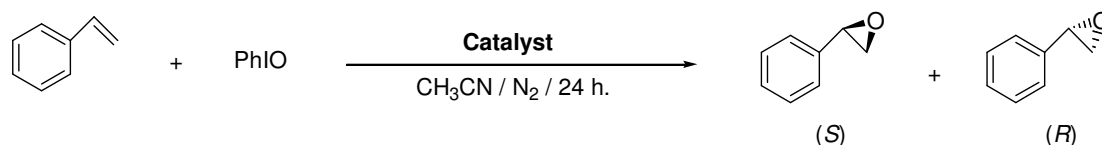
Table 4.4. Oxidation products ^a of olefins by PhIO catalyzed by **15**, **16**, **17** and **19**

Entry	Substrate	Catalyst	Epoxide Yield (%)	Epoxide e. e.(%)	1-Phenyl acetaldehyde Yield(%) ^c	Acetophenone Yield(%) ^c
1		Mn(II) 15	40 ^b	46 ^d	—	—
2		Mn(II) 15	25 ^b	20 ^d	—	—
3		Mn(II) 15	98 ^c	—	—	1
4		Cu(II) 16	—	—	50	42
5		Co(II) 17	53 ^c	—	20	24
6		Fe(II) 19	—	—	67	30

^a Products confirmed by ¹H-NMR spectroscopy. ^b Based on substrate consumed and determined by chiral column (CHIRALCEL OD-H) HPLC analysis. ^c Based on substrate consumed and determined by chiral column GC analysis (Supelco α -DEX 325, 30m length, 0.25mm id, 0.25 μ m film thickness). ^d Enantiomeric excess of epoxides, determined by chiral column (CHIRALCEL OD-H) HPLC analysis.

Anhydrous ether (10 mL) was added to the brown residue and the ether solution was carefully filtered. Then the ether was removed under reduced pressure and purified using short silica gel column from hexane. The product of the styrene was confirmed by ¹H-NMR spectroscopy (styrene epoxide $\delta \sim 3.84$ in CDCl₃). The

oxidation product yields and enantiomeric excess of styrene were determined by gas chromatography (GC). The gas chromatographic profile of authentic samples are shown in Chapter 2 (Figure 2.13). Gas chromatographic (GC) analysis of styrene oxidation products catalyzed by cobalt catalyst **17** is shown in Figure 4.8.



Scheme 4.5. Schematic representation of catalytic epoxidation of styrene.

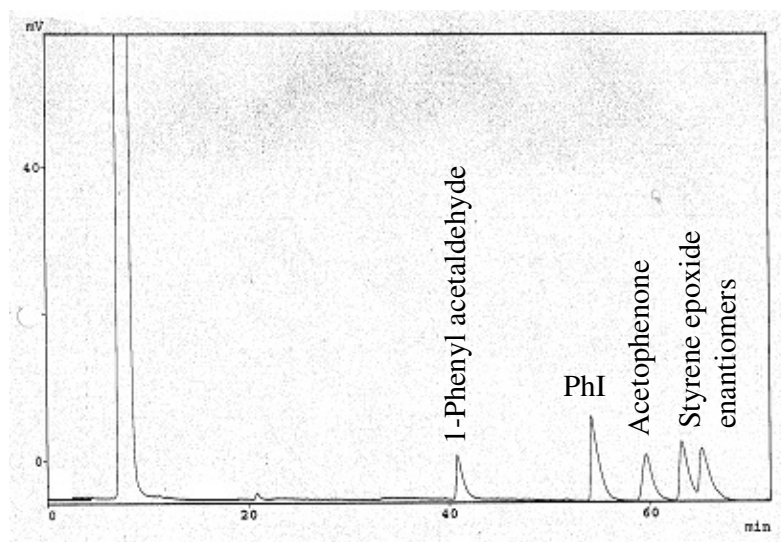


Figure 4.8. A representative gas chromatographic (GC) analysis of styrene oxidation products catalyzed by cobalt complex **17**.

The manganese catalyst **15** is promising for the epoxidation reactions of the styrene (yield 98%). The cobalt complex **17** favour for the oxidation of styrene yields to styrene epoxide (yield 53%). Complexes **16** and **19** favour for the oxidation of styrene yields to 1-phenylacetaldehyde and acetophenone.

4.6. Conclusions

New optically active Schiff base ligand **L**³ and its acyclic binuclear metal complexes **15–20** were characterized by analytical and spectral methods. All complexes show optical activity was confirmed by the circular dichroism studies.

The catalytic activities of the chiral Schiff base complexes were analyzed for the epoxidation of alkenes by a terminal oxidant. The manganese catalyst **15** is promising for the epoxidation reactions of the styrene (yield 98%). The cobalt complex **17** favour for the oxidation of styrene yields to styrene epoxide (yield 53%). Epoxidation of *trans*-stilbene catalyzed by **15**, yields up to 25% at room temperature with 20% of enantiomeric excess. Epoxidation of *cis*-stilbene catalyzed by **15**, yields up to 40% at room temperature with 46% of enantiomeric excess.

4.7. References

1. (a) R. A. Sheldon and J. K. Kochi, *Metal catalysed oxidations of organic compounds*, Academic Press, NY, **1981**, p. 81; (b) K. A. Jørgensen, *Chem Rev.*, **1989**, 89, 431; (c) B. Meunier, *Chem. Rev.*, **1992**, 92, 1411.
2. (a) J. P. Collman, X. Zang, V. J. Lee, E. S. Uffelman and J. I. Brauman, *Science.*, **1993**, 261, 1404; (b) Y. Naruta, in: R. A. Sheldon (Ed.), *Metalloporphyrins in Catalytic Oxidation*, Marcel Dekker, NY, **1994**, p. 241, Chap. 8.
3. (a) E. N. Jacobsen, in: I. Ojima (Ed.), *Catalytic Asymmetric Synthesis*, VCH, NY, **1993**, p. 159; (b) W. Zhang, J. L. Loebach, S. R. Wilson and E. N. Jacobsen, *J. Am. Chem. Soc.*, **1990**, 112, 2801.
4. (a) R. Irie, K. Noda, Y. Ito and T. Katsuki, *Tetrahedron Lett.*, **1991**, 32, 1055; (b) R. Irie, K. Noda, Y. Ito, N. Matsomoto and T. Katsuki, *Tetrahedron: Asymmetry.*, **1991**, 2, 481.
5. D. Das and C.-P. Cheng, *Dalton trans.*, **2000**, 1081.
6. (a) O. Hayaishi (Ed.), *Oxygenases*, Academic Press, NY, **1962**; (b) O. Hayaishi (Ed.), *Molecular Mechanics of Oxygen Activation*, Academic Press, NY, **1974**,

- p. 1; (c) K. D. Karlin and Z. Teyklár (Eds.), *Bioinorganic Chemistry of Copper*, Chapman & Hall, NY, **1993**.
7. (a) D. H. R. Barton, A. E. Martell and D. T. Sawyer (Eds.), *The Activation of Dioxygen and Homogenous Catalytic Oxidation*, Plenum, NY, **1993**; (b) J. Reedijk, (Ed.), *Bioinorganic Catalysis*, Marcell Dekker, NY, **1993**.
8. (a) Y. Natta, F. Tani, N. Ishihara and K. Maruyama, *Bull. Chem. Soc., Jpn.* **1993**, 66, 158; (b) R. L. Haltermann and S. T. Jan, *J. Org. Chem.*, **1991**, 56, 5253; (c) Y. Natta, N. Ishihara, F. Tani and K. Maruyama, *Chem. Lett.*, **1991**, 1933.
9. (a) J. T. Groves, Jr. W. J. Kruper and R. C. Haushalter, *J. Am. Chem. Soc.*, **1980**, 102, 6375; (b) J. T. Groves, Jr. W. J. Kruper, T.E. Nemo and R. S. Myers, *J. Mol. Catal.*, 1980, 7, 169.
10. T. Katsuki, *Coordination. Chem. Rev.*, **1995**, 140, 189.
11. (a) R. I. Kureshy, N. H. Khan, S. H. R. Abdi and K. N. Bhatt, *Tetrahedron Asymm.*, **1993**, 4, 1693; (b) R. I. Kureshy, N. H. Khan and S. H. R. Abdi, *J. Mol. Catal.*, **1995**, 96, 117; (c) R. I. Kureshy, N. H. Khan, S. H. R. Abdi and A. K. Bhatt, *J. Mol. Catal.*, **1996**, 110, 33; (d) R. I. Kureshy, N. H. Khan, S. H. R. Abdi, P. Iyer and A. K. Bhatt, *J. Mol. Catal.*, **1997**, 120, 101; (e) R. I. Kureshy, N. H. Khan, S. H. R. Abdi, P. Iyer and A. K. Bhatt, *J. Mol. Catal.*, **1998**, 130, 41; (f) R. I. Kureshy, N. H. Khan, S. H. R. Abdi, P. Iyer and S. T. Patel, *Polyhedron*, **1999**, 18, 1773; (g) R. I. Kureshy, N. H. Khan, S. H. R. Abdi, P. Iyer and A. K. Bhatt, *J. Mol. Catal.*, **2000**, 160, 217.
12. (a) W. Zhang and E. N. Jacobsen, *J. Org. Chem.*, **1991**, 56, 2296; (b) W. Zhang, J. L. Loebach and E. N. Jacobsen, *J. Am. Chem. Soc.*, **1990**, 112, 2801; (c) A. Hatayama, N. Hosoya, R. Irie, Y. Ito and T. Katsuki, *Synlett.*, **1992**, 407; (d) H. Sasaki, R. Irie and T. Katsuki, *Synlett.*, **1993**, 300; (e) H. Sasaki, R. Irie and T. Katsuki, *Synlett.*, **1994**, 356; (f) N. Hosoya, A. Hatayama, R. Irie, H. Sasaki and T. Katsuki, *Tetrahedron*, **1994**, 50, 4311.

13. (a) Y. N. Ito and T. Katsuki, *Bull. Chem. Soc. Jpn.* **1999**, 72, 603; (b) B. S. Lane, M. Vogt, V. J. DeRose and K. Burgess, *Synlett.*, **1994**, 255; (c) P. Pietikainen, *Tetrahedron Lett.*, **1994**, 35, 941.
 14. X.-W. Liu, N. Tang, Y.-H. Chang and M.-Y. Tan, *Tetrahedron Asymm.*, **2004**, 15, 1269.
 15. (a) A. I. Vogel, *Textbook of Practical Organic Chemistry*, 4th Ed. ELBS and Longman, **1978**; (b) D. D. Perrin, W. L. F. Armarego, D. R. Perrin, *Purification of Laboratory Chemicals*, Pergamon Press, London, **1966**.
 16. H. Saltzman and J. G. Sharefkin, *Org. Synth.*, **1973**, Coll. Vol. V, 658.
 17. SHELXTL Reference Manual, Version 5.1, Bruker AXS, Analytic X-Ray Systems, Inc., WI, **1997**.
 18. R. Thirumurugan, S. S. S. Raj, G. Shanmugam, H.-K. Fun, K. Chinnakali, S. Chantrapromma, M. Marappan and M. Kandaswamy, *Act Cryst.*, C54, **1998**, 780.
-

Chapter 5

Synthesis and structural characterization of some chiral acyclic and macro cyclic binuclear metal complexes and epoxidation reactions

5.1. Abstract

A new class of first row transition metal complexes of general formula $[M_2L^4]Cl_2 \cdot nH_2O$ with unsymmetrical dicompartmental chiral Schiff base macrocyclic ligand **L**⁴ was synthesized using 6, 6'-piperazine-1,4-diyl dimethylene bis(4-bromo-2-formylphenol), (R,R)-*trans*-1,2-diaminocyclohexane and metal salts. Structure of the chiral acyclic binuclear copper complex **21** was determined by X-ray crystallographic methods. Crystal data for copper complex **21**: Monoclinic space group $P2_1$, $a = 7.6061(6)$ Å, $b = 22.2607(16)$ Å, $c = 12.0995(9)$ Å, $V = 2017.0(3)$ Å³, $Z = 2$. In the macrocyclic ligand system there are two different N₂O₂ compartments; one has two piperazinyl nitrogens (amino) and two phenolic oxygens and the other compartment has two azomethine nitrogens (imino) and two phenolic oxygens as the coordination sites. Characterization of the acyclic binuclear copper(II) complex **21**, ligand **L**⁴ and its binuclear metal complexes **22–27** (M = Cu²⁺, **22**; Mn²⁺, **23**; Co²⁺, **24**; Ni²⁺, **25**; Fe²⁺, **26**; Zn²⁺, **27**) was carried out by microanalysis, ¹H-NMR, IR, UV/Vis- and CD spectral studies. They exhibit circular dichroism signals at room temperature.

The catalytic properties of these complexes in the olefins (*cis*-stilbene, *trans*-stilbene and styrene) oxidation reactions were investigated. The oxidations were carried out in CH₃CN using iodosylbenzene (PhIO) as the terminal oxidant at room temperature for 24 hours. The manganese catalyst **23** is promising for the epoxidation reactions of styrene (yield 96%). Catalytic activity of the other complexes viz. Cu²⁺, Co²⁺, Fe²⁺ (**22**, **24** and **26**) for the styrene oxidation reactions was also investigated.

Among these catalysts only Co^{+2} catalyst gave minor yields of epoxide. Epoxidation of *cis*-stilbene catalyzed by manganese complex **23**, yields up to 33% at room temperature with 85% of enantiomeric excess.

5.2. Introduction

Metal catalyzed oxidation of various organic substrates is of biochemical interest.¹ Optically active epoxides are known as versatile chiral building blocks in organic synthesis.² Many studies have been directed towards asymmetric epoxidation reaction of olefins. Sharpless *et al.* found that epoxidation of allylic alcohols using $\text{Ti}(\text{O}^i\text{Pr})_4$ /diethyl tartarate/*t*-butyl hydroperoxide derived system proceeded with high enantioselectivity.³ The iron complexes of porphyrins were found to be effective for the asymmetric epoxidation of unfunctionalized olefins.⁴ Kochi *et al.* reported manganese salen complex to be a useful catalyst for the epoxidation of olefins.⁵ Jacobsen *et al.* reported chiral (salen) manganese(III) complex was effective catalyst for the enantioselective epoxidation of unfunctionalized olefins.⁶ Katsuki *et al.* discovered a number of chiral (salen) manganese(III) complex by replacement of carbons by stereogenic centers on the aromatic ring part (C-3 and C-3' substituents) and those on the ethylenediamine part (C-8 and C-8' stereogenic centers).⁷ Very recently Jacobsen and Katsuki have reported an efficient catalytic system⁸ for several types of olefins with moderate to high enantioselectivity depending on the substitution degree of double bond using iodosylbenzene, NaOCl, H_2O_2 and periodates as terminal oxidants. Jian Gao *et al.* reported structurally defined chiral macrocyclic dicopper complexes for enantioselective oxidative coupling reactions.⁹

The aim of present work is to synthesize new macrocyclic chiral Schiff base ligand **L**⁴ and its metal complexes **22–27** and to examine the catalytic activity of the chiral Schiff base metal complexes.

5.3. Experimental

5.3.1. Chemicals and reagents

All chemicals and the solvents used in this work were of analytical grade and were used as obtained. The chemicals and the sources are as follows: 5-bromosalicylaldehyde and piperazine were purchased from Lancaster (England), CDCl_3 was obtained from Acros (India). (R,R)-*trans*-1,2-diaminocyclohexane was separated from the mixture of *cis*- and *trans*-1,2-diaminocyclohexane, according to the literature procedure.¹⁰ All metal salts were purchased commercially and used as received. HPLC grade solvents were used for spectral analysis. Iodobenzenediacetate, styrene, *cis*-stilbene and *trans*-stilbene were purchased from Aldrich chemicals. Iodosylbenzene was prepared according to literature procedure.¹⁷

5.3.2. Physical measurements

The ^1H -NMR spectra were recorded with a Bruker DRX-400 spectrometer using CDCl_3 as the solvent. Tetramethylsilane (TMS) was the internal standard. Elemental analyses were carried out on a Perkin-Elmer 240C CHN analyzer. Infra red spectra were recorded using KBr pellets on a Jasco-5300 FT-IR spectrophotometer. The UV-visible spectra were recorded with a Shimadzu model UV-3101PC spectrophotometer. The CD spectra were measured with a JASCO J-810 spectropolarimeter. Optical rotation was measured using an AUTOPOL-IV automatic polarimeter (readability $\pm 0.01^\circ$).

Gas chromatographic analyses were carried out on a Shimadzu GC 14B instrument equipped with a stainless steel packed column (5 m, 5 % SE 30) and a chiral capillary column (Supelco α -DEX 325, 30m length, 0.25mm id, 0.25 μm film thickness) and a flame ionization detector (FID). HPLC analyses of *cis*-stilbene epoxide and *trans*-stilbene epoxide products were carried out on a Shimadzu SCL-10A instrument equipped with CHIRALCEL OD-H using Class-VP program.

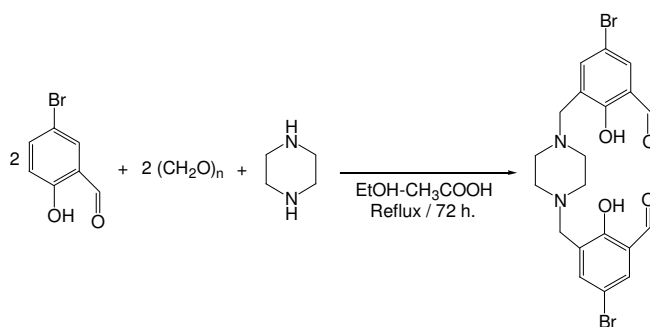
X-ray crystallography

X- ray data were collected for the crystal of copper complex **21** on Bruker-Nonius SMART APEX CCD single crystal diffractometer using graphite monochromated Mo-K α radiation (0.71073Å). The SMART software was used for intensity data acquisition and the SAINT-Plus software¹¹ was used for data extraction. In each case, absorption correction was performed with help of SADABS program.¹² The SHELXTL package¹³ was used for structure solution and least-squares refinement on F². All the non-hydrogen atoms were refined anisotropically. The ORTEP3¹⁴ and the PLATON¹⁵ softwares were used for molecular graphics.

5.3.3. Synthesis

5.3.3.1. 6, 6'-piperazine-1,4-diyl dimethylene bis(4-bromo-2-formylphenol)

A mixture of piperazine (2.2 g, 0.025 mol), paraformaldehyde (1.8 g, 0.06 mol) and 5-bromosalicylaldehyde (10.2 g, 0.05 mol) in ethanol-acetic acid solutions (100 mL 4:1 v/v) was refluxed for 72 hours and neutralized with a saturated solution of sodium carbonate after cooling to room temperature. Ethanol was removed by distillation and the product was further purified by silica gel column chromatography using chloroform-light petroleum (1:4 v/v) as the eluent (Yield: 90%). M. W.: 512.20 g mol⁻¹; M. P.: 217 °C; ¹H-NMR (CDCl₃): δ 1.8 (m, 8H, piperazine CH₂), 3.6 (m, 4H, benzylic CH₂), 7.0-7.4 (d, 4H, aromatic CH) and 9.85 (s, 2H, CHO); IR (KBr): 3450 (phenolic OH), 2840-2940 (N-CH₂), 1670 (CHO) and 1450 cm⁻¹ (aromatic skeleton). (This is the modified procedure from the literature procedure²⁰). Synthetic route is shown in Scheme 5.1.



Scheme 5.1. Schematic representation of the Mannich reaction.

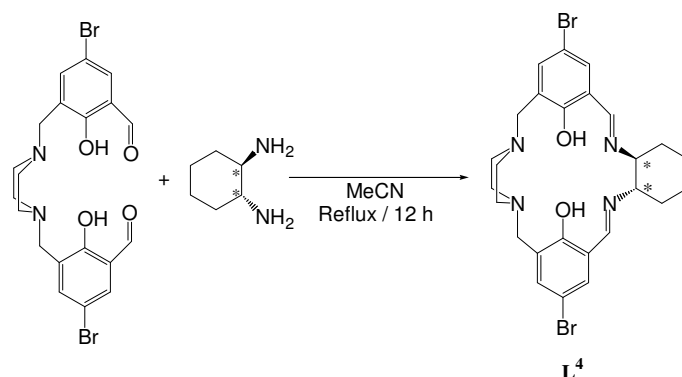
5.3.3.2. Resolution of *cis/trans*-1,2-diaminocyclohexane

A 500 mL beaker with magnetic stirrer was charged with L-(+)-tartaric acid (75 g, 0.50 mol) and distilled water (200 mL). The mixture was stirred at room temperature until complete dissolution occurred at which point a mixture of *cis*- and *trans*-1,2-diaminocyclohexane (120 mL, 97 mol) was added at a rate such that the reaction temperature just reached 70 °C. To the resulting solution was added glacial acetic acid (50 mL, 0.88 mol) at a rate such that the reaction temperature just reached 90 °C. A white precipitate was formed immediately upon addition of the acid, and the slurry was vigorously stirred as it was cooled to room temperature over 2 h.

The mixture was then cooled to ≤ 5 °C in an ice bath for 2 hours and the precipitate was collected by vacuum filtration. The wet cake was washed with 5 °C water (50 mL) and then rinsed with methanol (5 x 50 mL). The solid was dried by drawing air through the filter cake for 1 h. The product was then dried at 40 °C under reduced pressure to yield (R,R)-1,2-diaminocyclohexane mono-(+)-tartarate salt as a white solid (Yield: 80 g, 99%). To the dry compound in a separating funnel, saturated KOH (73 mL) solution was added and separated the upper layer. The compound was distilled under vacuum at 165–170 °C. The resulting enantiomeric excess of (R,R)-*trans*-1,2-diaminocyclohexane is ≥ 99 %.

5.3.3.3. Synthesis of new macrocyclic chiral Schiff base ligand, **L**⁴

To a solution of 6, 6'-piperazine-1,4-diyl dimethylene bis(4-bromo-2-formylphenol) (0.512 g, 1 mmol), in acetonitrile (25 mL) was added (R,R)-*trans*-1,2-diaminocyclohexane (0.114 g, 1 mmol). The reaction mixture was refluxed for 12 hours. The resulting yellow solid was collected by filtration and washed with acetonitrile. Recrystallization from chloroform gave the desired chiral ligand **L**⁴ as a yellow crystalline solid (Yield: 76%). The reaction sequence is shown in Scheme 5.2.



Scheme 5.2. Synthetic scheme for the macrocyclic chiral Schiff base ligand **L⁴**.

Characterization data for **L⁴**

Optical rotation $[\alpha]_D^{25}$: $-780 \cdot 10$ (c 1, chloroform); M. F.: $C_{26}H_{30}N_4O_2Br_2$; M. W.: $590.35 \text{ g mol}^{-1}$; IR ($\nu \text{ cm}^{-1}$, KBr pellet): 3443, 2930, 2856, 2810, 1628, 1448, 1375, 1290, 1134, 1024, 869, 700; ^1H NMR (CDCl_3 , δ , ppm): 8.26(d, 2H, $\text{HC}=\text{N}$), 7.17-7.4(m, 4H, Ar-H), 3.71(s, 4H, CH_2), 3.54 (q, 2H, CH), 2.55(s, 8H, CH_2), 1.88(s, 8H, CH_2); CD λ_{max} (mdeg) (CHCl_3): 344 (-130), 270 (-166); UV-Vis (CHCl_3) [$\lambda_{\text{max}}/\text{nm}$ ($\epsilon/\text{dm}^3 \text{ mol}^{-1} \text{ cm}^{-1}$)]: 335 (16000), 256 (34300); CHN Analysis: Calcd: C, 52.90; H, 5.12; N, 9.49%; Found: C, 53.06; H, 5.24; N, 9.63%; LCMS (m/z): 591 (M^+).

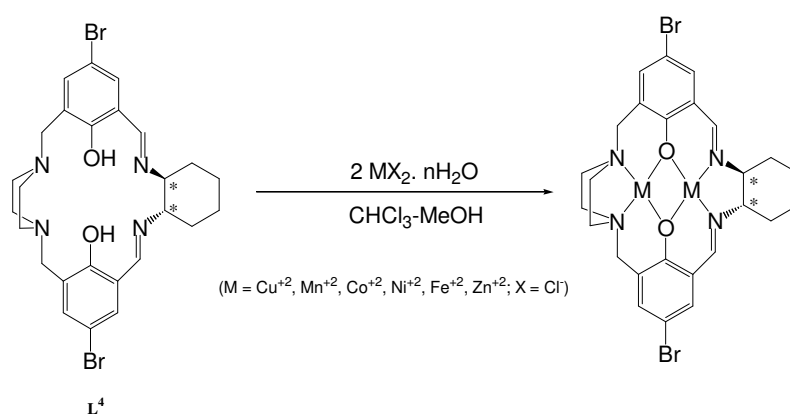
5.3.3.4. Synthesis of chiral acyclic binuclear copper complex, **21**

To a solution of **6**, 6'-piperazine-1,4-diylldimethylene bis(4-bromo-2-formylphenol) (0.256 g, 0.5 mmol), in methanol (25 mL) was added $\text{CuCl}_2 \cdot 4\text{H}_2\text{O}$ (0.170 g, 1 mmol) under reflux conditions for 1 hour. Then (R,R)-*trans*-1,2-diaminocyclohexane (0.114 g, 1 mmol) was added. The reaction mixture was refluxed for another 4 hours. The resulting reaction mixture was then concentrated using rotary evaporator. Recrystallization from methanol solution gave the green crystals suitable for X-ray single crystal analysis were obtained after 14 days (Yield: 68%).

5.3.3.5. General Synthetic procedure for complexes, **22–27**

To a solution of ligand **L⁴** (0.295 g, 0.5 mmol) in chloroform (20 mL) was added $\text{MX}_2 \cdot n\text{H}_2\text{O}$ (M = Cu, Mn, Co, Ni, Fe, Zn; X = Cl; n = 0-6) (1 mmol) dissolved in

methanol (20 mL). The reaction mixture was refluxed for 4 hours. The resulting solution was evaporated to half the volume and then allowed to cool by standing at room temperature. Solid compound was collected after the slow evaporation of the solvent at room temperature. The resulting chiral macrocyclic binuclear complex was recrystallised from chloroform to provide good yields. Generalized synthetic reaction sequence is shown in Scheme 5.3. Metal complex numbering sequences: ($M = Cu^{+2}$, **22**; Mn^{+2} , **23**; Co^{+2} , **24**; Ni^{+2} , **25**; Fe^{+2} , **26**; Zn^{+2} , **27**).



Scheme 5.3. Schematic representation of the macrocyclic chiral metal complexes.

5.3.3.6. Characterization data for complexes, 21–27

Characterization data for 21

M. F.: $C_{32}H_{46}Br_2N_6O_2Cu_2Cl_4 \cdot 4H_2O$; M. W.: $1047.52 \text{ g mol}^{-1}$; IR ($\nu \text{ cm}^{-1}$, KBr pellet): 3402, 3288, 3223, 3113, 2922, 2852, 1639, 1577, 1442, 1116, 1033, 684; CD λ_{max} (mdeg) (DMF): 397 (-134), 320 (-5); UV-Vis (DMF) [$\lambda_{\text{max}}/\text{nm}$ ($\epsilon/\text{dm}^3 \text{ mol}^{-1} \text{ cm}^{-1}$)]: 585 (400), 375 (2375), 273 (6632); CHN Analysis: Calcd.: C, 36.69; H, 5.20; N, 8.02%; Found: C, 36.73; H, 5.29; N, 8.16%.

Characterization data for 22

Yield: 70%; Colour: Green; M. F.: $C_{26}H_{28}N_4O_2 \cdot Br_2Cl_2Cu_2 \cdot 4H_2O$; M. W.: 858.39 g mol⁻¹; IR (ν cm⁻¹, KBr pellet): 3447, 1635, 1541, 1435; CD λ_{max} (mdeg) (DMF): 400 (-126), 317 (-5); UV-Vis (DMF) [λ_{max}/nm (ε/dm³ mol⁻¹ cm⁻¹)]: 580 (374), 377 (1315); CHN Analysis: Calcd.: C, 36.38; H, 4.23; N, 6.53 %; Found: C, 36.32; H, 4.35; N, 6.65%.

Characterization data for 23

Yield: 85%; Colour: Black; M. F.: $C_{26}H_{28}N_4O_2 \cdot Br_2Cl_2Mn_2 \cdot 4H_2O$; M. W.: 841.18 g mol⁻¹; IR (ν cm⁻¹, KBr pellet): 3468, 1624, 1547, 1431; CD λ_{max} (mdeg) (DMF): 477 (-2.36), 410 (-13), 330 (-45); UV-Vis (DMF) [λ_{max}/nm (ε/dm³ mol⁻¹ cm⁻¹)]: 414 (4947), 334 (6723); CHN Analysis: Calcd.: C, 37.12; H, 4.31; N, 6.66 %; Found: C, 37.26; H, 4.25; N, 6.74%.

Characterization data for 24

Yield: 73%; Colour: Brown; M. F.: $C_{26}H_{28}N_4O_2 \cdot Br_2Cl_2Co_2 \cdot 4H_2O$; M. W.: 849.17 g mol⁻¹; IR (ν cm⁻¹, KBr pellet): 3402, 1637, 1541, 1454; CD λ_{max} (mdeg) (DMF): 624 (32), 513 (-6), 423 (-37), 346 (-60); UV-Vis (DMF) [λ_{max}/nm (ε/dm³ mol⁻¹ cm⁻¹)]: 667 (600), 600 (580), 393 (7359); CHN Analysis: Calcd.: C, 36.77; H, 4.27; N, 6.60 %; Found: C, 36.69; H, 4.36; N, 6.82%.

Characterization data for 25

Yield: 85%; Colour: Orange; M. F.: $C_{26}H_{28}N_4O_2 \cdot Br_2Cl_2Ni_2 \cdot 4H_2O$; M. W.: 848.69 g mol⁻¹; IR (ν cm⁻¹, KBr pellet): 3406, 1624, 1543, 1454; CD λ_{max} (mdeg) (DMF): 413 (-24), 348 (-23); UV-Vis (DMF) [λ_{max}/nm (ε/dm³ mol⁻¹ cm⁻¹)]: 540 (127), 420 (3885), 340 (4952); CHN Analysis: Calcd.: C, 36.80; H, 4.28; N, 6.60 %; Found: C, 36.73; H, 4.16; N, 6.78%.

Characterization data for 26

Yield: 70%; Colour: Black; M. F.: $C_{26}H_{28}N_4O_2 \cdot Br_2Cl_2Fe_2 \cdot 4H_2O$; M. W.: 842.99 g mol⁻¹; IR (ν cm⁻¹, KBr pellet): 3368, 1626, 1554, 1435; CD λ_{max} (mdeg) (DMF): 550 (-9), 427 (-10), 368 (-34), 296 (-63); UV-Vis (DMF) [λ_{max}/nm ($\epsilon/dm^3 \text{ mol}^{-1} \text{ cm}^{-1}$)]: 490 (1813), 343 (7684); CHN Analysis: Calcd.: C, 37.04; H, 4.30; N, 6.65 %; Found: C, 37.16; H, 4.21; N, 6.83 %.

Characterization data for 27

Yield: 65%; Colour: Yellow; M. F.: $C_{26}H_{28}N_4O_2 \cdot Br_2Cl_2Zn_2$; M. W.: 790.02 g mol⁻¹; IR (ν cm⁻¹, KBr pellet): 1647, 1543, 1456; CD λ_{max} (mdeg) (DMF): 390(-121), 313 (-13), 280 (-63); UV-Vis (DMF) [λ_{max}/nm ($\epsilon/dm^3 \text{ mol}^{-1} \text{ cm}^{-1}$)]: 370 (13525); CHN Analysis: Calcd.: C, 39.53; H, 3.57; N, 7.09%; Found: C, 39.60; H, 3.62; N, 7.16%.

5.4. Results and discussion

The IR spectrum of the dicompartmental macrocyclic ligand **L**⁴ shows a $\nu(C=N)$ peak at 1628 cm⁻¹. Absence of $\nu(C=O)$ peak of 6,6'-piperazine-1,4-diyl dimethylene bis(4-bromo-2-formylphenol), at 1670 cm⁻¹ is indicative of Schiff base condensation. The IR spectra of the complexes **21–27** show bands at around 3400 cm⁻¹ corresponding to water molecules. $\nu(C=N)$ stretching bands at 1647 – 1624 cm⁻¹ confirm that the chiral Schiff base metal complexes are formed. A moderately new strong band appears at ~1543 cm⁻¹ and is indicative of a binuclear structure bridged by phenolic oxygens, which is not observed in the free ligand. The bands due to $\nu(C=C)$ stretching and bending modes appear at ~2935 cm⁻¹, ~2700 cm⁻¹ and as a strong band at ~1430 cm⁻¹. The CHN analytical data of the complexes match with the binuclear composition $[M_2L^4]Cl_2 \cdot nH_2O$. The circular dichroism (CD) and UV-vis spectra of the ligand **L**⁴ recorded in $CHCl_3$ solutions are shown in Figure 5.1. The UV-vis spectrum of the ligand **L**⁴ shows absorption bands at 335 nm and 256 nm. Circular dichroism bands appear at 344 nm and 270 nm. The electronic and circular

dichroism spectra of the binuclear complexes are recorded in N, N-dimethylformamide solution. The CD spectra bands of the complexes appeared at around 400 nm, 340 nm and the high intensity $\pi \rightarrow \pi^*$ transition band at near 280 nm. These CD signals confirm that the compounds are chiral. The circular dichroism and UV-vis spectra of the macrocyclic complexes are shown in Figure 5.6.

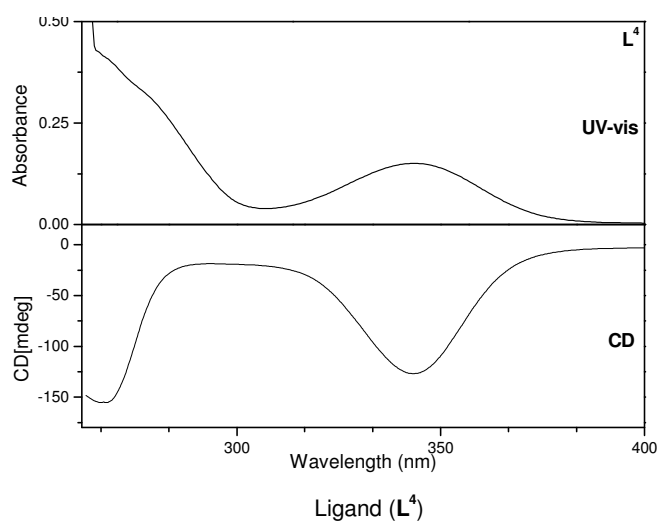


Figure 5.1. The CD and UV-vis spectra of the chiral macrocyclic ligand L^4 (concentrations= 1×10^{-5} M for UV-vis and 1×10^{-4} M for CD spectra in $CHCl_3$ solution).

5.4.1. X-ray crystallography of acyclic binuclear copper complex, **21**

Single crystals suitable for X-ray structure determination were obtained from methanol solution by the slow evaporation at room temperature. The binuclear copper complex crystallizes in monoclinic $P2_1$ space group.

Crystals of $[LCu_2Cl_4] \cdot 4H_2O$ **21** were characterized by elemental and spectral analyses. Single crystal X-ray structure determination data are given in Table 5.1. Bond lengths and bond angles are given in Table 5.2. The molecular structure of the acyclic binuclear copper(II) complex **21** is presented in Figure 5.2. In the molecular structure, each copper atom is five-coordinate with amino-nitrogen of cyclohexyl group (amine), imino-N (imine) and phenolic-O donors (from the chiral ligand) and two chloride ligands in a distorted square pyramidal geometry. The molecular

structure (chiral centers are C(1), C(6), C(27) and C(32)) has two imine nitrogen atoms, two amine nitrogen atoms and two piperazine nitrogen atoms are donor nitrogens. Interestingly, the two nitrogen atoms of the piperazine ring remains uncoordinated.

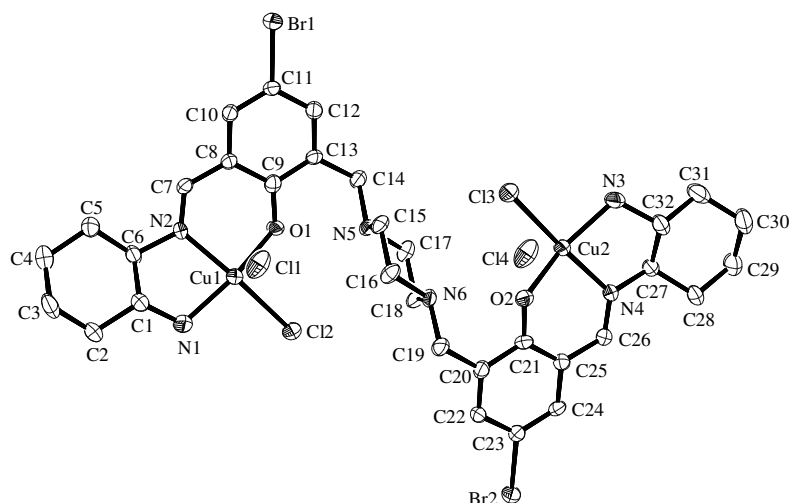


Figure 5.2. ORTEP diagram of the chiral acyclic binuclear copper(II) complex **21**. C(1), C(6), C(27) and C(32) are chiral centers. Thermal ellipsoids are at 30% probability level. Hydrogen atoms have been omitted for clarity.

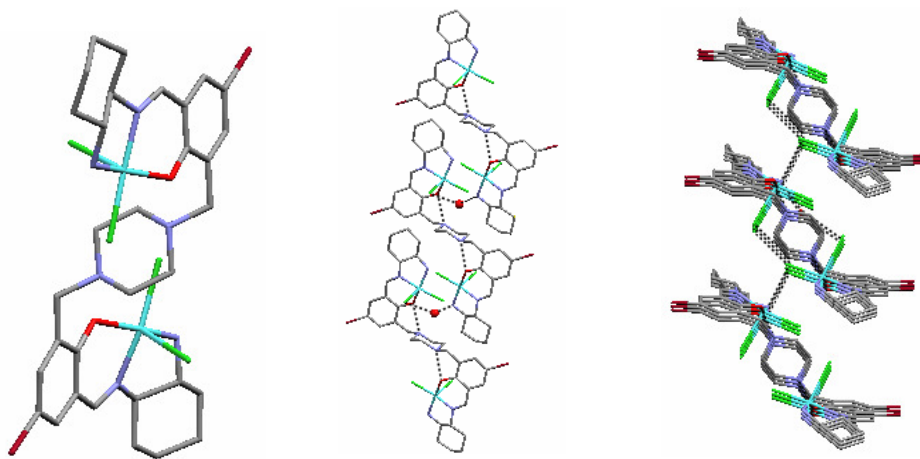


Figure 5.3. Molecular diagram of copper complex **21** (left: molecular twist; middle: intermolecular helix through the water molecules (red balls); right: crystallographic c-axis of intermolecular twist). (Colour: cyan: copper, red: oxygen, green: chlorine and blue: nitrogens).

Table 5.1. Crystallographic parameters of the binuclear copper complex, **21**

Compound	[LCu ₂ Cl ₄].4H ₂ O, 21
Empirical formula	C ₃₂ H ₅₄ Br ₂ N ₆ O ₆ Cu ₂ Cl ₄
<i>M</i>	1047.52
<i>T</i> /K	293(2) K
$\lambda/\text{\AA}$	0.71073
Crystal system	Monoclinic
Space group	<i>P</i> 2 ₁
<i>a</i> /\AA	7.6061(6)
<i>b</i> /\AA	22.2607(16)
<i>c</i> /\AA	12.0995(9)
$\beta/^\circ$	100.0840(10)
<i>U</i> /\AA ³ , <i>Z</i>	2017.0(3), 2
<i>D_c</i> /mg m ⁻³	1.715
μ/mm^{-1}	3.350
<i>F</i> (000)	1052
Crystal size/mm	0.06 x 0.14 x 0.30
θ range /°	1.71 to 28.28
Limiting indices	-10 ≤ <i>h</i> ≤ 10, -29 ≤ <i>k</i> ≤ 29, -16 ≤ <i>l</i> ≤ 15
Reflections collected	23441
Reflections [<i>I</i> > 2σ(<i>I</i>)]	9372
Data, parameters	9372, 493
Goodness-of-fit on <i>F</i> ²	0.954
Final <i>R</i> indices [<i>I</i> > 2σ(<i>I</i>)]	<i>R</i> 1 = 0.0494, <i>wR</i> 2 = 0.1028
<i>R</i> indices (all data)	<i>R</i> 1 = 0.0935, <i>wR</i> 2 = 0.1209

Table 5.2. Selected bond lengths (Å) and bond angles (°) of complex, **21**

Bond lengths			
N(1)-Cu(1)	1.970(6)	N(2)-Cu(1)	1.992(6)
N(3)-Cu(2)	1.998(6)	N(4)-Cu(2)	1.982(6)
O(1)-Cu(1)	1.912(4)	O(2)-Cu(2)	1.919(4)
Cl(1)-Cu(1)	2.643(2)	Cl(2)-Cu(1)	2.309(2)
Cl(3)-Cu(2)	2.298(2)	Cl(4)-Cu(2)	2.687(2)
C(1)-N(1)	1.447(9)	C(6)-N(2)	1.477(7)
C(7)-N(2)	1.277(8)	C(14)-N(5)	1.534(8)
C(15)-N(5)	1.471(8)	C(32)-N(3)	1.477(9)
C(19)-N(6)	1.492(9)	C(27)-N(4)	1.465(8)
C(9)-O(1)	1.320(9)	C(21)-O(2)	1.323(8)
C(11)-Br(1)	1.901(7)	C(23)-Br(2)	1.907(7)
C(13)-C(14)	1.496(10)	C(19)-C(20)	1.506(10)
Bond angles			
O(1)-Cu(1)-N(1)	164.2(2)	O(2)-Cu(2)-N(4)	91.8(2)
O(1)-Cu(1)-N(2)	89.6(2)	O(2)-Cu(2)-N(3)	157.4(3)
N(1)-Cu(1)-N(2)	83.1(2)	N(4)-Cu(2)-N(3)	84.5(2)
O(1)-Cu(1)-Cl(2)	89.85(15)	O(2)-Cu(2)-Cl(3)	89.25(16)
N(1)-Cu(1)-Cl(2)	94.46(19)	N(4)-Cu(2)-Cl(3)	175.54(17)
N(2)-Cu(1)-Cl(2)	168.15(17)	N(3)-Cu(2)-Cl(3)	92.84(19)
O(1)-Cu(1)-Cl(1)	93.94(15)	O(2)-Cu(2)-Cl(4)	96.65(16)
N(1)-Cu(1)-Cl(1)	100.5(2)	N(4)-Cu(2)-Cl(4)	85.77(16)
N(2)-Cu(1)-Cl(1)	94.42(16)	N(3)-Cu(2)-Cl(4)	105.3(2)
Cl(2)-Cu(1)-Cl(1)	97.43(8)	Cl(3)-Cu(2)-Cl(4)	98.42(8)
C(9)-O(1)-Cu(1)	123.1(4)	C(21)-O(2)-Cu(2)	123.6(4)

This is because the phenolic hydroxyl gets deprotonated and piperazine-N gets protonated during complexation. This kind of proton transfer is known in literature.¹⁶ There are two intra-molecular hydrogen bonds: N(5)····O(1) (2.641(5)) and N(6)····O(2) (2.637(7)). Also there is extensive inter-molecular hydrogen bonding interactions in the molecular structure **21**. The hydrogen bonding is extended through the uncoordinated lattice water molecules. The inter-molecular hydrogen bonded packing diagram of **21**, as shown in Figure 5.4.

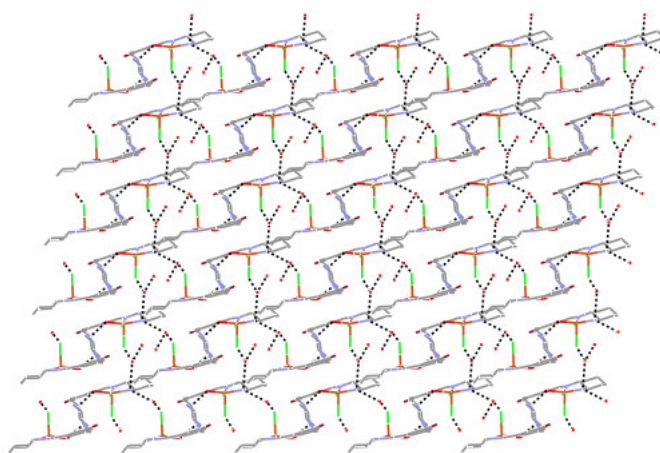


Figure 5.4. Inter-molecular hydrogen bonded packing diagram of the copper complex **21**.

There are four water molecules in the crystal lattice. The water molecule forms hydrogen bonding interactions to the coordinated axial chloride atom of the copper complex **21**. This hydrogen bonding is extended through the water molecules (Figure 5.3). The conformations of the piperazine and cyclohexyldiamine groups are found to be chair forms. Selected bond lengths and bond angles are given in Table 5.2. The average Cu(1)-N(1) and Cu(1)-N(2) bond distances are 1.970(6) and 1.992(6) Å, and the average Cu(2)-N(3) and Cu(2)-N(4) bond distances are 1.998(6) and 1.982(6) Å. The average Cu(1)-O(1) and Cu(2)-O(2) bond lengths are 1.912(4) and 1.919(4) Å. The average Cu(1)-Cl(1) and Cu(1)-Cl(2) bond distances are 2.643(2) and 2.309(2) Å and the average Cu(2)-Cl(3) and Cu(2)-Cl(4) bond distances are 2.298(2) and 2.687(2) Å respectively. The coordination geometry around the copper centre is distorted square pyramidal.

The IR spectrum of the acyclic copper complex **21** shows strong stretching band at around 1639 cm^{-1} due to the coordinated imine groups ($\text{C}=\text{N}$) and two bands at 3288 cm^{-1} and 3223 cm^{-1} are corresponding to the coordinated amine groups ($\text{C}-\text{NH}$) and band at 1577 cm^{-1} corresponds to coordinated phenolic oxygens.

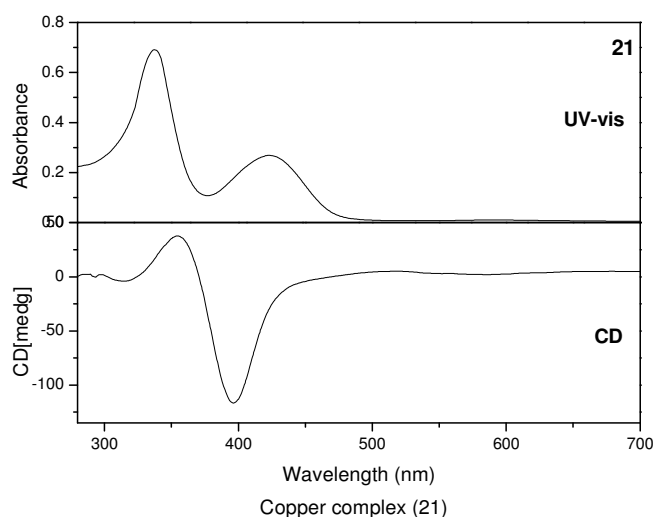


Figure 5.5. The CD and UV-vis spectra of the chiral acyclic binuclear copper complex **21** (concentrations= $1 \times 10^{-5}\text{ M}$ UV-vis and $1 \times 10^{-3}\text{ M}$ for CD spectra in DMF solution).

The broad band around 3402 cm^{-1} corresponds to the water molecules. The electronic and the circular dichroism spectra of the complex recorded in *N,N*-dimethylformamide solution (Figure 5.5) show a band at 585 nm and other strong absorption bands are observed at 375 nm and 273 nm. The 585 nm band is of d–d transition in square pyramidal geometry and the other bands correspond to ligand to metal charge transfer transitions and intra ligand charge transfer transitions. The circular dichroism spectrum shows two bands at 397(–134) and 320(–6) nm. These bands confirm that the complex is chiral. The analytical data of complex match with the binuclear composition of $[\text{LCu}_2\text{Cl}_4] \cdot 4\text{H}_2\text{O}$.

5.4.2. Copper complex $[\text{Cu}_2\text{L}^4]\text{Cl}_2 \cdot 4\text{H}_2\text{O}$, **22**

The chiral macrocyclic binuclear copper complex was synthesized by the procedure given in section 5.3.3.5. The binuclear copper(II) complex formation was

evident from the C=N stretching vibration frequency observed at 1635 cm^{-1} which is higher than the C=N frequencies (at 1628 cm^{-1}) observed for the free macrocyclic ligand **L**⁴. A moderately strong band at 1541 cm^{-1} appears in the complex which corresponds to the bridging C-O stretching vibrations. A broad band at 3447 cm^{-1} suggests the presence of lattice water.

The electronic and the circular dichroism spectra of the complex are measured in N,N-dimethylformamide solution (Figure 5.6). The complex exhibits d-d transition band at 580 nm. It may be noted that the λ_{max} values are observed at relatively lower energies compared to analogous symmetrical binuclear copper(II) complexes in which the metal ions are in planar environments. The moderately intense band observed at 377 nm is due to the overlap of the transition of the azomethine with the charge-transfer band from bridging phenolic oxygen to the vacant d-orbital of the copper(II). The circular dichroism spectrum of the copper complex shows the charge transfer transition band at 400(-126) and the band at 317(-5) nm is due to the intra ligand transition. The CHN analytical data agree with the binuclear composition of $[\text{Cu}_2\text{L}^4]\text{Cl}_2 \cdot 4\text{H}_2\text{O}$.

5.4.3. Manganese complex $[\text{Mn}_2\text{L}^4]\text{Cl}_2 \cdot 4\text{H}_2\text{O}$, 23

The chiral macrocyclic binuclear manganese complex was synthesized in good yields by the procedure given in section 5.3.3.5. The IR spectrum of the complex shows strong stretching band at around 1624 cm^{-1} due to the C=N group which is lower than the free ligand (C=N) frequency. Band at 1547 cm^{-1} corresponds to coordinated bridging phenolic oxygens. The broad band around 3450 cm^{-1} corresponds to the water molecules. The electronic and the circular dichroism spectra of the complex were recorded in N,N-dimethylformamide solution (Figure 5.6). The complex shows d-d transition band at 586 nm. An intense charge transfer band appears at 414 nm. This band is due to the charge transfer from phenolic oxygen to metal and also due to azomethine transitions. A strong peak observed at 344 nm is due to the intra ligand π - π^* transitions.

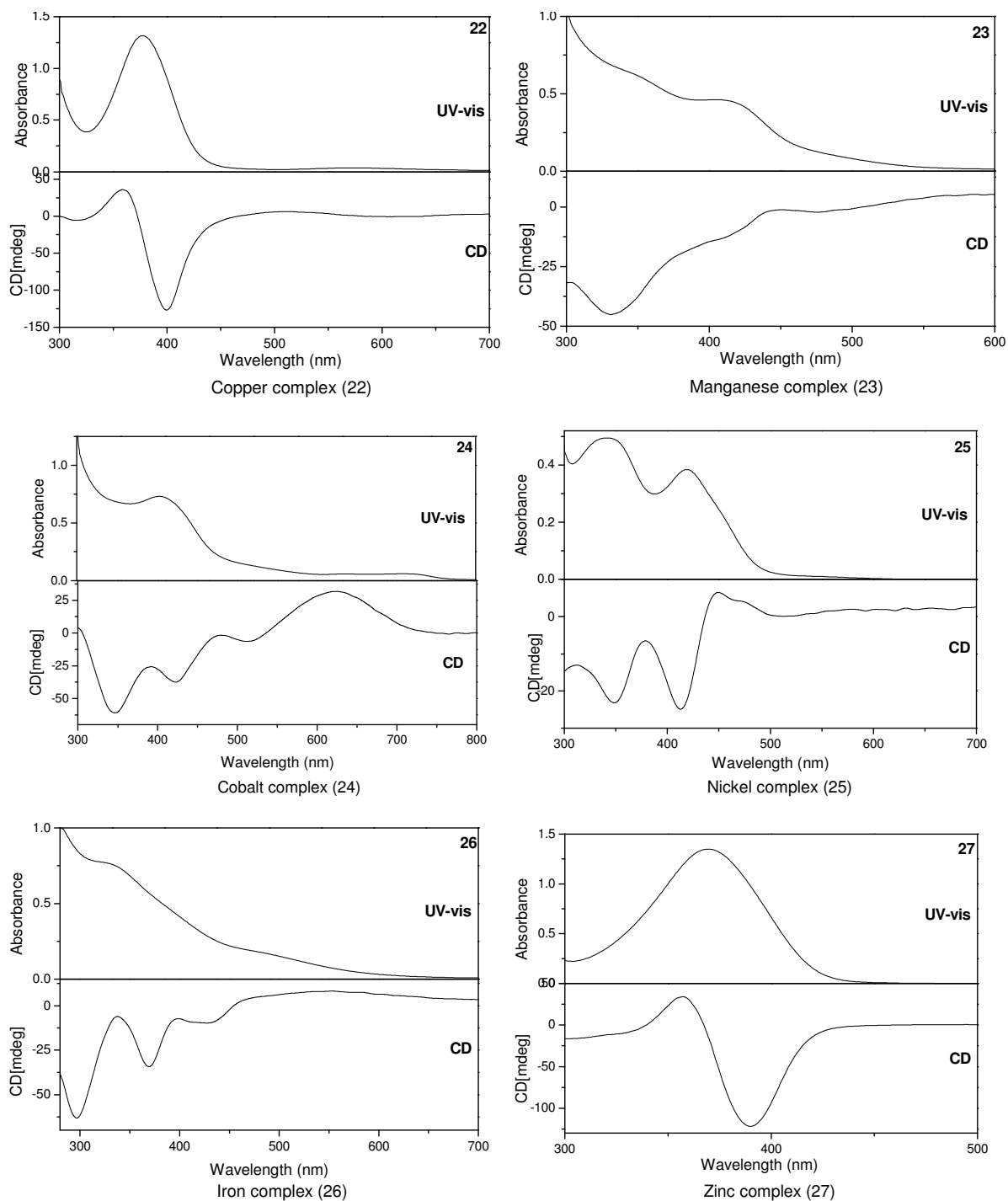


Figure 5.6. CD and UV-vis spectra of Cu^{2+} , Mn^{2+} , Co^{2+} , Ni^{2+} , Fe^{2+} and Zn^{2+} complexes recorded in DMF solutions (concentrations = $1 \times 10^{-3}\text{M}$ for CD and $1 \times 10^{-4}\text{M}$ for UV-vis spectra).

The circular dichroism spectrum of the complex shows intense peak at 332 (-45) nm and a shoulder band at 411(-12) nm. Appearance of these bands confirms the chirality. The analytical data of the complex match with the binuclear composition of $[\text{Mn}_2\text{L}^4]\text{Cl}_2 \cdot 4\text{H}_2\text{O}$.

5.4.4. Cobalt complex $[\text{Co}_2\text{L}^4]\text{Cl}_2 \cdot 4\text{H}_2\text{O}$, **24**

The chiral macrocyclic binuclear cobalt complex **24** was synthesized by the procedure given in section 5.3.3.5. The IR spectrum of the complex shows C=N stretching band at 1637 cm^{-1} and additional supporting band at 1454 cm^{-1} is indicative of bridging phenolic C-O groups. The broad band at 3402 cm^{-1} is due to the presence of lattice water. The electronic and circular dichroism spectra of the complex are recorded in N,N-dimethylformamide solution (Figure 5.6). The absorption spectrum shows three d-d transition bands at 667, 600 and 581 nm. A high intensity absorption band at 393 nm is due to the ligand to metal charge transfer transitions, band at 373 nm is due to the intraligand transition and the band at 230 nm is due to $\pi\text{-}\pi^*$ electronic transitions of the ligand.

The CD spectrum of the complex shows d-d transition bands at 624 (32) and 513 (-6) nm. The charge transfer region of the spectra shows band at 423(-37) nm and the high intensity $\pi\rightarrow\pi^*$ transition band at 346 (-60) nm confirms that the complex is chiral. The elemental analytical data of the complex agree with the binuclear composition of $[\text{Co}_2\text{L}^4]\text{Cl}_2 \cdot 4\text{H}_2\text{O}$.

5.4.5. Nickel complex $[\text{Ni}_2\text{L}^4]\text{Cl}_2 \cdot 4\text{H}_2\text{O}$, **25**

The chiral macrocyclic binuclear nickel complex was synthesized in good yields by the procedure given in section 5.3.3.5. The IR spectrum of the complex shows strong stretching band at around 1624 cm^{-1} corresponding to the C=N group and bridging phenolic oxygen band appears at 1543 cm^{-1} . Strong band appears for C=C at 1435 cm^{-1} and a broad band at around 3405 cm^{-1} corresponds to the water molecules.

The electronic and the circular dichroism spectra of the complex recorded in N,N-dimethylformamide solution (Figure 5.6) shows a shoulder band at 540 nm and two strong absorption bands are observed at 420 and 340 nm. The 540 nm band is of d–d transition in square planar geometry and the other bands correspond to the ligand to metal charge transfer transitions and intra ligand transition. The circular dichroism spectrum shows two bands at 413(-9) and 348(-10) nm. These bands confirm that the complex is chiral. The analytical data of complex match with the binuclear composition of $[\text{Ni}_2\text{L}^4]\text{Cl}_2 \cdot 4\text{H}_2\text{O}$.

5.4.6. Iron complex $[\text{Fe}_2\text{L}^4]\text{Cl}_2 \cdot 4\text{H}_2\text{O}$, **26**

The chiral macrocyclic binuclear iron complex **26** was synthesized by the procedure given in section 5.3.3.5. The IR spectrum of the complex exhibits three characteristic bands. The coordinated C=N stretching band occurs at 1626 cm^{-1} and phenolic bridging oxygen band appear at 1554 cm^{-1} . A broad band at around 3370 cm^{-1} corresponds to the water molecules. The electronic and circular dichroism spectra of the complex are recorded in N,N-dimethylformamide solution (Figure 5.6). The electronic spectrum shows d–d transition band at around 490 nm and a shoulder band at 440 nm due to the ligand to metal charge transfer transitions. A high intensity band observed at 343 nm is due to the intra ligand charge transfer transitions. In the circular dichroism spectrum, bands appear at 550 (-9), 427(-10) nm and high intensity bands at 368(-34) and 296(-63) nm. These bands confirm that the complex is chiral. The analytical data of the complex match with the binuclear composition of $[\text{Fe}_2\text{L}^4]\text{Cl}_2 \cdot 4\text{H}_2\text{O}$.

5.4.7. Zinc complex $[\text{Zn}_2\text{L}^4]\text{Cl}_2$, **27**

The chiral macrocyclic binuclear zinc complex was synthesized by the procedure given in section 5.3.3.5. The IR spectrum of the complex shows two strong stretching bands at 1647 cm^{-1} and 1543 cm^{-1} corresponding to the C=N and bridging phenolic oxygen groups. The electronic and CD spectra of the complex are recorded in N,N-dimethylformamide solution (Figure 5.6). The complex electronic spectrum

shows band at 370 nm due to the ligand to metal charge transfer transitions. The charge transfer region of the complex shows a high intensity band at 390(-121) nm and intra ligand transition band at 313 (-13) nm in the circular dichroism spectrum. These bands confirm that the complex is chiral. The analytical data of the complex agree with the binuclear composition of $[\text{Zn}_2\text{L}^4]\text{Cl}_2$.

5.5. Catalysis

To examine the activity of the chiral macrocyclic Schiff base metal complexes in the catalytic process, the alkenes oxidation reactions were studied. The epoxidation reactions were carried out in CH_3CN using iodosylbenzene (PhIO) as the terminal oxidant at room temperature. The oxidation reactions were run for 24 hours. In absence of the catalyst under similar reaction conditions, there is no reaction between oxidant and olefins.

5.5.1. Synthesis of Iodosylbenzene (PhIO)

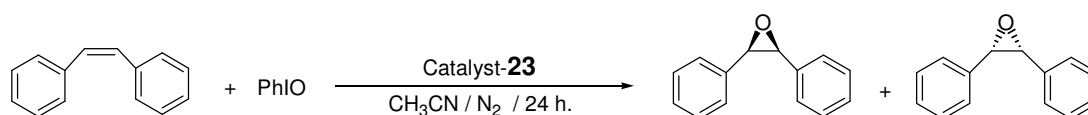
The iodosylbenzene (PhIO) used in the catalytic study as oxidant is prepared using a reported procedure.¹⁷ Finely ground iodosylbenzene diacetate (32.2 g, 0.10 mol) is placed in a 250 mL beaker and 150 mL of 3N sodium hydroxide is added over a 5 minute period with vigorous stirring. The lumps of solid that formed are triturated with a stirring rod or spatula for 15 minutes and the reaction mixture stands for an additional 45 minutes to complete the reaction. 100 mL of water is added, the mixture is stirred vigorously and the crude solid iodosobenzene is collected on a Büchner funnel, washed there with 200 mL of water and dried by maintaining suction. Final purification is effected by triturating the dried solid in 75 mL of chloroform in a beaker. The iodosylbenzene is separated by filtration and air-dried (Yield: 85%).



5.5.2. Epoxidation of *cis*-stilbene catalyzed by manganese complex, **23**

The chiral manganese catalyst **23** (0.022 g, 0.025 mmol) and *cis*-stilbene (0.180 g, 1 mmol) were dissolved in 5 mL acetonitrile. The reaction was initiated by the addition of iodosylbenzene (PhIO) (0.220 g, 1 mmol) and stirred at room temperature under nitrogen atmosphere for 24 hours.

After stirring, the mixture was concentrated in vacuum. Anhydrous ether (10 mL) added to the brown residue and the ether solution was carefully filtered. Then the ether was removed under reduced pressure and purified with column chromatography from hexane. The catalytic epoxidation reaction sequence of *cis*-stilbene is shown in Scheme 5.4.



Scheme 5.4. Schematic representation of catalytic epoxidation of *cis*-stilbene.

The product was confirmed by ¹H-NMR spectrum (*cis*-stilbene epoxide $\delta \sim 4.33$ in CDCl₃) of reported stilbene epoxide.¹⁸ HPLC analyses of *cis*-stilbene epoxide products were carried out on a Shimadzu SCL-10A instrument equipped with CHIRALCEL OD-H using Class-VP program (90:10 hexane / *i*-PrOH, 0.5 mL/min, 254 nm, retention times: 7.8 min for *cis*-stilbene; 10.78 min and 11.83 min for epoxides). The HPLC analysis profile of the *cis*-stilbene epoxide catalyzed by complex **23** is shown in Figure 5.7. HPLC analyses data percentage of enantiomeric excess of *cis*-stilbene epoxide catalyzed by complex **23**, as a function of time are given in Table 5.3. Epoxidation of *cis*-stilbene catalyzed by **23** yields up to 33% at room temperature with 85% of enantiomeric excess (Table 5.4 entry 1).

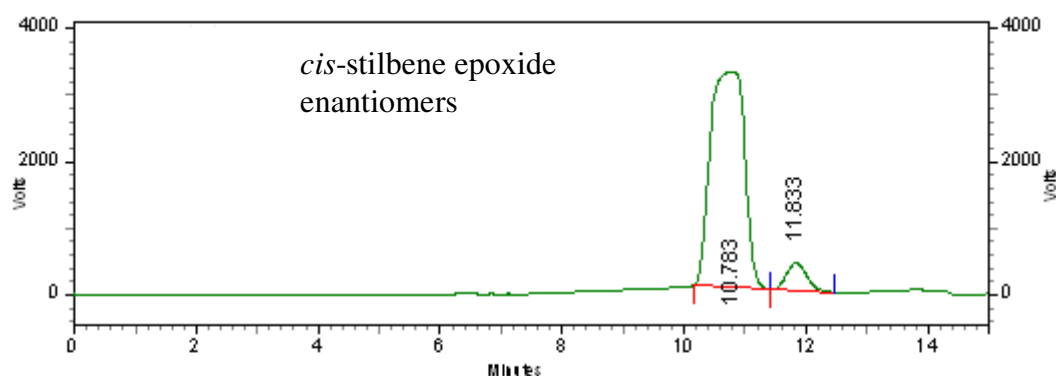


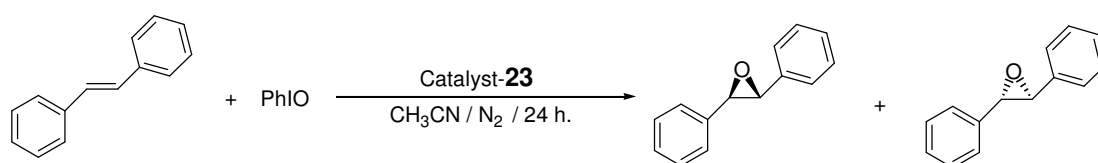
Figure 5.7. HPLC analysis profile of *cis*-stilbene epoxide catalyzed by complex **23**.

Table 5.3. HPLC analysis data profile of *cis*-stilbene epoxide, showing enantiomeric excess catalyzed by complex **23** as a function of time

Pk #	Retention Time	Area	Area %	Height	Height %
1	10.783	125290187	92.643	3236765	88.515
2	11.833	9950004	7.357	419994	11.485
Totals		135240191	100.000	3656759	100.000

5.5.3. Epoxidation of *trans*-stilbene catalyzed by manganese complex, **23**

The chiral manganese catalyst **23** (0.022 g, 0.025 mmol) and *trans*-stilbene (0.180 g, 1 mmol) were dissolved in 5 mL acetonitrile. The reaction was initiated by the addition of iodosylbenzene (PhIO) (0.220 g, 1 mmol) and stirred at room temperature under nitrogen atmosphere for 24 hours. After stirring, the mixture was concentrated in vacuum. Anhydrous ether (10 mL) added to the brown residue and the ether solution was carefully filtered. Then the ether was removed under reduced pressure and purified with column chromatography from hexane. The catalytic epoxidation reaction of *trans*-stilbene is shown in Scheme 5.5.



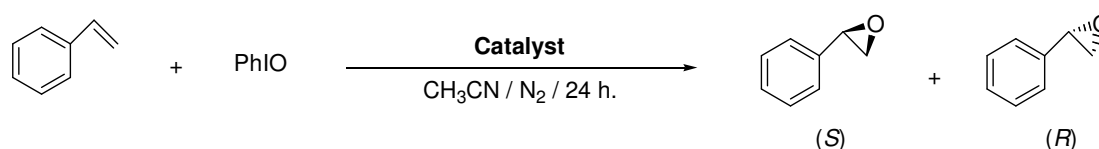
Scheme 5.5. Schematic representation catalytic epoxidation of *trans*-stilbene.

The product was confirmed by ^1H -NMR spectrum (*trans*-stilbene epoxide $\delta \sim 3.83$ in CDCl_3) of reported stilbene epoxide.¹⁹ HPLC analyses of *trans*-stilbene epoxide products were carried out on a Shimadzu SCL-10A instrument equipped with CHIRALCEL OD-H using Class-VP program (90:10 hexane / *i*-PrOH, 0.5 mL/min, 254 nm, retention times: 9.18 min for *trans*-stilbene; 10.53 min and 11.49 min for epoxides).

HPLC analysis data showing percentage of *trans*-stilbene epoxide catalyzed by complex **23**, as a function of time are given in Table 5.4 (entry 2). Epoxidation of *trans*-stilbene catalyzed by **23**, yields up to 17% at room temperature with 20% of enantiomeric excess.

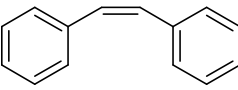
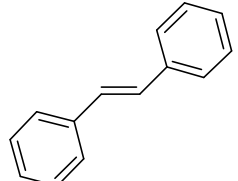
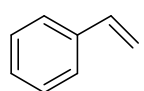
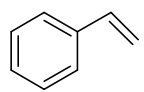
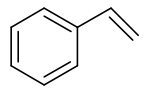
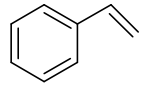
5.5.4. Epoxidation of styrene catalyzed by chiral complexes **22**, **23**, **24** and **26**

All the reactions were carried out by the same procedure. Oxidations of styrene by the chiral catalysts copper **22**, manganese complex **23**, cobalt **24** and iron **26** with iodosylbenzene (PhIO) as oxidant were carried out by the following procedure: The chiral catalyst (0.025 mmol) and styrene (0.104 g, 1 mmol) were dissolved in 5 mL acetonitrile. The reaction was initiated by the addition of iodosylbenzene (0.220 g, 1 mmol) and stirred at room temperature under nitrogen atmosphere for 24 hours (Scheme 5.6). After completion of the reaction, the solvent was removed under reduced pressure. Anhydrous ether (10 mL) was added to the brown residue and the ether solution was carefully filtered. Then the ether was removed under reduced pressure and purified using short silica gel column from hexane. The products were confirmed by ^1H -NMR spectroscopy (styrene epoxide $\delta \sim 3.84$ in CDCl_3).



Scheme 5.6. Schematic representation of catalytic epoxidation of styrene.

Table 5.4. Oxidation products ^a of olefins catalyzed by **22**, **23**, **24** and **26**

Entry	Substrate	Catalyst	Epoxide Yield(%)	Epoxide e. e.(%)	1-Phenyl acetaldehyde Yield(%) ^c	Acetophenone Yield(%) ^c
1		Mn(II) 23	33 ^b	85 ^d	—	—
2		Mn(II) 23	17 ^b	20 ^d	—	—
3		Mn(II) 23	96 ^c	5 ^e	—	—
4		Cu(II) 22	50 ^c	—	44	3
5		Co(II) 24	14 ^c	—	54	24
6		Fe(II) 26	65 ^c	4 ^e	32	—

^a Products confirmed by ¹H-NMR spectroscopy. ^b Based on substrate consumed and determined by chiral column (CHIRALCEL OD-H) HPLC analysis. ^c Based on substrate consumed and determined by chiral column GC analysis (Supelco α -DEX 325, 30m length, 0.25mm id, 0.25 μ m film thickness). ^d Enantiomeric excess of epoxides, determined by chiral column (CHIRALCEL OD-H) HPLC analysis. ^e Enantiomeric excess of epoxides, determined by chiral column GC analysis (Supelco α -DEX 325, 30m length, 0.25mm id, 0.25 μ m film thickness).

The oxidation product yields and enantiomeric excess of the styrene were determined by gas chromatography (GC) analysis. Gas chromatographic analyses were carried out on a Shimadzu GC 14B instrument equipped with a chiral capillary column (Supelco α -DEX 325, 30m length, 0.25mm id, 0.25 μ m film thickness) and a flame ionization detector (FID). Column temperature programmed at 90 °C, Injector and Detector temperatures programmed 200 °C with nitrogen as carrier gas.

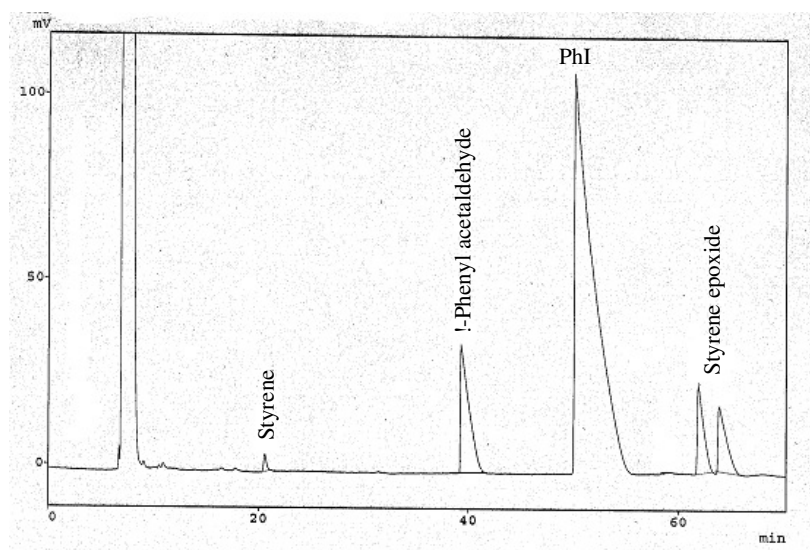


Figure 5.8. A representative gas chromatographic (GC) analysis of styrene oxidation products catalyzed by copper catalyst **22**.

The oxidation product yields and enantiomeric excess of styrene were determined by gas chromatography (GC). Gas chromatography of authentic samples is shown in Chapter 2 (Figure 2.13). The amount of epoxide formed on epoxidation of styrene and the enantiomeric excess of the epoxide catalyzed by complex **22** as a function of time are shown in Figure 5.8. The percentage of epoxide yields and the enantiomeric excess of the epoxides are given in Table 5.4 (entries 3-6). The manganese catalyst **23** is encouraging for the epoxidation reactions of the styrene (yield 96%).

5.6. Conclusions

New optically active macrocyclic binuclear Schiff base metal complexes have been synthesized. The chiral acyclic binuclear copper complex **21** was characterized by X-ray crystallographic analysis. The chiral macrocyclic ligand **L⁴** and its macrocyclic binuclear complexes **22–27** were characterized by analytical and spectral methods. All complexes show optical activity was confirmed by the circular dichroism studies.

The catalytic activities of the chiral Schiff base complexes were determined for the epoxidation of alkenes by a terminal oxidant. The manganese catalyst **23** is promising for the epoxidation reactions of the styrene (yield 96%). The other complexes favour for the epoxidation reactions of styrene yields to styrene epoxide with 1-phenylacetaldehyde and acetophenone as side products. Epoxidation of *trans*-stilbene catalyzed by manganese complex **23**, yields up to 17% at room temperature with 20% of enantiomeric excess. Epoxidation of *cis*-stilbene catalyzed by **23**, yields up to 33% at room temperature with 85% of enantiomeric excess.

5.7. References

1. R. A. Sheldon and J. K. Kochi, “*Metal-catalyzed Oxidations of Organic Compounds*”; Academic: New York, **1981**.
2. B. E. Rossiter, In “*Asymmetric Synthesis*” ed. By J. D. Morrison, Academic Press, New York, **1986**, vol. 5, p. 193.
3. T. Katsuki and K. B. Sharpless, *J. Am. Chem. Soc.*, **1980**, 102, 5974.
4. J. T. Groves and P. Viski, *J. Org. Chem.*, **1990**, 55, 3628.
5. K. srinivasan, S. Perrier and J. K. Kochi, *J. Am. Chem. Soc.*, **1986**, 108, 2309.
6. (a) W. Zhang, J. L. Loebach, S. R. Wilson and E. N. Jacobsen, *J. Am. Chem. Soc.*, **1990**, 112, 2801; (b) Jay F. Larrow and Eric N. Jacobsen, *J. Org. Chem.*, **1994**, 59, 1939.
7. (a) R. Irie, K. Noda, N. Matsumoto, Y. Ito and T. Katsuki, *Tetrahedron Lett.*, **1990**, 31, 7345; (b) R. Irie, K. Noda, N. Matsumoto, Y. Ito and T. Katsuki,

- Tetrahedron Lett.*, **1991**, 32, 1055; (c) R. Irie, K. Noda, Y. Ito, N. Matsumoto and T. Katsuki, *Tetrahedron Asymmetry.*, **1991**, 2, 481.
8. (a) E. N. Jacobsen, in *Catalytic Asymmetric Synthesis*, Ed. I. Ojima, VCH, **1993**, 159; (b) T. Katsuki, *Coordination. Chem. Rev.*, **1995**, 140, 189; (c) J. P. Collman; X. Zhang; V. J. Lee; E. S. Uffelman; and J. I. Brauman, *Science*, **1993**, 261, 1404.
 9. J. Gao, J. H. Reibenspies and A. E. Martwell, *Angwe. Chem. Int. Ed.*, **2003**, 42, 6008.
 10. Jay F. Larrow and Eric N. Jacobsen, *J. Org. Chem.*, **1994**, 59, 1939.
 11. SMART & SAINT Software Reference Manuals, Version 6.22, Bruker AXS Analytic X-Ray Systems, Inc., Madison, WI, **2000**.
 12. G. M. Sheldrick, SADABS, Software for Empirical Absorption Correction, University of Göttingen, Germany, **2000**.
 13. SHELXTL Reference Manual, Version 5.1, Bruker AXS, Analytic X-Ray Systems, Inc., WI, **1997**.
 14. L. J. Farrugia, *J. Appl. Cryst.*, **1997**, 30, 567.
 15. A. L. Spek, *Platon, Molecular Graphics Software*, University of Glasgow, UK, **2001**.
 16. H. Pizzala, M. Carles, W. E. E. Stone, and A. Thevand, *J. Chem. Soc., perkin trans. 2.* **2000**, 935.
 17. H. Saltzman and J. G. Sharefkin, *Org. Synth.*, **1973**, Coll. Vol. V, 658.
 18. K. Srinivasan, P. Michaud and J. K. Kochi, *J. Am. Chem. Soc.*, **1986**, 108, 2309.
 19. D. Das and C.-P. Cheng, *J. Chem. Soc., Dalton Trans.*, **2000**, 1081.
 20. R. Thirumurugan, S. S. S. Raj, G. Shanmugam, H. -K. Fun, K. Chinnakali, S. Chantrapromma, M. Marappan and M. Kandaswamy, *Act Cryst.*, C54, **1998**, 780.
-

Scope of the future research work

The present study revealed the synthesis and structural characterization of chiral Schiff base metal complexes and their catalytic activity.

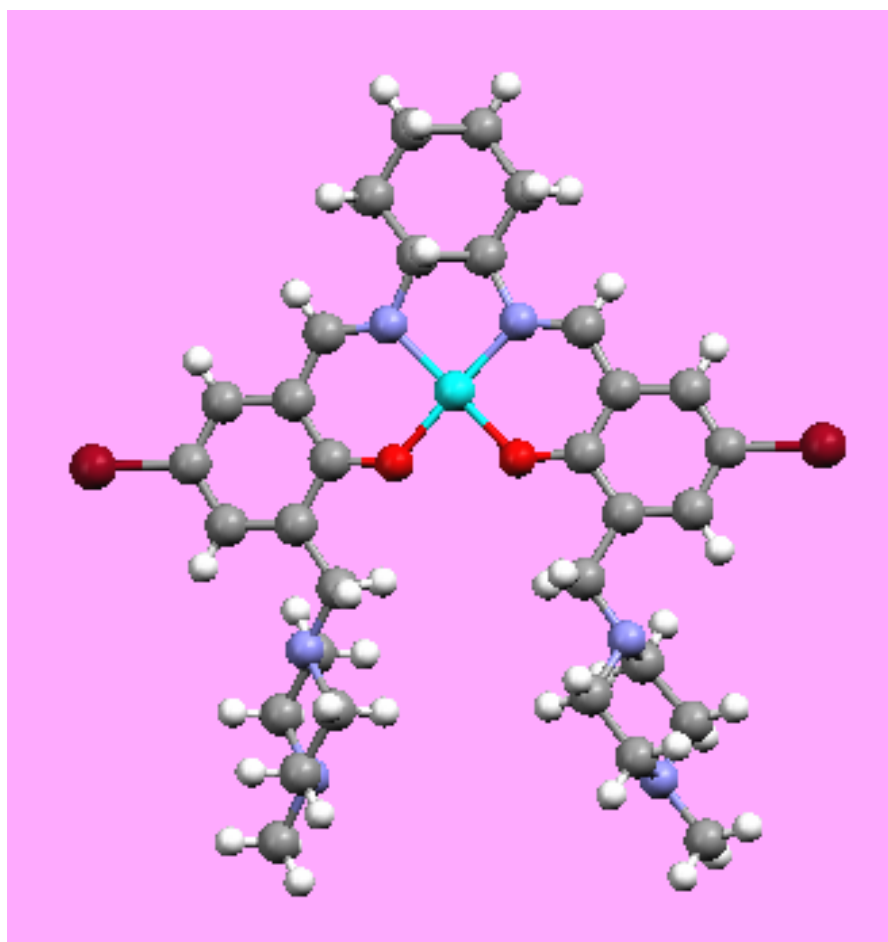
We examined the asymmetric epoxidation of *cis*-stilbene, *trans*-stilbene and styrene using some of the synthesized complexes as catalysts. But we did not make any further attempt to optimize the reaction conditions like the optimum amount of catalyst needed and other conditions normally required to be done for asymmetric epoxidation of several olefins.

One can explore these chiral catalysts for cyclopropanation reactions, borohydride reduction reactions, hydroxylation reactions, alkynyl addition reactions, hydrocyanation reactions and aziridination of olefins...etc.

List of Publications

1. Synthesis and structural characterization of complexes from the NOS ligating Schiff base of dfp: structurally different molecules in the unit cell of the manganese complexes. N. Mangayarkarasi, **Maddela Prabhakar** and Panthapally S. Zacharias, *Polyhedron.*, **2002**, 21, 925.
2. Self assembly of a fluorescent chiral Zn(II) complex that leads to supramolecular helices. **Maddela Prabhakar**, Panthapally S. Zacharias and Samar K. Das, *Inorg. Chem.*, **2005**, 45, 2585 (*most accessed top 5 article in jan-jun 2005*).
3. Water-chloride interactions: Left- and right-handed aqua-chloro supramolecular helices anchored by a chiral Schiff base nickel complex. **Maddela Prabhakar**, Panthapally S. Zacharias and Samar K. Das, *Inorg. Chem. Commun.*, **2006**, 9, 899.
4. A chiral Schiff base binuclear copper (II) complex, which is molecularly twisted and inter-molecular hydrogen bonded $\text{NH}_2 \cdots \text{H}_2\text{O} \cdots \text{Cl}$ interactions. **Maddela Prabhakar**, Panthapally S. Zacharias and Samar K. Das (*manuscript under preparation*).
5. Synthesis and X-ray crystallographic studies of a tetranuclear chiral Schiff base copper complex. **Maddela Prabhakar**, Panthapally S. Zacharias and Samar K. Das (*to be communicated*).
6. Synthesis and X-ray crystal structure of reduced Schiff base octanuclear copper complex. **Maddela Prabhakar**, Panthapally S. Zacharias and Samar K. Das (*to be communicated*).

7. Synthesis and X-ray crystallographic studies of a chiral Schiff base mononuclear copper complex. **Maddela Prabhakar**, Panthapally S. Zacharias and Samar K. Das (*to be communicated*).
 8. X-ray crystal structure of a chiral Schiff base ligand, its metal complexes synthesis, characterization and catalytic activity. **Maddela Prabhakar**, Panthapally S. Zacharias and Samar K. Das (*to be communicated*).
 9. Synthesis and X-ray crystallographic studies of a chiral Schiff base mononuclear nickel(II) complex. **Maddela Prabhakar**, Panthapally S. Zacharias and Samar K. Das (*to be communicated*).
 10. Synthesis and structural characterization of macrocyclic chiral Schiff base metal complexes and their catalytic activity towards epoxidation reactions of olefins. **Maddela Prabhakar**, Panthapally S. Zacharias and Samar K. Das (*to be communicated*).
-



X-Ray Crystal Structure of Chiral Schiff Base Nickel Complex 1